THERMAL-MECHANICAL ANALYSIS OF SYSTEM-LEVEL ELECTRONIC PACKAGES FOR SPACE APPLICATIONS

by

Adrien Pascal Lambert

A thesis submitted in partial fulfillment
of the requirements for the degree

of

Master of Science

in

Mechanical Engineering

MONTANA STATE UNIVERSITY
Bozeman, Montana

November 2012

APPROVAL

of a thesis submitted by

Adrien Pascal Lambert

This thesis has been read by each member of the thesis committee and has been found to be satisfactory regarding content, English usage, format, citation, bibliographic style, and consistency and is ready for submission to The Graduate School.

Dr. Ahsan Mian

Approved for the Department of Mechanical and Industrial Engineering

Dr. Christopher Jenkins

Approved for The Graduate School

Dr. Ronald W. Larsen

STATEMENT OF PERMISSION TO USE

In presenting this thesis in partial fulfillment of the requirements for a master's degree at Montana State University, I agree that the Library shall make it available to borrowers under rules of the Library.

If I have indicated my intention to copyright this thesis by including a copyright notice page, copying is allowable only for scholarly purposes, consistent with "fair use" as prescribed in the U.S. Copyright Law. Requests for permission for extended quotation from or reproduction of this thesis in whole or in parts may be granted only by the copyright holder.

Adrien Pascal Lambert

November, 2012

TABLE OF CONTENTS

TABLE OF CONTENTS - CONTINUED

LIST OF TABLES

LIST OF FIGURES

LIST OF FIGURES - CONTINUED

Figure Page

LIST OF FIGURES - CONTINUED

Figure Page

LIST OF FIGURES - CONTINUED

Figure Page

ABSTRACT

A position sensitive radiation sensor is being designed in conjunction with a field programmable gate array (FPGA) in order to further harden space flight computers against cosmic radiation. The system functionality is such that it requires a stack of PCB's that power and support the radiation sensor. The stacked architecture introduces limitations in terms of mechanical stability that must be addressed.

Mechanical characterization of system electronics must be performed in order to ensure that a new system will not fail under normal operation. This is especially true for systems subjected to harsh environments such as space flight. System level packaging must be employed in order to prevent damaging these systems. Factors such as weight constraints, system architecture, mechanical, and thermal loading must be considered, especially in space applications.

During development of the sensor, different test beds were employed in order to characterize the radiation sensor and it's supporting electronic systems. The most common preliminary tests are high altitude balloon tests which allow the sensor to experience cosmic radiation at high altitudes, consistent with space flight operations.

Each balloon test has mechanical and thermal criteria that must be met in order to survive flight. These criteria include resistance to vibration loading, as well as the ability to maintain system operational temperatures inside a payload as it ascends through the atmosphere. Finite element analysis (FEA) was used to evaluate primary system architecture, system support structures, as well as the flight payload in order to determine if the system would survive preliminary, and future, testing. System level architecture and test payloads were designed using SolidWorks cad software. ANSYS FEA software was used to create thermal models which accurately simulated convective cooling through the atmosphere, and solar radiation loading on the exterior of the payload. Vibration models were performed in order to find the natural frequencies of the subsystem, as well as characterize the response to applied vibrations.

Conclusions from each model show that the system will survive expected test loading at a wide range of vibration frequencies, and maintain a thermally stable environment in order to prevent damage to the internal electronic systems.

1. INTRODUCTION

Radiation and Flight Computers

Flight computers require much more rigorous design and testing than their ground based counterparts. High altitude, and space based environments are subject to a significantly higher dose of solar radiation than that of ground level. The earth's atmosphere absorbs and reflects nearly half of the incoming solar radiation incident to our planet, Figure 1-1. Before this energy is diminished, it hits the outer atmosphere with a magnitude of 1368 W/m^2 (NASA Earth Obsevatory).

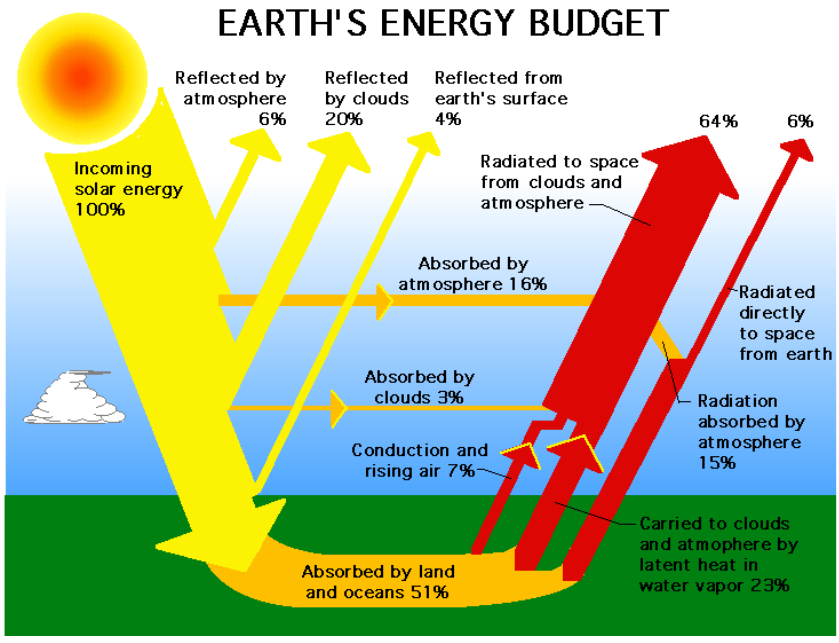

Figure 1-1: Earth energy balance (NASA Earth Obsevatory)

Cosmic radiation has several detrimental effects on digital integrated circuits. These effects come from the physical phenomenon of a high-energy particle passing

through the semiconductor material and creating an ionized electron/hole pair. Ionizing Radiation Transients are radiation strikes that by themselves do not cause permanent damage to the materials in a device but do result in a charge accumulation in the diffusion region of the transistor. The ionizing of the diffusion region causes free charge to be created. If this charge has a large enough magnitude, it will cause the output of the logic circuit to produce a voltage which can be observed as a state change by a receiving gate, causing a program faults.

As a result, space flight computers must be additionally hardened against radiation strikes that can cause faults in their programming. Heavy duty shielding can often be used to help harden electronics against radiation when weight is not an issue. However, most flight applications require a minimal mass design in order to save fuel and improve overall efficiency and maneuverability. Therefore, thick shielding is not the preferred method of radiation hardening when limiting mass is a concern.

In order to mitigate programming faults due to radiation strikes, a combination of redundant systems and repair protocols are used. To that end, a multidisciplinary group of engineering students at MSU has been designing and developing a new radiation tolerant computing (RTC) system that decreases the time needed to repair these electrical systems. By using a position sensitive radiation sensor, targeted repair protocols can be implemented directly to the affected systems once a radiation strike is detected. The sensor detects the potential for Single Event Upsets (SEUs) due to cosmic radiation and feeds the information to a many tiled computing system implemented on a Field Programmable Gate Array (FPGA). The many tiled computer architecture allows for

system redundancy should one or more tiles become compromised by an SEU. These redundancy tiles in the FPGA are identical in size and structure. Each tile contains its own processor and can be partially reconfigured during operation. Based on the information from the radiation sensor, the computer system reconfigures itself into different operating modes including high-performance, low-power, and fault-tolerant. Additionally, if a strike with enough energy to potentially cause a fault is detected, processes can be moved from the affected tile circuitry to another redundant tile's circuitry while the damaged tile is reconfigured to its pre fault state in real time. This system saves time by preemptively beginning repairs on a tile known to have experienced a radiation strike before an actual fault is observed (Buerkle, 2012).

Fault Mitigation System

The final reversion radiation sensor is a multi-channel, double sided silicon chip with aluminum strips that make the channels. The top channels are oriented orthogonally to the bottom channels. This allows the sensor to detect radiation strikes in the X direction with the top channels, and in the Y direction with the bottom channels, as seen in Figure 1-2.

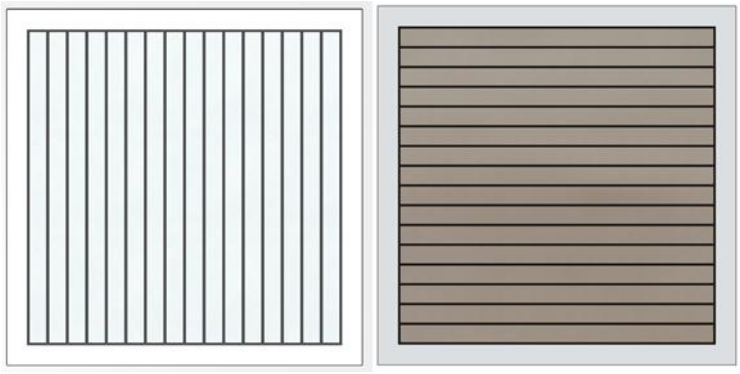

Figure 1-2: Radiation sensor, top and bottom view

As previously discussed, the radiation sensor must be positioned above the circuitry it is helping to protect in order for the system to work. Therefore, stacked system architecture is required for testing and development of this system. The stacked test system architecture uses two packaged sensors stacked above one another, along with an FPGA board to process detection of radiation particles that strike the sensors. A power conversion board sits below the FPGA board to regulate power needed for individual components of the test system, Figure 1-3. A more detailed explanation of the design and fabrication processes of both the radiation sensor and its surrounding circuitry can be found in a design group member, and previous graduate student's thesis (Buerkle, 2012).

The goal of using two stacked sensors is to determine the angle of incidence of a radiation particle as it passes through first the top sensor, and then the bottom one. Another benefit to the stacked design is that the entire assembly has a relatively small footprint, in this case, a four inch square. The small footprint allows for a smaller test payload enclosure which saves space during flight testing.

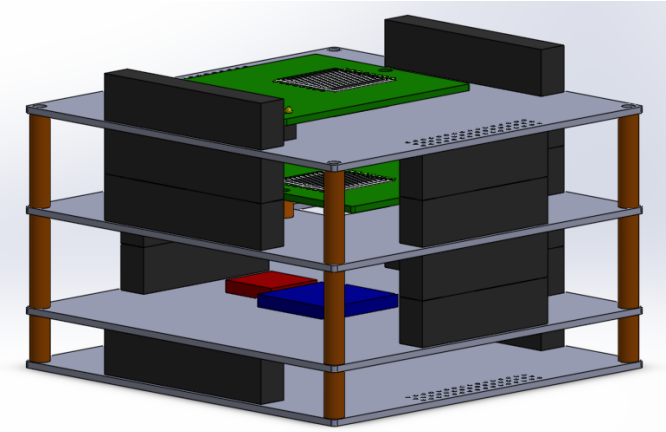

Figure 1-3: Test payload system architecture

Stacked system architecture poses some problems with regards to vibration response. Larger stacks can be prone to failure due to applied mechanical vibrations. Such vibrations can occur especially when the system is employed in test rockets, or other aircraft. Typical sounding rocket launches can result in an excitation frequency ranging from 20 to 2000 Hz (NASA Goddard Space Flight Center, 2005). In order to prevent damage, it was important that each component of the system stack must be properly supported.

Packaging

Damage to printed circuit board (PCB) systems is typically prevented with the use of packaging. Packaging is the use of sturdier materials to encase or support the more fragile systems. This allows the packaging material to take applied stresses away from the fragile materials such as wire bonds/ traces, and thin wires themselves. Packages are usually made of either ceramic, metal, or plastics. Ceramic packaging is made of several layers stacked around a sensitive device to protect it. The individual ceramic layers are held together with epoxy or a strong adhesive. Ceramics have very high strength,

especially in compression and can also protect against radiation depending on the thickness of the packaging. Unfortunately, ceramic packaging adds a considerable amount of weight which is not desirable for aerospace applications. Metal packaging lends strength to the overall structure; however, the metal must be electrically insulated from the rest of the system in order to avoid a short in the circuitry. The high thermal conductivity of metals can also heavily affect the overall operating temperature of the system. Plastic packaging is very versatile and can provide a good balance between strength and weight. Typically, plastic packaging is employed using a plastic ball grid array (PBGA) to surround system devices as seen in Figure 1-4. This ball grid array is then melted to form a solid plastic casing. A major drawback to encasing every system in plastic packaging is that the low thermal conductivity of plastic can often trap heat inside the packaging which can potentially overheat the very system being protected.

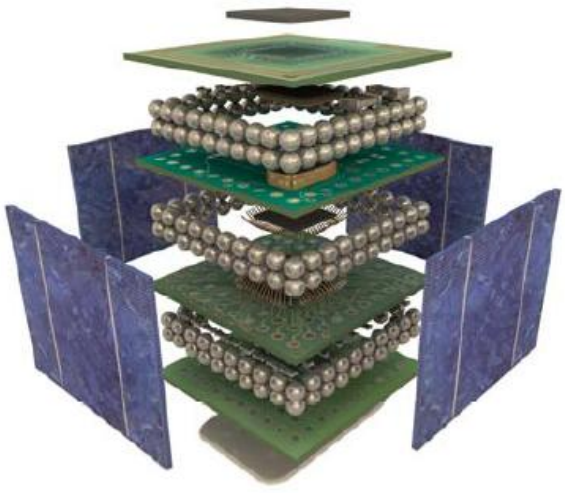

Figure 1-4: Example of stacked packaging using a plastic BGA and outer case material

While the different types of packaging undeniably provide added strength, each is not without their drawbacks, most notably added weight. It is important to note that of

the three different types of packaging discussed; only heavy ceramic packaging can provide protection from radiation. Therefore, flight systems must rely on means other than packaging to protect against harmful radiation strikes.

Development of the position sensitive radiation sensor repair system will greatly aid in the protection against radiation. During flight testing of the system, it was important to ensure that operating temperatures were kept within an acceptable range, as well as to maintain structural integrity.

High Altitude Testing

In order to characterize the radiation sensors response to real world radiation strikes, various high altitude test platforms were employed. While the sensor underwent rigorous laboratory testing initially, it was important to ensure that it would perform as expected in an actual flight environment. To that end, two different types of high altitude balloon tests were utilized. Each balloon test consisted of a large balloon attached to several test payloads of various projects.

The first type of balloon test was the Balloon Outreach, Research, Exploration, and Landscape Imaging System (BOREALIS) test sponsored by the Montana Space Grant Consortium (MSGC). This test consisted of a large atmospheric weather balloon that carried a string of test payloads up to an altitude of just below 100,000 ft. The typical BOREALIS configuration can be seen in Figure 1-5.

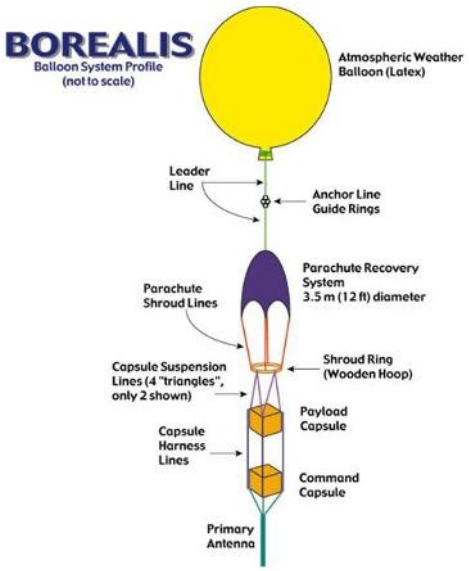

Figure 1-5: BOREALIS configuration (Montana Space Grant Consortium, 2011)

Each BOREALIS flight typically ascends to its maximum altitude at a nearly constant rate of roughly 5m/s. Once the maximum altitude is reached, the external pressure acting on the weather balloon is reduced so much that it causes the balloon to burst. Once the balloon bursts, string of payloads falls until the air is dense enough to deploy the parachute recovery system. With the parachute deployed, the test payloads descend back to earth at a speed of around 7m/s. After landing, the payloads are collected and the data is retrieved. Typically, the total balloon flight time is around two hours.

The second type of high altitude balloon testing was the NASA/LSU High Altitude Balloon Student Program (HASP). This test procedure lasts much longer than that of BOREALIS, and as such, is subject to a much harsher thermal environment. The HASP platform is a large framework suspended below a huge zero pressure balloon. The test frame is designed to carry up to twelve student payloads to a maximum altitude of

roughly 36 kilometers or 120,000 feet. This maximum altitude is reached at a climb rate of about 1000 feet per minute, or 5 m/s. This is nearly exactly the same climb rate as that of the BOREALIS test platform. The duration of the flight time can last anywhere between 15 and 20 hours. The HASP framework includes a standard mechanical, power and communications interface for all student payloads to connect with. The fully assembled HASP frame with attached student payloads can be seen in Figure 1-6.

Figure 1-6: Suspended HASP frame and payloads (LSU Department of Physics and Astronomy, 2012).

Once the HASP test frame is launched, it takes around two hours to reach its maximum float altitude. Once maximum altitude was reached, the balloon floats for roughly ten hours while the various payloads conduct tests. After 18 hours of total flight time, the balloon is released from the flight frame. Then the flight frame free falls down

to around 90,000 feet where the parachute deploys, and begins to slow the decent. From there, the entire apparatus floats down to earth in just under an hour.

High altitude testing, along with preliminary on the ground lab tests were instrumental in early development of radiation sensor development.

2. BACKGROUND

The following contains basic background information on the design process, and testing of the radiation sensor, the techniques used in testing, as well as an overview of the thermal and mechanical environments of various test rigs and the engineering theories behind the design process.

Laboratory Sensor Testing

During early sensor development, preliminary testing was performed in a laboratory in order to ensure that the sensor was responding to radiation stimulus. Laboratory testing was used first in order to ensure that only quality sensors were sent up in the following balloon tests. Laboratory testing began with the use of an infra-red laser aimed at various positions on the sensor. After the infra-red testing, new sensors were taken to a lab with krypton radiation particles that were shot at the sensor, again in various locations to ensure that the sensor was reading radiation strikes with positional accuracy.

Balloon Test Thermal Environments

BOREALIS

Due to the inherently short flight time of the BOREALIS payload, the thermal requirements were a bit different than those of the HASP test. Since the BOREALIS payload never stopped changing in altitude, its heat transfer treatment was entirely in the transient regime. As the balloon rose in altitude, the test payload was exposed to varying

ambient conditions. The ambient temperature is important as it affects the amount of heat lost to convection from the outside of the payload structure. Because the ambient temperature was always at or below the internal temperature of the payload, the structure would be continuously cooled through convection heat transfer into the atmosphere. Another way the payload was being cooled is through radiation heat transfer. The payload sides would radiate heat out to any cooler surface, or to space itself. However, radiation heat transfer would also bring heat into the payload. The major source of incoming radiation was due to the sun. As previously discussed, the incoming solar radiation at lower altitudes is much less than that of higher altitudes. Obviously Incoming solar radiation is at its maximum outside earth's protective atmosphere. A small portion of solar energy would also be reflected back up from the earth towards the payload. In addition to the thermal energy hitting the payload, the radiation sensor and its surrounding electrical systems generated their own heat from inside the test payload. The stacked system architecture generated a combined heat rate of 7 W throughout the structure continuously. This high heat generation rate meant that the test payload was being heated by both internal and external sources simultaneously. The thermal energy balance for the payload can be seen in Figure 2-1, where Q denotes thermal energy transfer. While heat is transferred through all of the exterior surfaces of the payload, only the total heat transfer for each mode of transfer is shown in the energy balance figure.

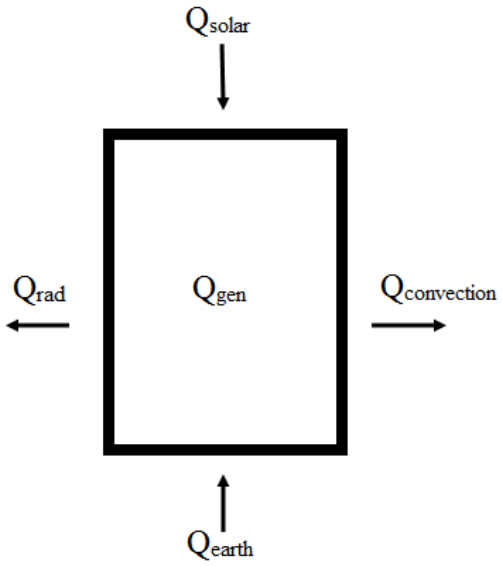

Figure 2-1: Balloon test payload energy balance

HASP

The HASP test payload and RTC systems were designed and fabricated to be exactly the same as each other. This was done in order to streamline the design and fabrication processes. The HASP test conditions were very similar to the BOREALIS conditions during the ascent and descent portions of the flights. This was due to both tests having a nearly identical ascent speed and maximum altitudes that were fairly close. The major difference in the HASP flight occurred during the 10 hour period where the HASP structure maintained its maximum altitude of 120,000 feet. While the thermal energy balance of the test payload looked the same as the BOREALIS one shown in Figure 2-1, the time spent at maximum altitude had some significant effects on the thermal energy transfer from radiation and convection. At maximum altitude, the heat transfer due to conduction was completely negligible because of the extremely thin atmosphere. This meant that there was no cooling effect through convection during the

majority of the HASP flight. While convection heat transfer becomes minimal at altitude, the amount of thermal energy from solar radiation is maximized. With little to no atmosphere present, none of the incoming solar energy would be absorbed or reflected, allowing all of the solar radiation to hit the test payload uninhibited.

Positional Effects on Incident Solar Radiation

Many variables affect just how much solar energy would in fact be transferred to the payload itself. Time of day, time of year, as well as which way the payload walls faced all had an effect on the intensity of incident radiation applied to the payload. This is due to the tilt of the earth as it orbits the sun. The effect on the amount of incident solar radiation at a specific time of year is illustrated best by Figure 2-2 comparing the summer and winter solstices.

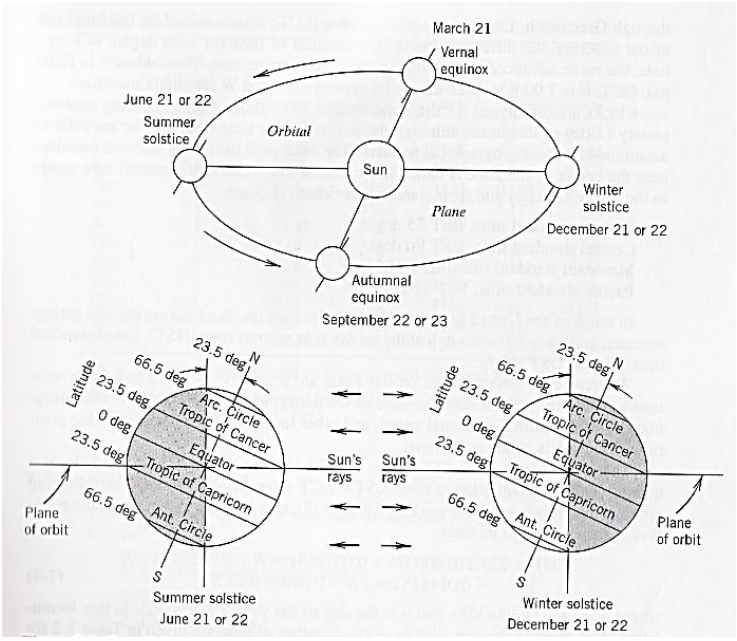

Figure 2-2: The effect of the earth's tilt and rotation about the sun (McQuiston, Parker, & Spitler, 2005)

The time of day also has a significant impact on solar radiation. The time of day helps determine the angle of the sun's rays incident to the earth. This solar altitude angle, or beta angle, can then be used in order to determine the angle of incidence on a given object. In order to apply a time of day towards determining the solar beta angle, a standard way of measuring time at any position on the earth must be used. This standard measurement is called local solar time (LST) and it is found using two additional values.

The first factor is known as the local civil time (LCT) and is determined by the longitude of the observer as seen in Equation 2-1 where Local Standard Time is simply the local time as seen on a clock, L_L is the location longitude, and L_S is the standard meridian (longitude) of the location's time zone. Standard meridians for the four time zones in the lower 48 states are shown in Table 2-1.

$$LCT = Local\ Standard\ Time - (L_L - L_S) * \left(\frac{4\ min}{\deg W}\right) \qquad \text{Equation 2-1}$$

Table 2-1: Standard meridians for US time zones

TIME ZONE	CENTRAL STANDARD LATTITUDE (L_S)
Eastern Standard Time, EST	75 deg W
Central Standard Time, CST	90 deg W
Mountain Standard Time, MST	105 deg W
Pacific Standard Time, PST	120 deg W

The second factor used in calculating the local solar time is called the equation of time, or EOT. The EOT is a numerical relationship developed in order to determine the LST from the LCT and is shown in Equation 2-2

$$\begin{aligned} \text{EOT} = 229.2 * ((&0.000075 + 0.001868 * \cos(\text{N}) \\ &- 0.032077 * \sin(\text{N}) - 0.014615 \\ &* \cos(2\text{N}) - 0.04089 * \sin(2\text{N})) \end{aligned} \qquad \text{Equation 2-2}$$

where N is the angle of the earth's rotation around the sun at the given day in degrees. N can quickly be calculated using the numeric day of the year, d_n, and Equation 2-3.

$$N = \left[(d_n - 1) * \left(\frac{360\ deg}{365}\right)\right] \qquad \text{Equation 2-3}$$

Finally the local solar time can be calculated using Equation 2-4 in order to get the hour angle, h, as seen in Figure 2-3.

$$\text{LST} = \text{LCT} + \text{EOT} \qquad \text{Equation 2-4}$$

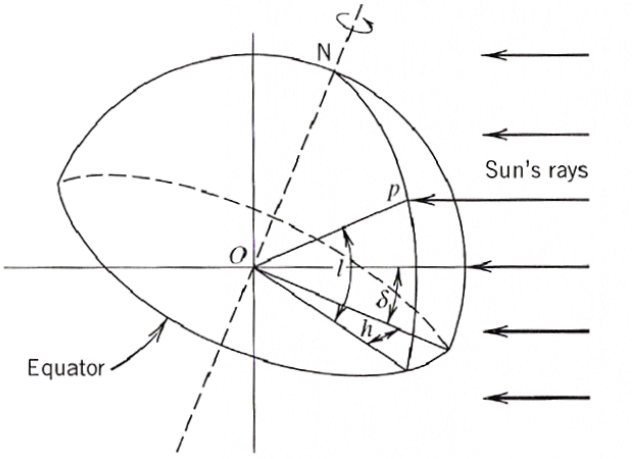

Figure 2-3: Latitude l, hour angle h, and sun's declination δ (McQuiston, Parker, & Spitler, 2005)

Lastly, the angle of incidence, the angle between the normal vector of a surface, known as the surface azimuth, and the solar altitude angle, β, has an effect on how much radiation energy is transferred due to radiation. The angle of incidence, θ, is used to determine the radiation form factor, a coefficient ranging between 0 and 1 that factors how much of the total incoming radiation actually is incident on a surface at a given angle. In order to calculate the angle of incidence the surface solar azimuth must also be known. Figure 2-4 shows the surface solar azimuth γ, the solar altitude angle β, the surface azimuth ψ, and the tilt angle α for an arbitrary surface. Detailed calculations of all the relevant angles and the resulting radiation form factors for each face of the payload can be seen in APPENDIX A.

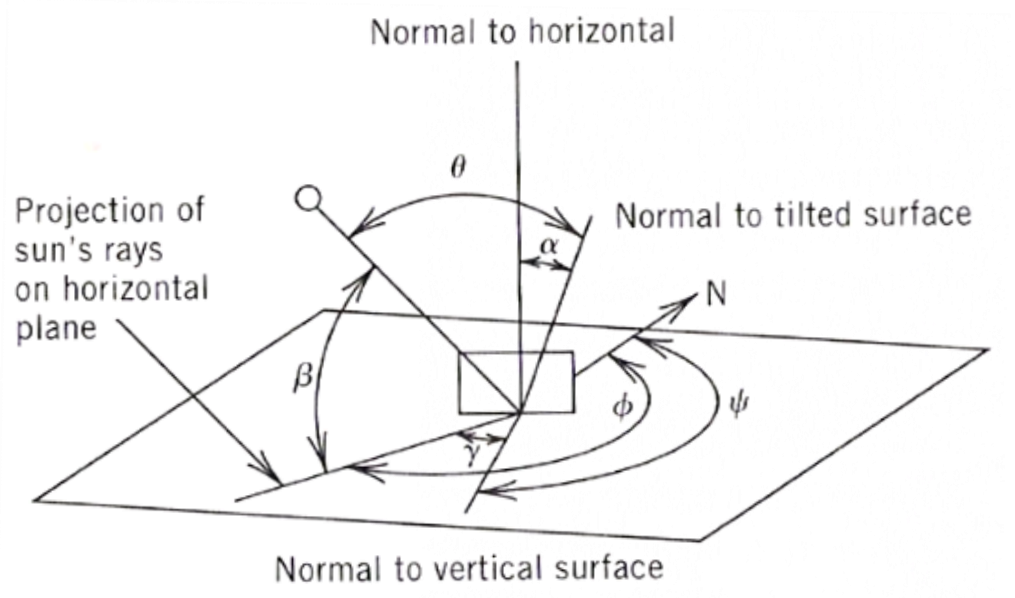

Figure 2-4: Relevant solar and position angles for an arbitrary surface (McQuiston, Parker, & Spitler, 2005)

Test Payload Physical Structure

As previously stated, the same test payload would be used for both the BOREALIS and HASP tests. In order to integrate with the larger HASP frame that supported the various test payloads, several requirements needed to be met. These requirements included a maximum height and footprint of the payload, as well as a mass limit and are shown in Table 2-2 (LSU Space Sciences Group, 2009).

Table 2-2: HASP mechanical requirements

Mass	Footprint	Height
3 kg	15 cm x 15 cm	30 cm

A mechanical interface mounting plate for the payload was also provided for HASP. The mounting plate was made of 1/4" thick PVC material and includes areas strictly to be used for mounting the plate to the frame of the HASP structure, and a middle section for the test payload to be mounted to, as seen in Figure 2-5.

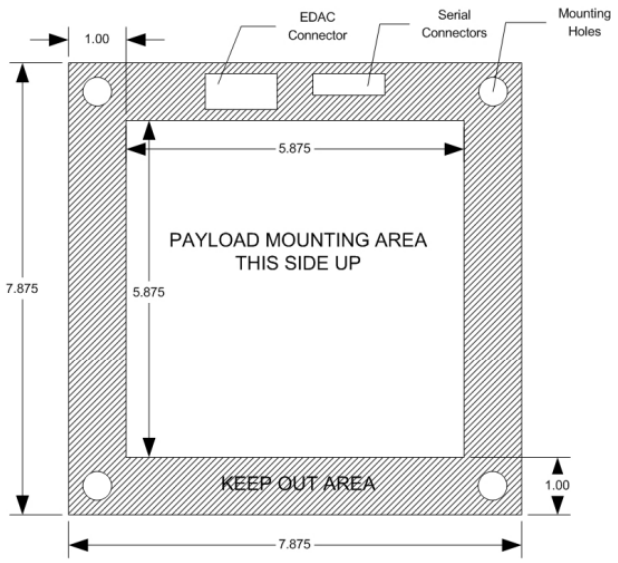

Figure 2-5: Small payload mechanical interface plate. All dimensions are in inches

The basic design for the test payload was based off legacy designs for the BOREALIS payloads. This structure was essentially made out of a foam insulation box that would enclose whatever system was being tested at altitude. While outer dimensions would be controlled by the guidelines set by the HASP interface requirements, features such as insulation thickness as well as material selection and internal systems placement would need to be considered. The insulation used would simply be polystyrene foam insulation readily available at most hardware stores. An outer layer of fiberglass was added in order to provide structural strength against any inertial loads during flight. The final version of the proposed payload design can be seen in Figure 2-6, where the front two panels of insulation have been made transparent to better show the internal RTC system.

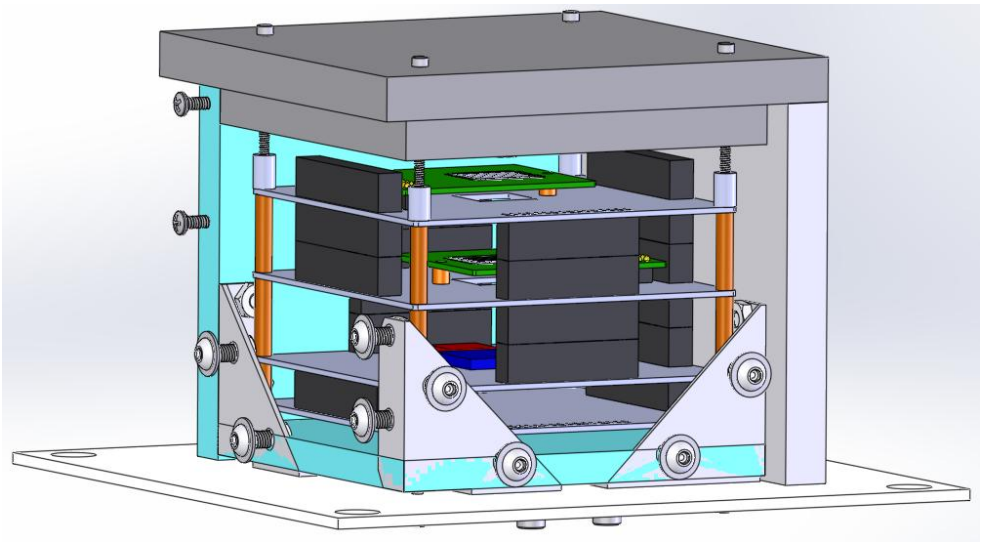

Figure 2-6: HASP test payload model (final revision)

The final internal system sent up in the HASP test ended up using only one sensor instead of two stacked over each other. This was done in order to simplify the computing

system, as a result of only one of the FPGA boards working correctly at the time of launch.

Heat Transfer Theory

Thermal energy transfer, or heat transfer, is a very important consideration in mechanical design. Generally, heat transfer occurs when there is a temperature gradient, thus causing thermal energy to flow from high temperature regions to lower ones. Heat transfer occurs through three different processes, or modes. These three modes are conduction, convection, and radiation.

Conduction

Conduction is the transfer of thermal energy from more energetic to less energetic particles of a substance due to interactions between the substances' molecular and atomic particles. This mode of heat transfer allows thermal energy to travel from higher temperature regions to lower temperature regions within a substance. While heat conduction can occur in a solid, liquid or a gas, it is most prevalent in solids. With regards towards radiation sensor development, conduction is the mode of heat transfer that allows for thermal energy to be transferred through the solid matter of the sensor test payload as well as the system hardware itself. The rate at which heat is transferred by conduction is defined by Fourier's Law and is expressed, for steady state conduction, by the following equation.

$$q'' = -k\left(i\frac{\partial T}{\partial x} + j\frac{\partial T}{\partial y} + k\frac{\partial T}{\partial z}\right) \qquad \text{Equation 2-5}$$

Where q" [W/m^2] is the heat flux, k [W/m*°K] is the thermal conductivity of the material, and T [°K] is the temperature (Incropera, Dewitt, Bergman, & Lavine, 2007). The thermal conductivity is an inherent material property and can easily be found for common materials. Composite materials, such as printed circuit boards which are made of a fiber glass and epoxy composite, will have two separate materials with two separate thermal conductivities. In the event of a composite material, often the bulk thermal conductivity must be found either experimentally, or by using a rule of mixtures. Fortunately, many common composite materials, such as FR4, have been tested by the manufacturer for many of their thermo-physical properties, including thermal conductivity. In many cases, Equation 2-5 can be simplified into a one or two dimensional equation in order to simplify analysis. This is possible if it is known that there is negligible heat transfer in a given direction.

Convection

The second form of heat transfer is convection, which is based on motion. Convection heat transfer can occur due to random molecular motion known as diffusion, or the motion of a bulk fluid or gas. Diffusion based convection occurs when a fluid is moving very slowly, or not at all. This can occur in enclosed spaces with minimal ventilation. Bulk fluid convection heat transfer can occur due to either forced convection, or free convection. Forced convection occurs when the fluid or gas flow is caused by external means, such as a fan, pump, or atmospheric winds. Another example of forced convection is if an object is moving through the air, such as a car driving down the road. This is mathematically treated the same as if the car was stationary and wind

was flowing over it at the same speed. Free convection refers to flow that is induced by buoyant forces caused by temperature gradients in a fluid. This temperature gradient often causes density variations in the fluid, which causes less dense fluids to rise above denser or colder ones. This rise and fall of fluids at different densities causes heat transfer as higher temperature fluids bring thermal energy to colder ones. While forced and free convection can occur independently, it is important to note that both can occur simultaneously. Heat transfer due to convection is described by Newton's Law of Cooling,

$$q_{conv}" = h\Delta T \qquad \text{Equation 2-6}$$

where q_{conv}" [W/m^2] is the convective heat flux at the surface, h [W/m^2°K] is the convection coefficient between a surface and the convective fluid, and ΔT is the temperature difference between the surface and that of the convective fluid (Incropera, Dewitt, Bergman, & Lavine, 2007).

Convection heat transfer was initially relevant during the BOREALIS high altitude test because most of the flight time was in atmosphere, with very little time spent at maximum altitude. This meant that, for most of the flight, the test payload was exposed to heat loss from convection to the atmosphere. As the test payload rose in altitude, the surrounding air decreased in temperature. Eventually, the surrounding air starts to heat back up due to the increase in solar heating. In order to get a good approximation of the surrounding atmosphere as the payload ascends, a mathematical

model was used. The model predicts the temperature, pressure, and density of air at different altitudes, and can be seen in Figure 2-7.

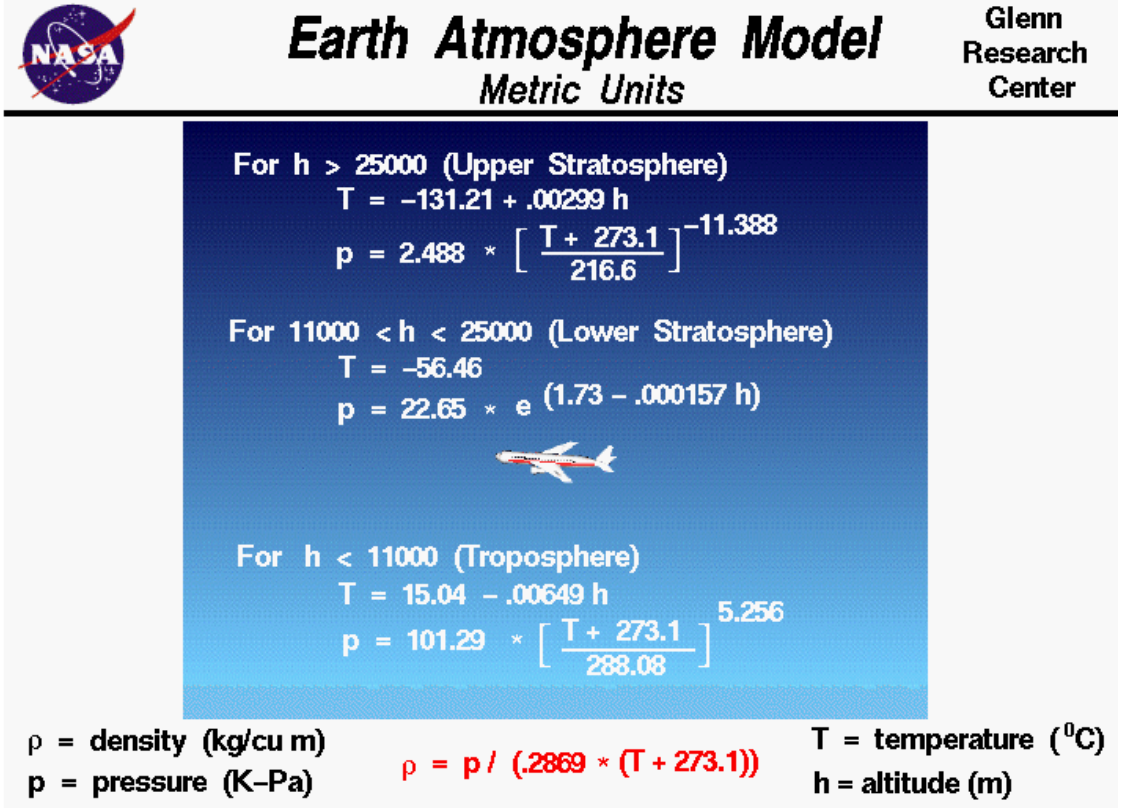

Figure 2-7: Earth atmosphere model, (Benson, 2010)

Using the mathematical model, the atmospheric temperature with respect to altitude was plotted in order to compare the temperatures with the altitudes reached by the BOREALIS test payload. As can be seen in Figure 2-8, the most extreme temperature conditions occur during the middle portion of the flight.

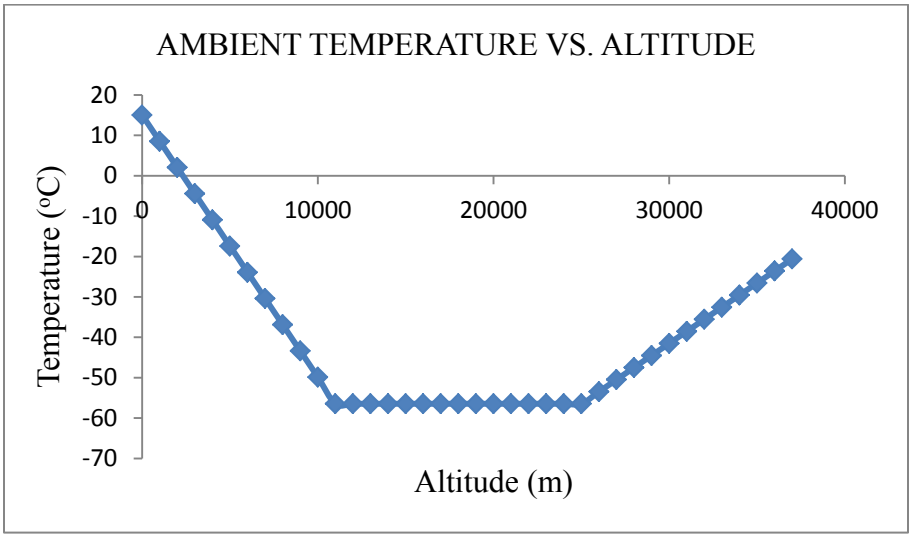

Figure 2-8: Atmospheric temperature vs. altitude

Another important property of a convection fluid, in this case air, is the viscosity. In order to obtain the viscosity of air with respect to altitude, Southerland's Formula was used. Southerland's Formula relates viscosity to temperature,

$$\mu = \mu_o * \frac{T_o + C}{T + C}\left(\frac{T}{T_o}\right)^{3/2} \qquad \text{Equation 2-7}$$

where μ [Pa*s] is the dynamic viscosity of air at altitude, μ_o [Pa*s] is a known reference viscosity usually taken at sea level, T [°K] is air temperature at altitude, T_o [°K] is a known reference temperature taken at the same altitude as the reference viscosity, and C[°K] is the Southerland's temperature constant for a given material. As viscosity is temperature dependent, it depends on altitude in the same fashion. Again, the minimum viscosity levels correspond with the minimum temperature values throughout the atmosphere. The viscosity of air was important in obtaining certain flow characteristics for convection calculations. Most importantly, the viscosity was used to determine the

Reynolds number of the flow. This was made fairly simple as the test platforms ascended at a nearly constant rate. Therefore, the only changing variables were viscosity and density. Initially, the side walls of the test payload were modeled as parallel flow over a flat plate. In order to perform the analysis, the Reynolds number had to be calculated in order to define the flow regime, determine the Nusselt number, and the corresponding convection coefficient. The flow regime refers to a flow being laminar or turbulent along its path. It is important to know whether the fluid flow is turbulent or laminar as it affects how the Nusselt number relates to the convection coefficient. Depending on the conditions, both laminar and turbulent flow can exist along the length of the payload wall. Turbulence is defined by a critical Reynolds number; in this case, the transition Reynolds number is $5*10^5$. As long as the maximum Reynolds number was below $5*10^5$, the flow would be laminar. This was found using Equation 2-8 where Re_{max} is the maximum Reynolds number for the given flow, ρ [kg/m3] is the density of the air, V [m/s] air flow velocity, L [m] is the length of the payload wall, and μ_{min} [Pa*s] is the minimum dynamic viscosity of the air travelled through (Incropera, Dewitt, Bergman, & Lavine, 2007).

$$Re_{max} = \frac{\rho V L}{\mu_{min}} \qquad \text{Equation 2-8}$$

Due to the low density and velocity of the test platforms, the flow regime was determined to be entirely laminar over the full length of the payload wall. Therefore, a strictly laminar correlation could be used over the entire length of the structure. A more detailed development of the convection model can be seen in APPENDIX B.

It is important to note that convection heat transfer does not play a significant role in high altitude tests such as HASP because so little of the overall flight time is spent in atmosphere. At maximum altitude, the air is so thin that there simply is not enough fluid substance for significant convection to occur. This can clearly be seen in Figure 2-9, where air density is plotted with respect to altitude. At only 30,000 meters the air density is down to roughly 1.4% of its density at sea level. The minimal effect of convection can most easily be seen by examining Equation 2-6, and noting that the convective coefficient, h, and the temperature gradient, ΔT, are relatively small.

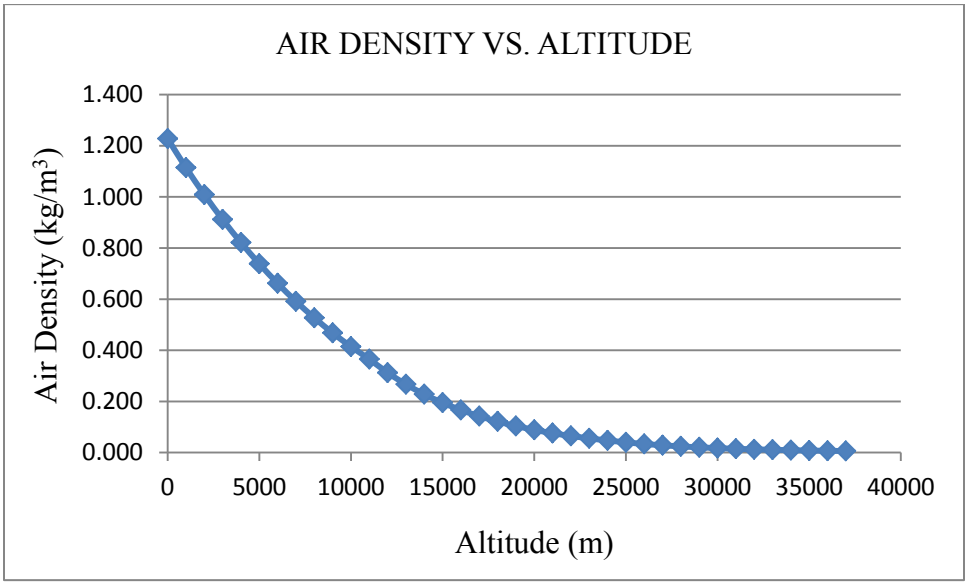

Figure 2-9: Air density with respect to altitude

Radiation

The third form of heat transfer is radiation. Radiation heat transfer is the process of thermal energy being emitted by matter that is at a nonzero temperature. This emission of thermal energy is independent of matter, and may be attributed to changes in

the electron configurations of the matters atoms or molecules. Radiation energy is the only form of heat transfer that occurs independently of a material medium, and is instead transferred by electromagnetic waves, or photons. In fact, radiation heat transfer actually occurs most efficiently in a vacuum (Incropera, Dewitt, Bergman, & Lavine, 2007). For this reason, it is easy to see how radiation heat transfer plays such an important role in space applications.

The total amount of thermal energy emitted by a surface is given in Equation 2-9

$$E = \varepsilon\sigma {T_s}^4 \qquad \text{Equation 2-9}$$

where T_s is the absolute temperature (K) of the surface, σ is the Stefan-Boltzmann constant (σ = 5.67*10-8 W/m^2*K^4), and ε is a surface radiative property called emissivity. Emissivity gives a measure of how well a surface can emit thermal energy relative to an ideal or black body. The values can range from 0 to 1.

If radiation heat transfer is occurring between a small surface at T_s and a much larger isothermal surface or surroundings at T_{sur}, then the net rate of radiation heat flux from the surface can be expressed as the following.

$$E = \varepsilon\sigma\left({T_s}^4 - {T_{sur}}^4\right) \qquad \text{Equation 2-10}$$

Radiation heat transfer can also occur due to incident radiation on a surface from the surface's surroundings. It is important to note that not all of the incoming irradiation, G, is absorbed into the surface. Instead, the irradiation absorbed by the surface G_{abs}, is

limited by its absorptivity, another surface radiative property also ranging from 0 to 1, and is given by

$$G_{abs} = \alpha G \qquad \text{Equation 2-11}$$

Absorptivity and emissivity of a material are two very important factors in determining how much thermal energy a surface will absorb, and how much it will emit. Both of these factors were heavily considered in test payload material selection and design.

Finite Element Analysis

The finite element analysis software used in this project was ANSYS v. 13, both the classic APDL version as well as Workbench. Finite element analysis (FEA) is a numerical computation technique commonly used in the engineering design process. The solution process uses known boundary conditions along with characteristic differential equations, which are dependent on the physics of each particular problem, in order to numerically solve for dependent field variables, such as temperature, everywhere in a known domain of independent variables (Hutton, 2004). Boundary conditions are specified values of the dependent field variables at a given location. For example, a common boundary condition for structural analyses could be a specified displacement at certain boundaries of the structure. Usually boundaries such as fixed ends of support structures can be said to have zero displacements. The independent domain variables usually consist of known constitutive properties such as the modulus of elasticity or thermal conductivity of a material. Although numerical solution techniques can be very accurate, it is important to note that the results obtained are close approximations, not

100% exact results. As long as the finite element solution method is used properly, it can be an extremely powerful tool in the engineering design process.

FEA Solution Process

In order to obtain a solution, FEA first discretizes the body being analyzed in a process called meshing. This refers to dividing the known domain into many finite elements with points, or nodes, at each of its vertices. Each node represents a specific point in the field where the value of each specific field variable is calculated. Many elements include additional nodes located along border lines in between the vertex nodes. Elements come in a huge variety of shapes and sizes and can have as little as two nodes, or upwards of 20. One of the most basic element types is a simple line element. Line elements are often used to represent beams or trusses in structural analyses. Two dimensional area elements, used for surfaces or planar problems, as well as three dimensional volume elements used for representing various solid structures also exist. An example of a basic 8 node brick element, a type of volume element, can be shown in Figure 2-10.

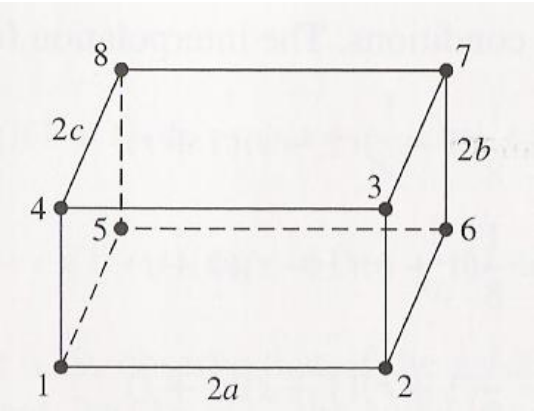

Figure 2-10: 8 node brick element (Hutton, 2004)

Adjacent finite elements share common nodes along their boundaries. This allows for continuity between the nodes, and therefore, across the entire body of elements. It is important to note that the more nodes in a model, the more simultaneous equations the software must solve. Because of this, there are limitations on the number of nodes available for use in most FEA software. With a limited number of nodes and elements, one must make sure that the geometry being analyzed is not overly complicated. Complex geometries always require more elements to represent than simple ones, and therefore take a longer time to solve. One cannot simply model an exact representation of a complex assembly in FEA software and expect to solve an analysis. Strategies such as geometry simplification, and or the use of sub models are often necessary. Sub models are simply substructures, or separate components, of an entire assembly. If detailed analysis of a complex part is desired, it is often beneficial to try and figure out the boundary conditions of the substructure in order to run a separate analysis on it.

Meshing

Meshing is a complex process with many different strategies to help ensure solution accuracy. As previously mentioned, meshing discretizes a body in order to reduce an infinite dimensional problem to a finite dimensional one. Meshing begins with element selection. Current FEA software employs a huge variety of element types with varying behaviors and degrees of freedom. Therefore, careful element type selection is a very important step, as the elements used will help define the analysis. It is important to

use elements that represent the behavior of the physical body being analyzed. For example, if a thermal analysis is being performed, thermal elements with a single temperature degree of freedom should be selected. This allows the software to specifically solve for temperatures throughout the body. Other elements can be used with varying degrees of freedom to include structural effects, magnetic or electric field effects, fluid flow effects, and special surface effects such as contact between surfaces, to name a few.

Often it is necessary to alter the elements after an initial mesh has been performed. Element size, shape, and density have a significant effect on solution accuracy. The geometry where the elements are placed also plays an important role. If the geometry is complex in shape, then the elements must be adjusted to accurately reflect that complexity. For example, when meshing circular entities, each curve is often made from many small straight edge elements that approximate the curvature as seen in Figure 2-11.

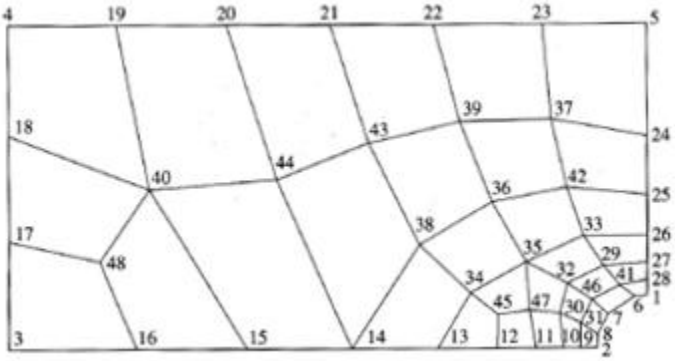

Figure 2-11: Coarse mesh using quadrilateral elements on a curved feature. (Hutton, 2004)

As a result, elements representing curvature need to be very small in order to accurately represent a curved structure. The process of making elements smaller in order to more accurately represent complex geometries is known as mesh refinement. A mesh refinement process for the geometry shown in Figure 2-11 can be seen in Figure 2-12.

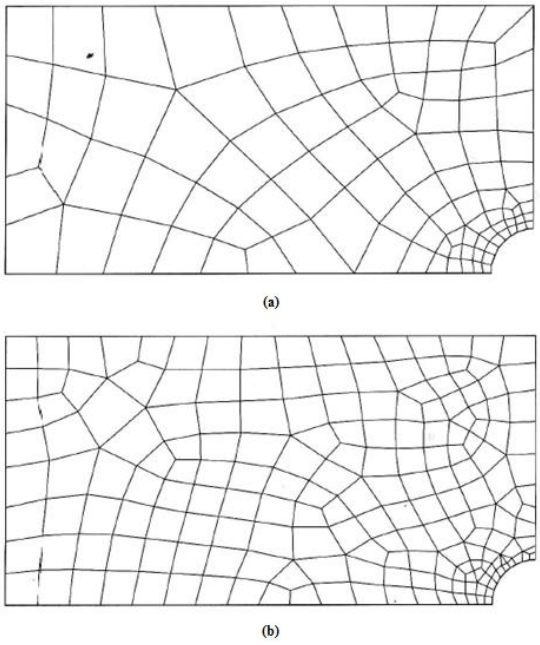

Figure 2-12: (a) First level mesh refinement on curvature. (b) Additional mesh refinement on curvature

An alternative to using many quadrilateral elements to represent curvature is to use a higher order element. A higher order element is an element with more nodes than vertices. This usually means that there are mid-side nodes in between the vertex nodes. These mid-side nodes can allow for curvature along element boundaries. A higher order version of the brick element in Figure 2-10 can be seen in Figure 2-13. Node displacement for this higher order element exhibit quadratic behavior instead of a linear one. This is what allows the element edges be curved, however, the quadratic behavior

further increases the complexity of the constituent equations relating each node to one another. Another drawback with the use of higher order elements is the drastic increase in the total amount of nodes used in a model. It is usually customary to only use these high order elements in small portions of the geometry where they are absolutely necessary.

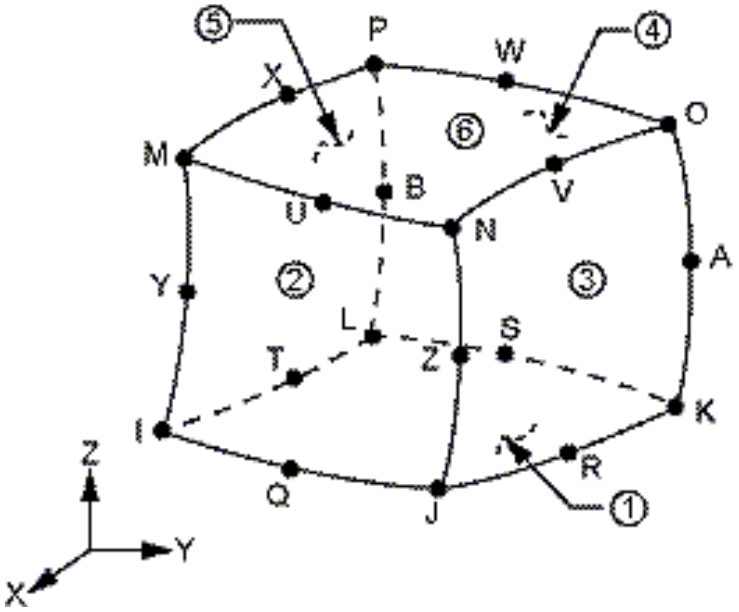

Figure 2-13: 20 node solid element

Advantages of FEA

FEA is extremely useful for design purposes as it provides accurate results along with a high level of flexibility with regards to changes made in an analysis. The use of FEA software can greatly help reduce the costs during a design process. It allows for the testing and improvement of various designs. Conventional destructive testing can often be both costly and time consuming. With FEA software, many different variations of a

structure, or substructure, can be tested in a variety of different ways. Instead of fabricating new parts and continuously physically testing them, changes can simply be made by editing part files. With care, the use of input codes can be parameterized in order for quick and easy changes with a few keystrokes. Aside from geometry and component changes, FEA can also be used to help with material selection for various parts. Again, changing various material properties can be done by simply altering input codes. With complex structures made of a large variety of materials, the use of FEA can be invaluable in testing how changes of material properties or part configuration affect the overall design.

3. VIBRATION ANALYSIS

While much of the design of the electronic systems surrounding the radiation sensor were constrained primarily by electrical requirements such as power requirements and electrical conductivity, several important mechanical requirements also had to be addressed. As this radiation tolerant computing (RTC) system was still in early stages of development and testing, many structural loading environments are unknown except for those of the high altitude balloon tests. Obviously failure of materials was a concern, as well as thermal concerns. However, without knowing the types of future test vehicles used in further evaluation of the system, the applied vibration loading was unknown.

FEA Analyses

The main goal of the vibration analyses was to lay the groundwork for continued vibration studies applied toward various future test vehicles for the radiation tolerant computing system. The most important result desired was to obtain the natural frequencies of the support structure so that these natural frequencies could be avoided when used in future test platforms. As previously discussed, using an all-inclusive detailed assembly of the entire test payload was impossible. The many holes, interconnect pins, and other tiny features in the components were just too complex to be meshed in the software (recall Figure 1-3.) Both geometry simplification and sub-modeling techniques were employed. Depending on the analysis, several different models and sub models were used.

Geometry Treatment

As the radiation sensor was the most critical and fragile component of the system, a sub model was used for just the sensor and its immediately surrounding package board and amp board. This sub model can be seen in Figure 3-1, where the sensor is the gray component in the center of the green package board. Below the package board is the gray signal amplification (AMP) board. As previously mentioned, specific vibrational loading was unknown at the time of analysis. To that end, a model was created that could be easily edited to represent a variety of loading scenarios.

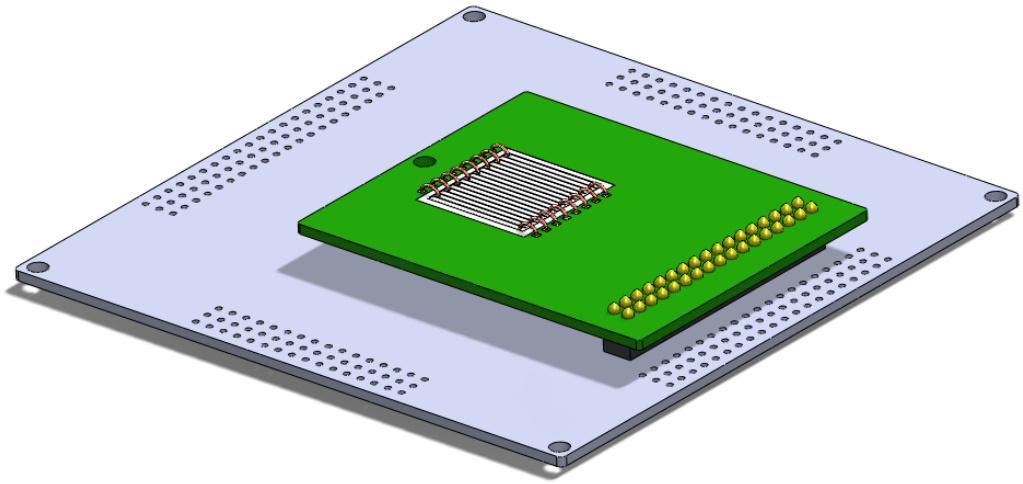

Figure 3-1: Radiation sensor, package board, and amplification board assy.

Starting with the sub model shown in Figure 3-1, geometry simplification was done in order to decrease the complexity of the parts, and therefore limit the maximum amount of nodes and elements used in the FEA software. The first thing done was to eliminate all of the small holes along the edges of the amp board. These holes were merely for interconnection pieces to stack different system boards on top of each other. The next feature to be removed was the thin copper wires (center of Figure 3-1)

connecting the sensor channels to the package board contact pads. These thin wire traces did not provide any real structural integrity as the sensor was held in place by a thin layer of epoxy. Lastly, the use of symmetry was employed. The only viable symmetry plane in the design passes directly through the center of the sensor and runs longitudinally with the package board. The end result of geometry simplification can be seen below in Figure 3-2, and is the sub-model that all further vibration analyses were modeled after.

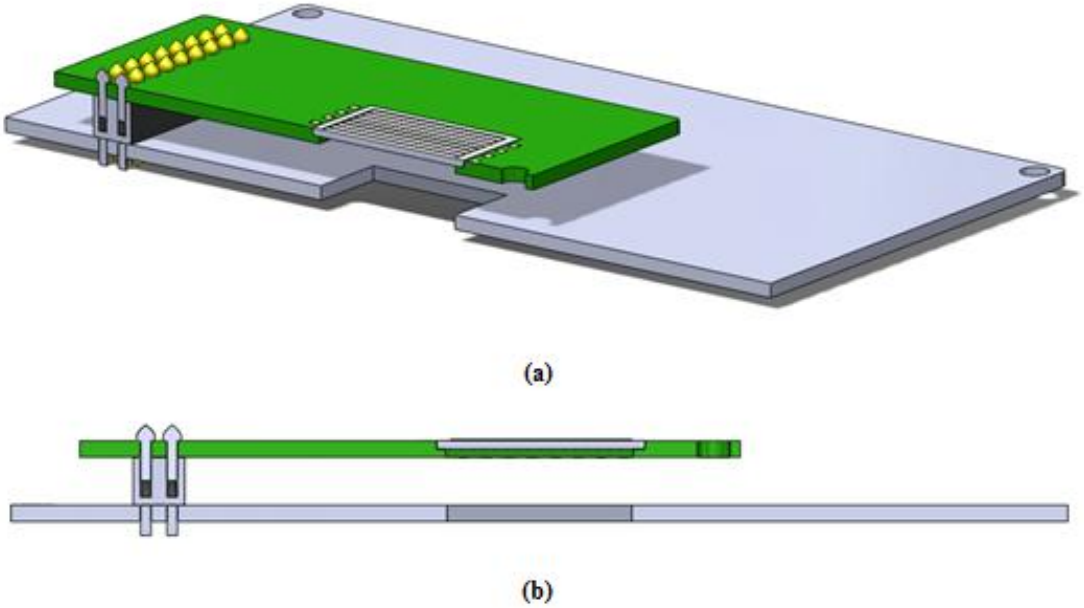

Figure 3-2: (a) Simplified sensor, package, and amp assy.
(b) Symmetry plane view

Two Dimensional Model

Initially, a very simple two dimensional model was used in a modal analysis for the sub-model shown in Figure 3-2 (b). This was done by outlining every geometric feature on the symmetry plane and using that as a two dimensional outline for the analysis structure. As a two dimensional model was fairly small, the cross section of the

copper wires, as well as the epoxy holding them in place was included in the geometry. The two dimensional geometry was modeled from the bottom up. This means that input the input code used keypoints to define corners of all the two dimensional areas. Next, lines were drawn to connect each keypoint. Lastly, areas were generated from the lines. The input code for geometry, as well as the rest of the analysis can be seen in APPENDIX C. The purpose of this two dimensional model was simply to help identify mode shapes for the sub-assembly. Mode one was of particular interest because it should be the most comparable with the three dimensional modal results.

Element Selection and Meshing: Once the geometry was modeled it had to be meshed into finite elements. For this analysis, a higher order two dimensional plane element was chosen called PLANE183. Although the use of a higher order element added more nodes to the analysis, it also reduced the necessary number of elements needed to accurately represent flexure deformation throughout the structure. PLANE183 elements can be either an 8 node quadrilateral element, or a 6 node triangular element, and both exhibit quadratic displacement behavior. Each node has two degrees of freedom which are translations in the nodal x and y directions (ANSYS, Inc., 2011). The geometry, node locations and element coordinate system can be seen in Figure 3-3.

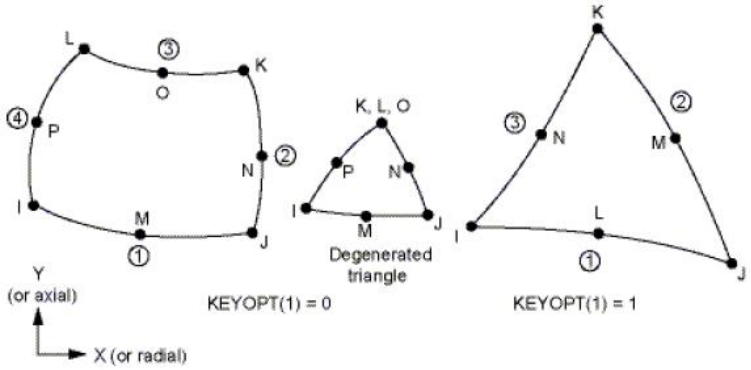

Figure 3-3: PLANE183 geometry and node locations

With the element selected, the model was then meshed. Initially a coarse mesh was used to quickly ensure the model was behaving as expected. Once the model yielded initial results, a mesh refinement process was used to ensure accuracy.

Mesh Refinement: Once the simulation appeared to be running properly, the process of mesh refinement was begun. While overall element sizing was reduced, targeted mesh refinement was also performed. This was done by selecting and meshing important areas such as the sensor, epoxy, copper wires, and interconnection pins first and at a smaller size, as seen in Figure 3-4 and Figure 3-5. This was done by selecting the important lines that formed the borders to the important geometry and using the LESIZE command, as seen in APPENDIX C.

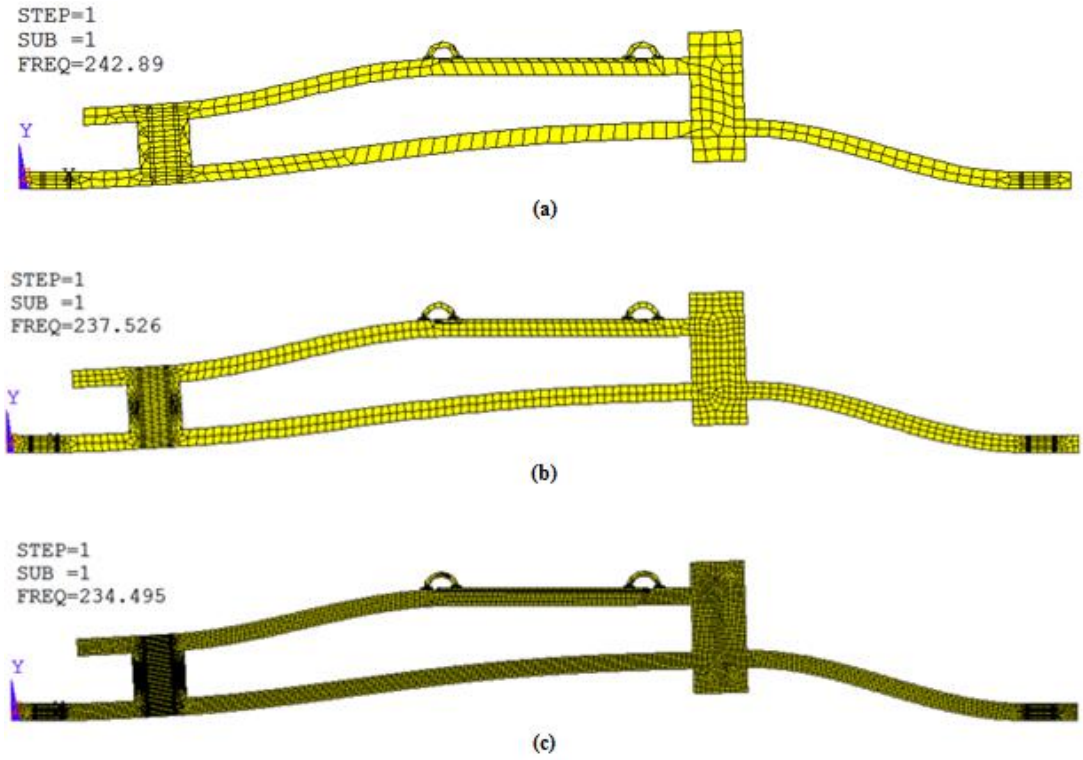

Figure 3-4: First three levels of mesh refinement

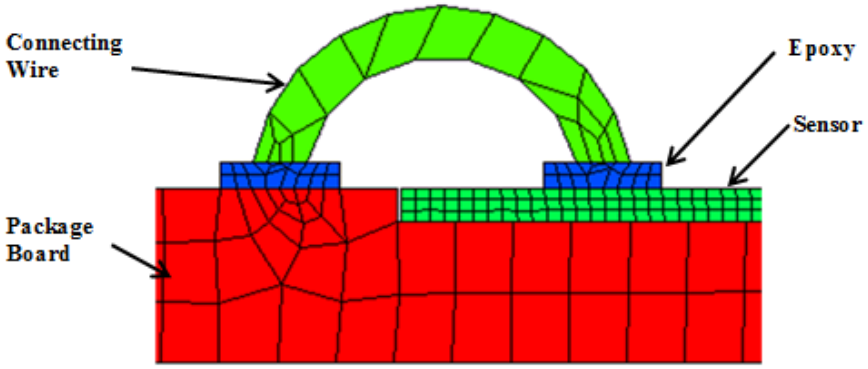

Figure 3-5: Mesh refinement at sensor, epoxy, and connecting wire

Figure 3-4 shows the first three levels of mesh refinement over the entire body, while Figure 3-5 shows the targeted mesh refinement at the sensor, conductive epoxy, and connecting wire. Two additional levels of mesh refinement were performed after the

refinement shown in Figure 3-4(c) in order ensure that ensure as much accuracy as possible. While the minimum element length was not further decreased, the element size used for the larger geometries such as the package and AMP boards was continuously decreased, thus increasing the total number of elements as seen in Table 3-1. The mode 1 natural frequencies of each level of mesh refinement were then compared with the total number of elements in the model. Once the solution started to converge, as seen in Figure 3-6, it was determined that the mesh density was adequately refined.

Table 3-1: Mesh Refinement Values

Min. Element Length (in)	No. of Elements	Mode 1 F_n (Hz)
0.01	526	242.89
0.005	1405	237.53
0.001	8741	234.5
0.0005	29386	231.28
0.0005	36771	230.64
0.0005	46856	229.996

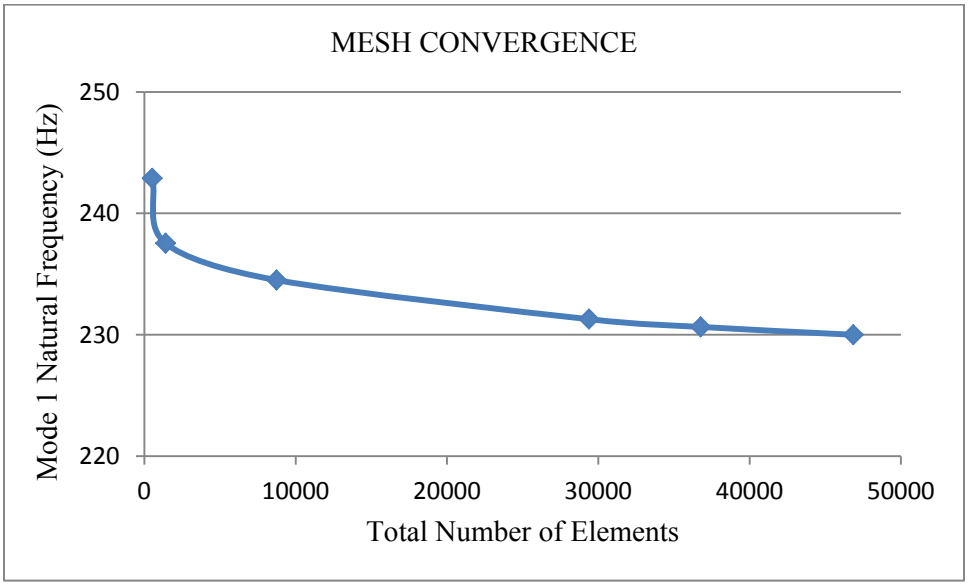

Figure 3-6: Mesh refinement convergence

Boundary Conditions: The 2D cross section model was supported by the pin holes on each end of the AMP board. To simulate the way a pin would constrain the board, the bottom edge of each pin hole, as well as the outside vertical edge was constrained. The bottom edge was fixed in all directions, x, y, and z, while the vertical edges were only fixed in the x direction, as shown in Figure 3-7. Lastly, every node was fixed in the Z direction (UZ =0) in order to ensure strictly two dimensional behavior.

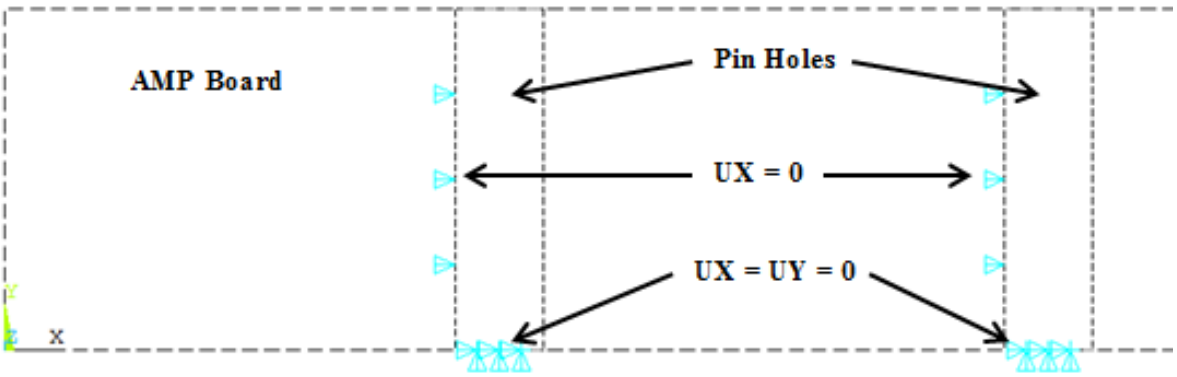

Figure 3-7: Left side boundary conditions

With the model fully constrained, the last input code defined the desired solution. A modal analysis type was defined and told to solve for the first five mode shapes. The resulting mode shapes and the natural frequency of each will be detailed in the RESULTS chapter.

Three Dimensional Model

The geometry for the first revision of the 3-D model looked very much like the structure shown in Figure 3-1 (a). Instead of modeling the structure from the bottom up as in the 2D analysis, a top down approach was used. The top down approach to modeling uses components called primitives. The use of primitives allows for the user to

create areas and or volumes directly without having to first specify keypoints, lines, and areas. While the top down approach to modeling does not allow for as much direct control of line numbering and reference, it does allow for much more rapid generation of geometry. Once the geometries are formed it was extremely useful to name various selections with the use of components, see the input code in APPENDIX C. Round support bolts and bolt holes were used, as well as cylindrical bushings. While these structures were modeled exactly like the parts being used to assemble the physical structure, they added a great deal of complexity to the model. The thousands of small, irregular elements needed to model the multiple curvatures would not connect to the neighboring regions of geometries. This resulted in a huge amount of elements being needed in the areas of complex geometry, as well as in transition regions in between the irregular elements, and the mapped, or regular ones. This approach resulted in the necessary amount of elements greatly exceeding the maximum amount of elements allowed by ANSYS.

To solve the problems caused by the curvature, the corner support bolts were converted into squared representations of the bolts. As the bolts themselves were not of great importance to the analysis, it was decided that changing them from being round to squared would not be a problem. Careful consideration was taken to ensure that the new square bolts had close to the same volume, and therefore the same mass, as the circular ones.

The final revision of the meshed geometry can be seen in Figure 3-8. Different mesh densities can be seen throughout the structure in order to accommodate for specific

geometric complexities. One important geometric feature to note is the connecting pins that join the package board to the interconnect device mounted on the AMP board. There is a slight gap intentionally included so that the package board does not sit flush with the top face of the connector, Figure 3-9. This was done to more accurately reflect the real connection conditions as the pins do not fully go into the connector piece. A good example of targeted mesh refinement can also be seen in Figure 3-9.

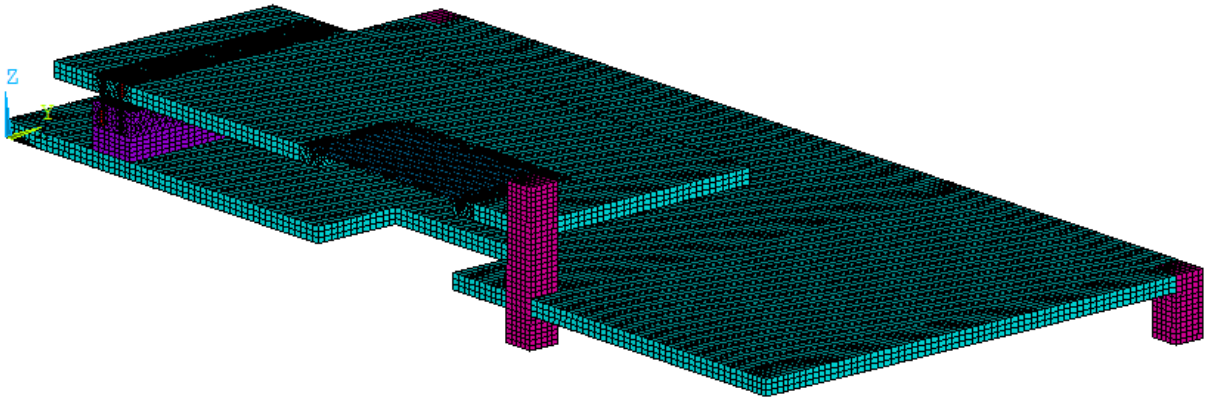

Figure 3-8: Final meshed structure for 3D vibration models

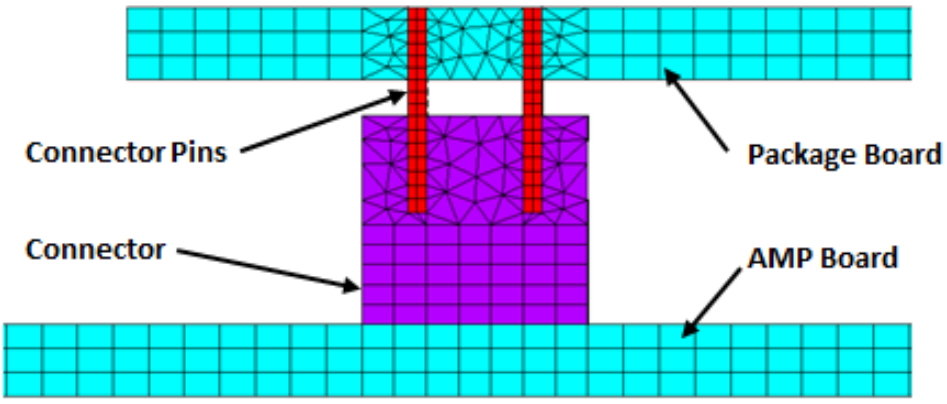

Figure 3-9: Detail view of package board and AMP board interface

Element Selection and Meshing: In order for this model to be meshed properly, several different types of elements were selected. The first element used was a lower

order solid structural element called SOLID185. The element is defined by eight vertex nodes, each having three degrees of freedom; displacement in the x, y, and z directions as seen in Figure 3-10. This lower order element was chosen in order to help keep the total number of nodes down and was used in all of the volumes that used mapped meshing. Elements generated with mapped meshing can be identified in Figure 3-9 as the quadrilateral elements. In order to set up the mapped mesh in various structures components of the geometry, volumes first had to be subdivided into portions with no geometric irregularities. Each volume that was to be discretized with a mapped mesh could only have a total of six areas defining it. The connector shown in Figure 3-9 best illustrates this concept where the top half is a free mesh while the bottom half employed a mapped mesh. A free mesh was required in the top half because the pin holes in the connector created a geometry that was too complex for a mapped volume mesh. The entire connector was not free meshed in order to help minimize the total element count.

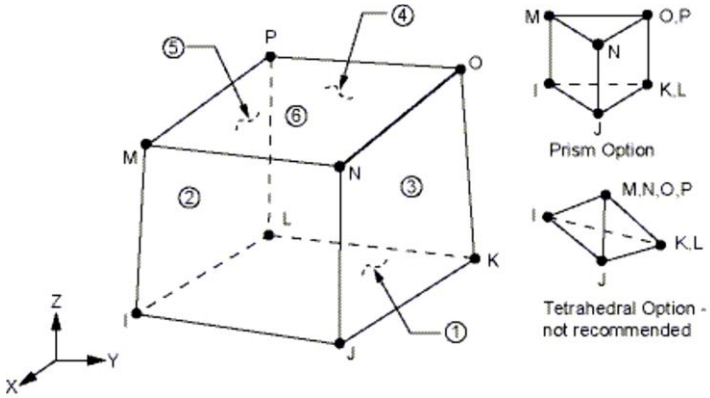

Figure 3-10: Solid185 structural element (ANSYS, Inc., 2011)

The second element selected was a higher order version of SOLID185 and was simply called SOLID186. This element was a 20 node quadrilateral element with

allowances for tetrahedral degeneration when used in irregular regions. Again, each node had three degrees of freedom in displacement, UX, UY, and UZ. The additional nodes in SOLID186 allowed for quadratic behavior along the element boundaries which greatly helped with element stability in irregularly shaped volumes.

Mesh Refinement: Mesh refinement was once again performed based on convergence of the modal analysis solution just as in the 2D analysis. As previously discussed, great care was taken in refining the mesh around critical areas of the geometry, while less critical or complex volumes were kept as course as possible, without sacrificing accuracy, in order to minimize the element count. Figure 3-11 shows the mesh refinement around the sensor and at the connection pins where they interface with the package board.

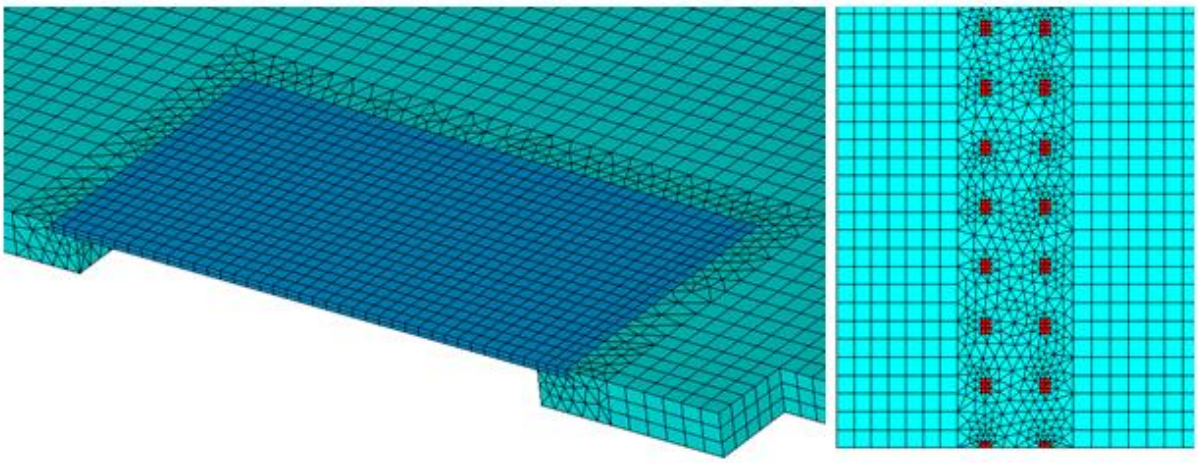

Figure 3-11: Mesh refinement at sensor (left) and connection pins (right)

Boundary Conditions: In the 3D simulation, the first boundary condition set was at the base of the corner bolts. Just as in the actual RTC system, the corner bolts were

fixed in all three degrees of freedom against displacement as seen in Figure 3-12. Lastly, all the nodes on the symmetry plane were fixed in the Y direction so as to allow for displacement in only the X and Z directions in accordance with symmetry conditions. Once the model was fully constrained, a modal analysis was performed to determine the first five natural frequencies for the structure.

Figure 3-12: Support bolt displacement constraints

Lastly, a harmonic analysis was made with the exact same geometry and meshing as used in the modal analysis. However, instead of fixing the corner support bolts, a harmonic force load was applied in order to simulate a forced vibration load from an external support structure. For this analysis, a 0.1 g force was applied at a frequency ranging from 5 to 60 Hz in each test axis. This applied loading was based off the General Environmental Verification Standard (GEVS) given for small sounding rocket test platforms from NASA Goddard Space Flight Center (NASA Goddard Space Flight Center, 2005).

4. THERMAL ANALYSES

Before the radiation tolerant computing (RTC) system could be tested with high altitude balloon tests, a test payload had to be designed. The test payload needed to withstand the physical environment it would be subjected to during the BOREALIS and HASP flights. Thorough consideration of thermal environments was especially important due to the stresses developed in materials undergoing thermal loading, as well as the important requirement of maintaining system temperatures inside the operating ranges of the various electrical components. The most temperature sensitive system component was the FPGA processor with a temperature range spanning from -50 °C to 120°C. In order to solve the energy balance shown in Figure 2-1, several thermal simulations were run. Development of the models was performed over a great many iterations until the temperature results became reasonable. The following sections will outline the various thermal models used and how they were developed in order to help design the test payload used for both high altitude balloon tests.

Test Payload Analysis

As previously discussed, the amount of time the test payload would spend in the lower atmosphere was much less than that of the time spent in the upper atmosphere. Therefore, while convection heat transfer was somewhat cooling the outside of the payload, it was certainly not as important as the amount of thermal energy being transferred due to solar radiation, or internal heat generation of the system during operation. In order to ensure that the internal systems would not get too cold during their

ascent, cold room tests were performed to simulate the time spent in the cold portion of the atmosphere. These tests revealed that the internal systems would never reach a temperature below 20°C, which was well above the minimum operating temperature. These early tests concluded that cooling would not be a concern for the system.

The major concern was due to the solar heating the payload would experience at the maximum test altitudes. The use of FEA analysis was then put toward solving the thermal concerns for the HASP test flight. Each input code was made so that certain geometries were parameterized in order for quick and easy adjustments to things such as insulation thicknesses, as well as placement of internal structures. This allowed for quick adjustment while running multiple analyses in order for optimization of these features.

Maximum Altitude Analysis

In order to test for the worst thermal conditions of the HASP flight, a simulation was made to represent the eight to ten hour float at 120000 feet. At this altitude, convection heat transfer, both inside and outside the payload was neglected. This was due to the atmosphere being too thin to support any significant heat transfer due to convection. Therefore, the payload thermal energy balance was altered from Figure 2-1 to look like Figure 4-15.

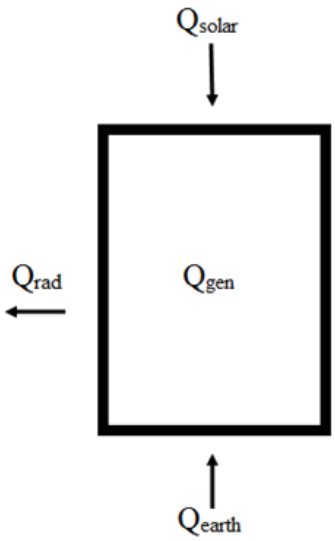

Figure 4-1: Max altitude energy balance

Geometry Treatment: Once again, geometry simplification was crucial. All of the fasteners that held the insulation in place were eliminated. The internal RTC system stack was also reduced to include only the circuit boards that produced the most heat. Initially, the payload included two FPGA boards, the major contributors to heat generation. These boards were modeled as a solid volume made entirely of the FR4 material. The surrounding payload structure included the PVC mount plate, a bottom piece of insulation on top of that, as well as the side and top pieces of the polystyrene insulation as seen in Figure 4-2. Note that the use of symmetry was employed as in the previous analyses.

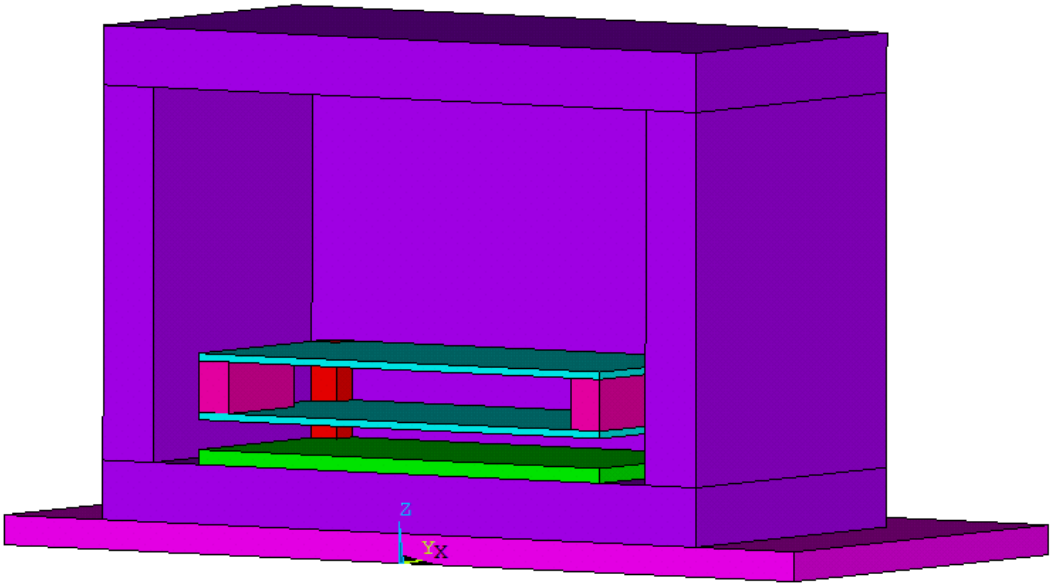

Figure 4-2: Initial model architecture

As previously mentioned, the actual HASP flight only sent one FPGA board and one sensor up to be tested. That resulted in the top internal circuit board being removed so that only one board was generating a significant amount of heat as seen in Figure 4-3.

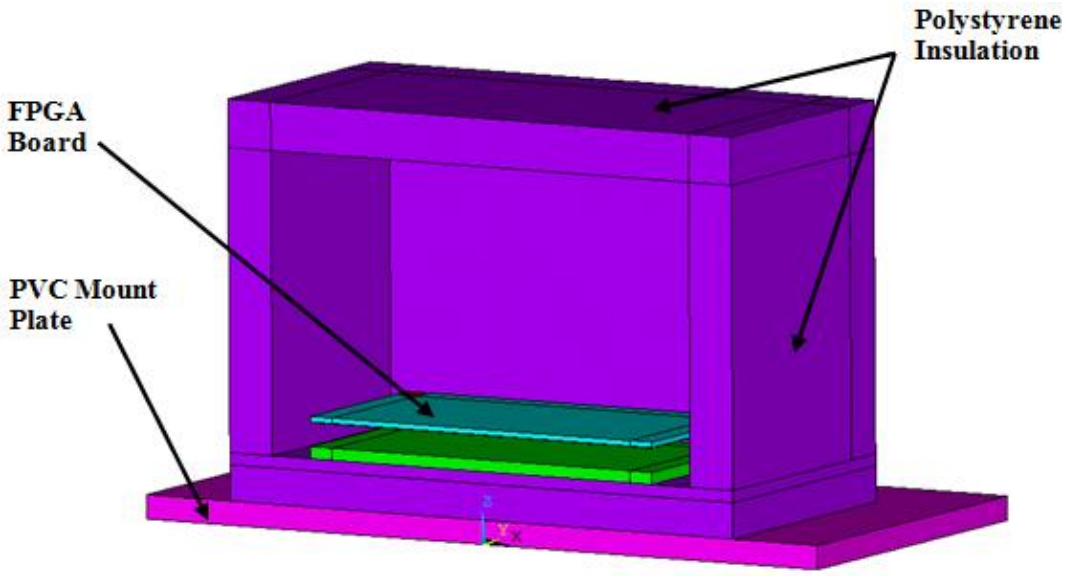

Figure 4-3: HASP payload model, final configuration

System Heat Generation: While each system component generated a certain amount of heat, it was impossible to perfectly model the distributed heat generation throughout the system using FEA software. Again, geometric simplification was essential in order for the simulations to even run. In order to keep the geometry simple enough for analysis, initial simulations used only the FR4 material for two internal system boards. The heat generation was placed in the center of the board in order to mimic the physical system. The actual source of heat generation was from the FPGA processor positioned in the center of the PCB. While this provided the simplest geometry, it was very inaccurate and provided extremely high temperatures as a result. This was mostly due to the extremely poor thermal conductivity of the FR4 material.

Material Properties in PCB Modeling: One important thing to note is the material properties of the PCB structure. Initially each PCB was set to only have the FR4 material. While the PCB was mostly made out of FR4, it also had several copper components, most notably, several copper ground planes that went throughout the entire board. This is a significant difference, especially in thermal analyses due to the vast discrepancy of thermal conductivity between FR4 and copper. As FR4 is essentially fiber glass in an epoxy resin, it has an extremely poor thermal conductivity. This meant that any heat generated in a volume made entirely of FR4 would essentially be trapped. The low thermal conductivity would inhibit any transfer of thermal energy out of the material. The thermal conductivities of payload materials can be seen in Table 4-1.

Table 4-1: Thermal conductivity of payload materials

Material	FR4	Polystyrene	Copper	Aluminum
Thermal Conductivity [W/m°K]	0.27	0.036	401	177

The result of the first version of the thermal model yielded extremely high temperatures due to the thermal energy being trapped in the FR4 material and having nowhere to go. This effect is shown in Figure 4-4.

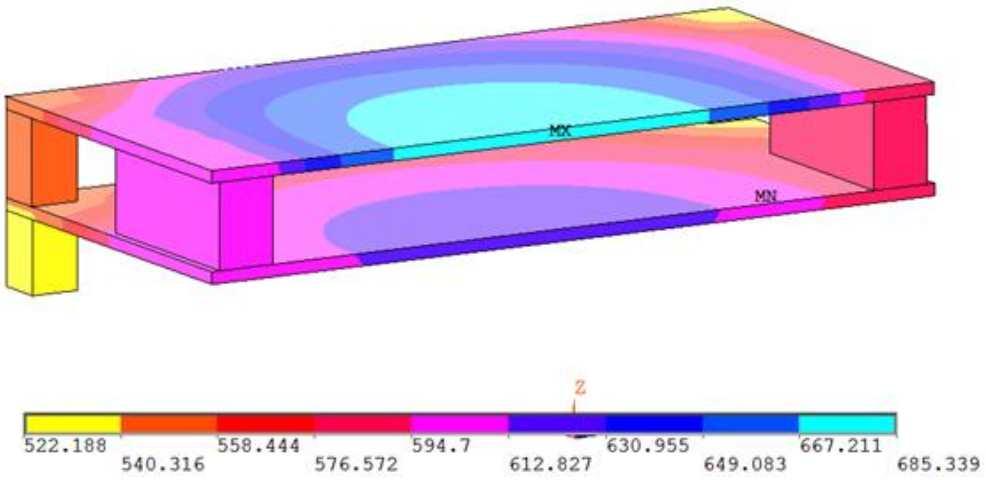

Figure 4-4: Solid FR4 temperature results [°K]

Note that the highest temperature regions are isolated exactly where the heat generation source was placed. Another important factor that led to thermal energy being trapped in the RTC system structure was that the aluminum support posts, seen in the back left corner of the structure shown in Figure 4-4, did not go through the bottom insulation slab to the exterior of the payload.

Model Improvement: In order to improve the model accuracy, the PCB structure had to be improved. Using the FR4 material for the heat generation volume was too inaccurate. In reality, the metal components of the FPGA board were responsible for the heat generation. To improve the model, the copper ground planes were added to the structure of each PCB board. The copper ground planes not only better represented the actual structure, but their high thermal conductivity provided a path for thermal energy to spread through the PCB instead of being trapped at the point of generation. The copper ground plane for the FPGA board, see Figure 4-5, was only 0.0045" thick, but that small addition to the model geometry greatly improved solution accuracy.

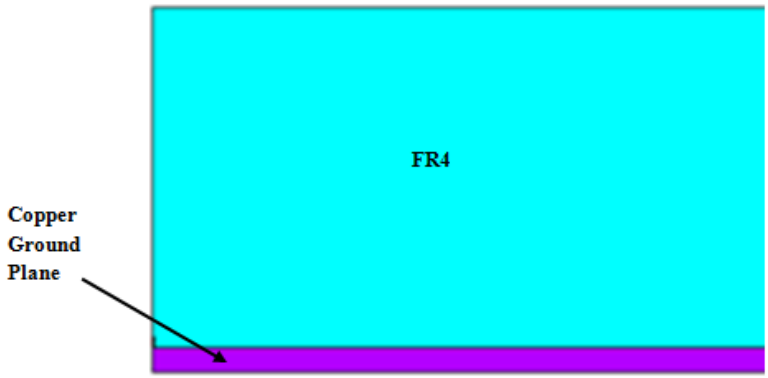

Figure 4-5: PCB with copper ground plane included

The copper ground planes presented a problem with regards to meshing. In order to produce an accurate mesh, the elements in the copper ground plane had to be very small. The incredibly small thickness of the ground plane meant that a longer horizontal element length would create a very poor aspect ratio for the element. If the aspect ratio, the elements width to height ratio, was too high, the element would become unstable and provide inaccurate results. In order to maintain an acceptable aspect ratio, a fine mesh

had to be defined on the ground plane, as well as any other geometries that shared coincident nodes, including the FPGA board and the support bushings. The final mesh density, with the proper aspect ratio, of the ground plane and FPGA board can be seen in Figure 4-6 where the elements on the top are the FPGA elements, and the thin elements on the bottom are the copper ground plane elements.

Figure 4-6: FPGA and ground plane mesh density

The second improvement to the model was to make the corner support bushings go all the way through the insulation. This allowed thermal energy conducting through the ground plane to enter the aluminum support, and eventually get to the exterior of the payload. Once there, the thermal energy could be radiated outward toward the earth. The decision was made to direct thermal energy down through the bushings to radiate towards earth in order to prevent over cooling the structure. If metal heat pipes were connected to the exterior of the sides of the payload, they might pump too much heat out to the coldness of space. By directing the thermal energy towards earth, a much higher temperature than space, the amount of thermal energy lost would be limited. This ensured that the structure would only pump thermal energy out toward earth as long as it was at a higher temperature than that of the earth. If the interior system ever reached a temperature below that of the earth, the direction of heat flow would be reversed. This strategy would help keep the internal system within its operating temperature range,

without either over heating it, or over cooling it. This concept of radiating thermal energy to surroundings of a known temperature is illustrated in Equation 2-10.

A copper heat sink was also connected to the corner support bushings directly below the FPGA board. The goal was to direct as thermal energy out of the bushings and into the heat sink. The heat sink was added mostly to aid in thermal control during the HASP integration test which will be outlined in the HASP Integration Analysis section. The effects of these component changes will be detailed further in the RESULTS and ANALYSIS chapter.

Lastly, additional alterations to the model geometry, as well as the internal system heat generation were performed with an eye toward the future development and testing of the radiation tolerant computing system. One such alteration was the simple variation of internal heat generation. While initial studies used the heat generated by a single FPGA processor, different generation values were used to see the effect of the change. This would help provide initial response data for future designs with varying components and heat generation.

The next alteration was the addition of a slight gap between the copper ground plane and the corner bushings. Future PCB designs may include a gap between the copper ground plane, and the corner holes for bushings. The expected result of a gap in the copper material would be an increase in maximum temperature experienced by the system structure. This would be due to the much lower thermal conductivity in the FR4 material filling the gap in the copper material. By varying the gap thickness, the effect on the maximum temperature reached in the structure could be tested. The gap width ranged

from zero, meaning there was direct contact between the copper ground plane and bushings, to 0.01 inches of FR4 material in between the ground plane and the bushing. The addition of the small gap in the ground plane made further volume subdivision and subsequent mesh density refinement necessary for the model to maintain accuracy while staying under the maximum node count limit of the software. The ground plane gap, and new element mesh density, can be seen in Figure 4-7 and Figure 4-8.

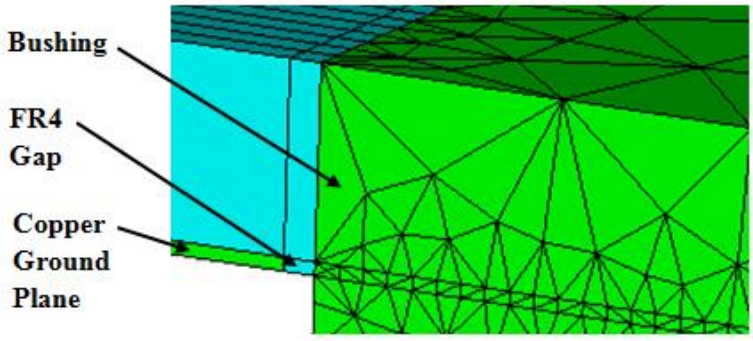

Figure 4-7: Gap in copper ground plane

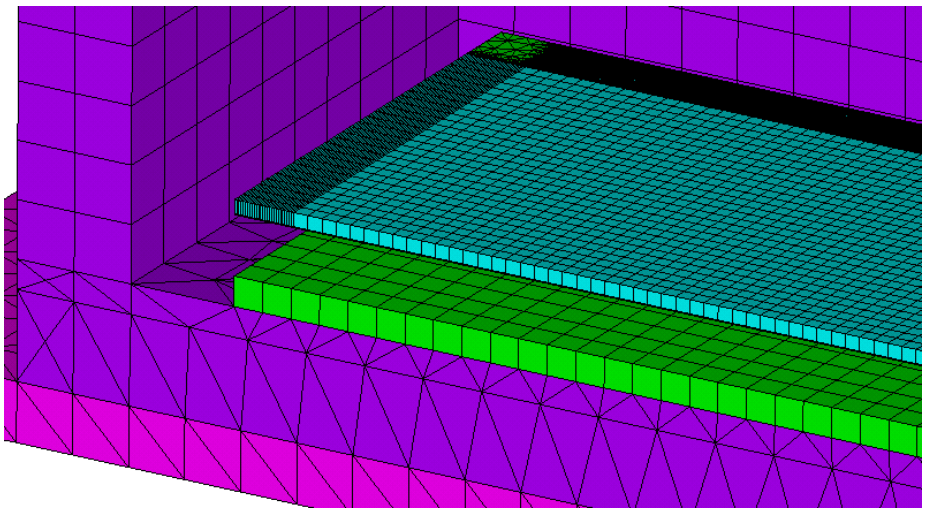

Figure 4-8: Mesh refinement after gap addition

Element Selection and Meshing: As this was a strictly thermal analysis, new elements had to be selected for the payload structure. The first element used for most of the structure was a 3D thermal solid element called SOLID70. The element allowed for 3D thermal conduction and had eight nodes, each with a single degree of freedom, temperature. The element geometry, as well as the geometry of its degenerate shapes looked exactly the same as the SOLID185 structural element shown in Figure 3-10. Although the low order SOLID70 element allowed for degenerate shapes to mesh irregular geometry, it often resulted in unstable elements being created. This instability was usually due to extreme angles between the edges of narrow degenerate elements along with poor aspect ratios.

In order to mesh some of the more complex regions of the geometry, a higher order thermal solid element, called SOLID90, was used. This element was exactly like the SOLID70 element except it included mid-side nodes, shown in Figure 4-9. The mid-side nodes allowed for curved element edges, which improved element quality and stability when in degenerate forms.

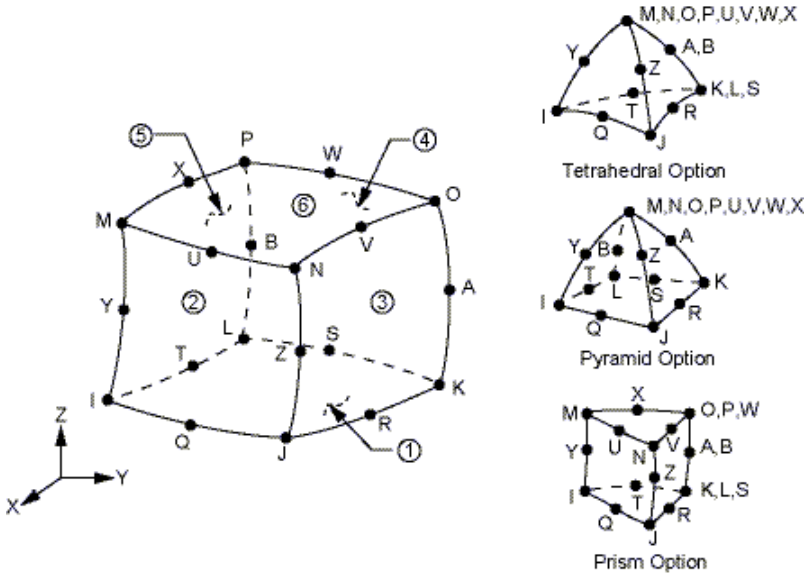

Figure 4-9: Solid90 thermal element (ANSYS, Inc., 2011)

The last element used in the maximum altitude analysis was used to allow for thermal surface effects, in this case radiation. The element, called SURF152, was a 2D element that was laid over the outside faces of the 3D solid thermal elements. This versatile element allowed the user to specify whether mid-side nodes would be used or not. Mid-side nodes were not used in this analysis as the surfaces experiencing radiation were all rectilinear in nature and thus did not require higher order elements to mesh them. Another option was the use of an extra node that was out in space a specified distance away from the surface element. This extra node was used to set reference temperatures for either radiation or convection effects. This analysis used the extra node for reference temperatures of both space, as well as the earth ground temperature. This allowed the top and sides of the test payload to radiate heat out into space, and the bottom of the structure to radiate heat back towards earth.

Great care was taken in meshing the entire structure with regards to mapped meshing and element sizing. Each component was divided into six sided sub-volumes in order to use mapped meshing wherever possible, as seen in Figure 4-10.

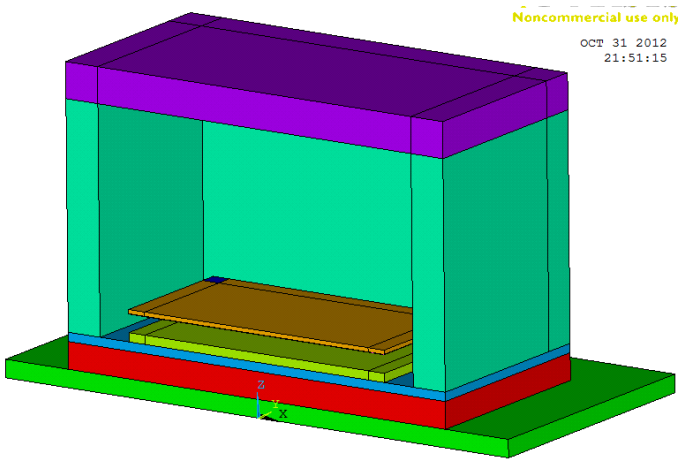

Figure 4-10: Subdivided payload volumes

Mapped meshing was crucial because it allowed the use of the lower order SOLID70 element which contained far less nodes than the higher order SOLID90. This allowed an accurate mesh to be created while preventing the model from quickly exceeded the software's node limit of 260,000. Once the volumes were subdivided, the mapped meshing was performed in order of smallest element size to largest. As previously discussed, the ground plane, FPGA board, and support bushings had to be meshed first with the fine mesh density (small element size.) The heat sink was meshed next with a slightly coarser mesh density. The top and side insulation volumes were then meshed with a much more coarse mapped mesh.

Once the mapped meshing processes were complete, the remaining volumes were free meshed. The mount plate was meshed first with a coarse free mesh still using the lower order SOLID70 element. Next the bottom half of the base insulation was meshed

with the same coarse mesh density. Lastly, the top portion of the base insulation was free meshed with the higher order SOLID90 element. The higher order element was used in this volume to allow for a smoother transition between the different mesh densities on either side of the sub-volume currently being meshed. This resulted in more accurate elements being created with acceptable aspect ratios. The final meshed structure can be seen in Figure 4-11, where the different colored volumes represent different materials.

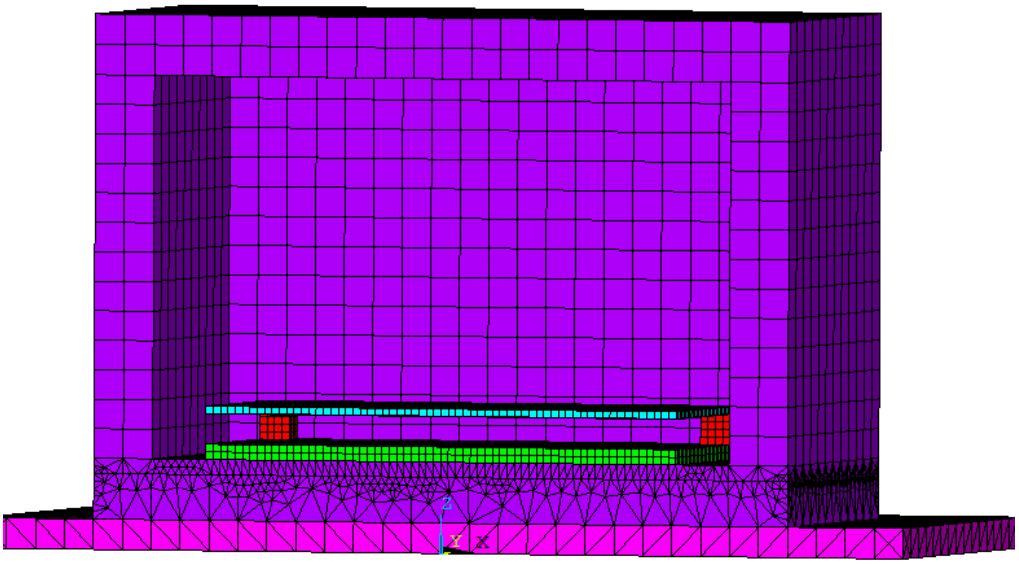

Figure 4-11: Completely meshed payload structure

Boundary Conditions: The last elements added to the model also defined the boundary conditions. The SURF152 elements were meshed directly over the exterior faces of the payload insulation, shown in purple of Figure 4-11 and the PVC mount plate, shown in pink in Figure 4-11. These elements were defined as radiation elements with a specified emissivity. Each face of SURF152 elements was also given an extra node that defined the temperature of the matter that the face was radiating to. This meant that the

side and top faces had a reference temperature equal to the temperature of space, while the bottom face used a reference temperature of the earth.

Thermal Loading: The first set of thermal loads applied to the model included the loads due to the incident solar irradiation. These loads were applied to the SURF152 elements as a heat flux. Surface emissivity, absorptivity, and the radiation form factor were accounted for as outlined in the BACKGROUND chapter. The emissivity and absorptivity were controlled as material properties for the thin surface elements. Solar angles and times were calculated for the date and time when maximum altitude was reached, as well as the location in Fort Sumner, NM. The relevant data is shown in Table 4-2.

Table 4-2: Solar incidence angles input data

Date	Local Time	Latitude	Longitude
Sept. 10, 2012	9:30 AM	34 ° N	104 ° W

Each face of the payload was given its own surface flux load due to solar radiation and calibrated for its relative position, as can be seen in APPENDIX A. As the entire HASP structure was free to rotate about its vertical axis, it was decided to orient the payload along the cardinal directions for ease of radiation form factor computation. Once the radiation form factors were calculated, the largest radiation load was applied to the largest face, the back face, in order to ensure that a worst case scenario of heating was analyzed (Figure 4-12.)

The final thermal load applied was the internal heat generation of the FPGA board. This was implemented as a body load and was applied to the ground plane in the FPGA board over its volume. The final form of the model with exterior flux loads applied can be seen in Figure 4-12, note the varying flux values as a result of the varying angles of incidence.

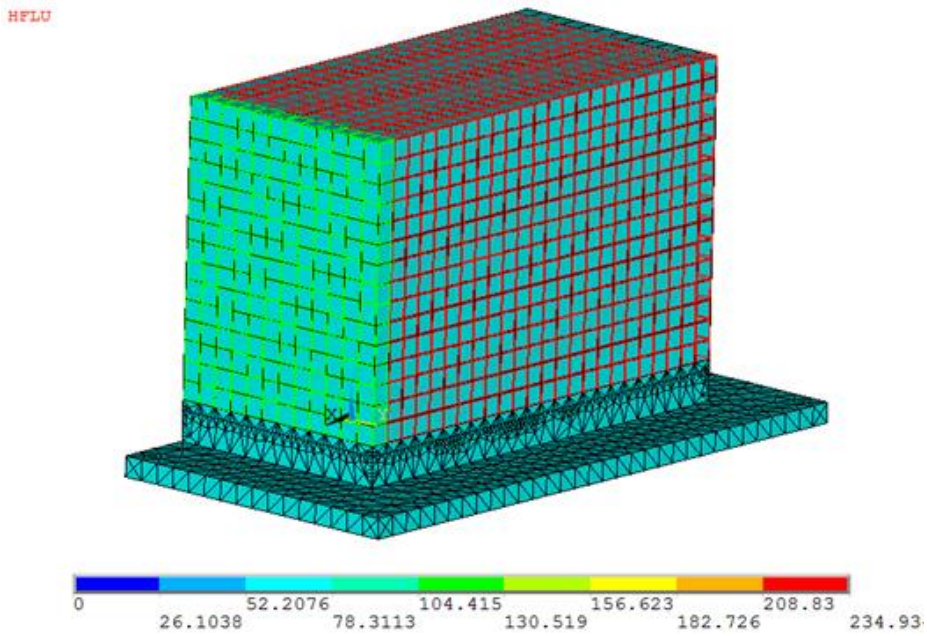

Figure 4-12: Meshed and loaded model before solution

HASP Integration Analysis

Before the payload would be allowed to fly on the HASP structure, an integration test had to be passed. The thermal integration test consisted of the system being placed in a pressurized furnace in order to stress test the payloads thermal capabilities. The thermal test would consist of a cooling cycle where the test chamber was set to -50°C at 1atm of pressure. These conditions would be held for one hour. Then the pressure was reduced down to 5 millibar while the temperature remained constant and again, the

conditions were held for one hour. Finally the test chamber was brought back up to 1 atm of pressure and heated up to 50°C and held for an hour. Then the pressure was reduced back down to 5 millibar and the temperature was maintained for yet another hour.

Due to the high heat generation of the RTC system, as well as the successful flight in the BOREALIS test, which had similar low temperature ambient conditions, it was deemed unnecessary to overly analyze the cold portion of the integration test.

However, the high temperature stress test brought about some overheating concerns. Without being able to radiate thermal energy out to the cold space environment, the main source of payload cooling was lost. Therefore, a transient analysis that would reflect the high temperature conditions was made. The payload geometry was essentially the same as that of the maximum altitude test, but instead of empty space inside the insulation, there was now air, seen in orange in Figure 4-13.

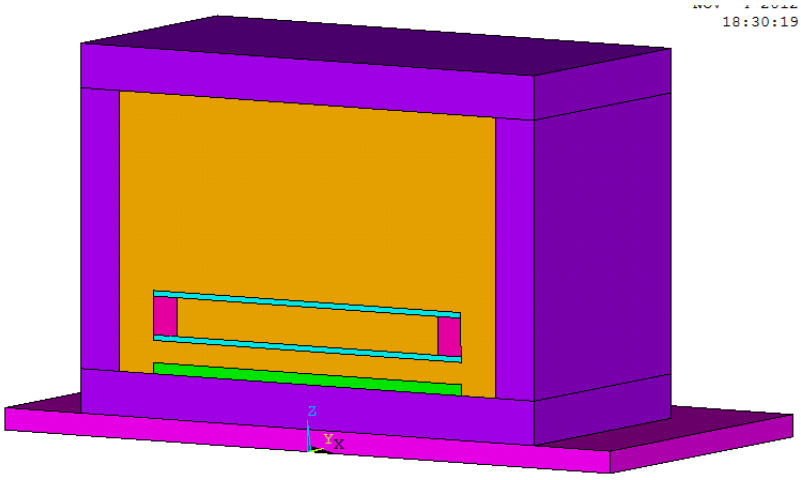

Figure 4-13: Integration test model with internal air

Geometry and Meshing: Since the first part of the heating was done at atmosphere, convection heat transfer had to be considered. The solid thermal elements

used to mesh the model were exactly the same as those used for the maximum altitude model. Further volume subdivision was required in order to generate an adequate mesh as seen in Figure 4-14.

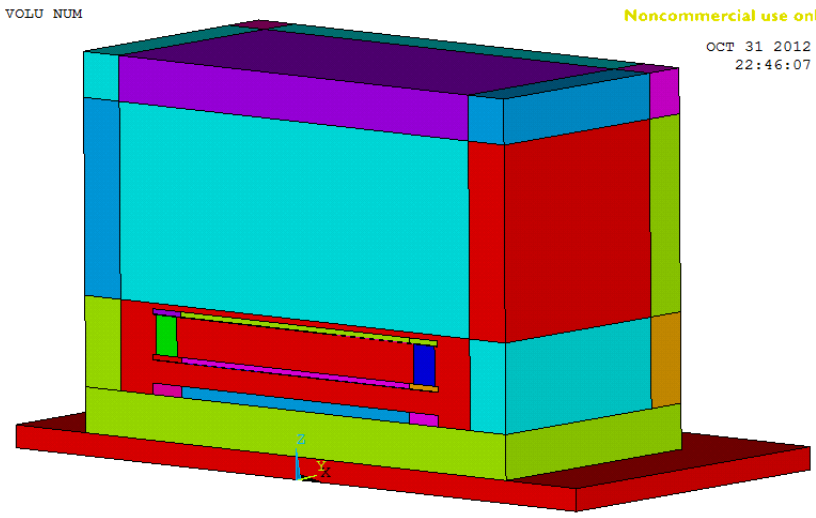

Figure 4-14: Subdivided integration model

Thermal Loading: One important distinction between the two models is the lack of radiation surface elements. Instead of creating surface effect elements, convection loads were applied directly to all exterior faces of the model. The loads were applied by defining the convection film coefficient, as well as the ambient, or bulk fluid temperature. The bulk fluid temperature was set to 50°C while the convection coefficient was calculated using the free convection formulation detailed in APPENDIX B. The simulation was then run for one hour at a constant temperature to simulate the integration test conditions. A cold test was also simulated using a bulk fluid temperature of -50°C and run for an hour as well.

System Level Thermal Expansion Analysis

Once estimates of maximum temperature values were obtained, simple steady state thermal simulations were run to test for the effects of thermal expansions and contractions due to the heating and cooling of the structure. Thermal expansion was a concern due to the many different materials used in the system with varying coefficients of thermal contraction. As the package board was fixed at each end by pins and a support bolt, stresses would develop due to the expansion or contraction of the material between the fixed supports. If too much deflection were to occur, the thin sensor could fail as it was very fragile, especially in flexure. For this model, the geometry shown in Figure 3-2 was used with the corner bolts added at each corner for support.

Element Selection Meshing and Boundary Conditions

As this analysis was fairly simple, ANSYS Workbench was used because of its ability to easily import structures and assemblies directly from CAD software. Another benefit to the ANSYS Workbench software was the ease of meshing the complicated structure. Instead of requiring an input code for everything, ANSYS Workbench uses a graphic user interface (GUI) for much of its processes. In this case, the software was told that structural elements were needed for the analysis. Sizing was then specified for various regions as well as specific meshing methods for certain geometries. The AMP board, as well as the sensor, were defined using a sweep method in order to keep the element shapes as uniform as possible. The remaining geometries were then allowed to be free meshed with size and transition of elements controlled by the program under the

prescribed guidelines of size and transition rates. The mesh method was set as a hexahedral dominant mesh method. This robust method worked best for imported CAD structures because of its high adaptability to complex geometries. The method tries to use hexahedral element shapes wherever possible with the option of using tetrahedral elements in transition or complex areas. Again, the bottoms of the corner support bolts were fixed against translation on all three axes. The completely meshed structure can be seen in Figure 4-15.

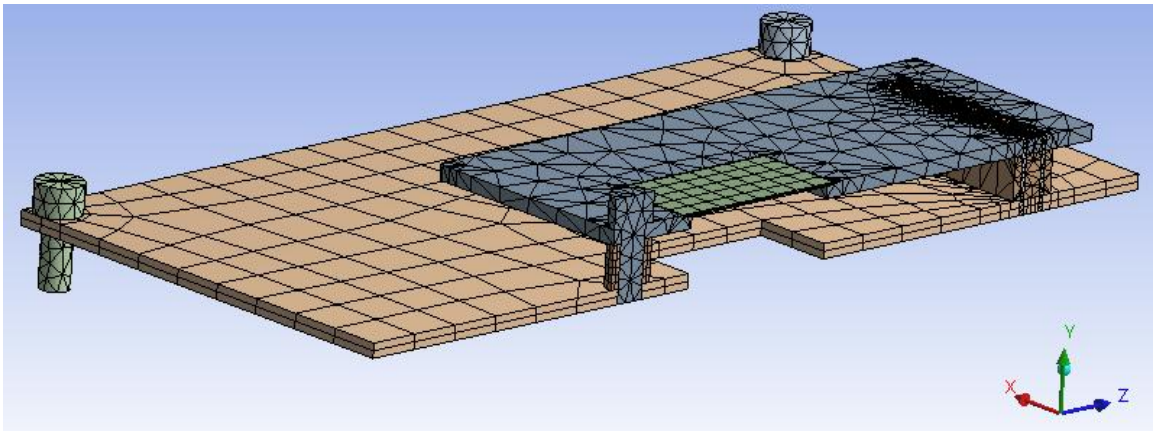

Figure 4-15: Meshed thermal expansion model

Component & Material Selection and Optimization

As previously mentioned, there were several material driven factors that affected the payloads overall mechanical, and thermal performance. Certain materials were chosen to help facilitate the thermal stability of the structure. Other considerations such as mass, product availability and cost were also considered. The following is a brief description of the critical material selections and their relevant constitutive properties.

Payload Exterior

As previously mentioned, the payload exterior was comprised of several panels of Polystyrene extruded foam insulation. While it did not have the lowest thermal conductivity on the market, it was fairly close, and readily available in both 1" and 1/2" thick panels. Several Iterations of the maximum altitude simulation model were run in order to determine the effect of changing the thickness of the insulation. The 1" thick panel was slightly too wide to fit within the allotted area so different iterations were performed ranging between 1/4" and 3/4" thicknesses. It was found that these slight thickness alterations did not significantly affect the maximum FPGA temperature and so it was decided to use the stock 1/2" thick insulation in order to facilitate the fabrication process. A thin layer of fiberglass was then wrapped around the insulation panels to lend stiffness and strength to the overall structure. Once the fiberglass had set, the exterior surfaces were painted with Krylon Flat White #1502 paint. This paint, along with the rough surface finish of the fiberglass, vastly increased the emissivity of the outer surface of the structure to 0.95. This extremely high emissivity value allowed the structure to radiate thermal energy out to space, and back to earth in an extremely efficient manner.

Internal Structure

As previously mentioned, much of the internal RTC system components were already designed and fabricated. However, much of the fasteners and PCB connectors still needed to be selected. The selection process was made fairly simple by balancing structural stability with cost effectiveness and availability. Structural stability was achieved by ensuring that there was no free hanging, or unsupported edges on any of the

PCBs, while minimizing the free space between stacked boards. The use of metal, instead of plastic standoffs at each corner of the PCBs also helped to facilitate conduction of thermal energy out of the PCB stack and toward the bottom of the structure. Table 2-1 illustrates the vast differences in thermal properties between different payload components.

Table 4-3: Thermal properties for various payload materials

Material	Thermal Conductivity [W/m*K]	Specific Heat [J/kg*K]
Polystyrene	0.036	1200
FR4	0.27	915
Plastic Connectors	0.42	1500
2024 Aluminum	177	875
Copper	401	385

5. RESULTS and ANALYSIS

Vibration Studies

Two Dimensional Result

The initial two dimensional model yielded satisfactory results with regards to mode shapes. The first mode shape was exactly as expected and can be seen in Figure 5-1. The first mode shape met the expectations as the maximum displacement was centered on the highest concentration of mass in the geometry. This corresponded to the aluminum support bolt on the right end of the sensor package board, the large rectangle to the right in Figure 5-1.

Figure 5-1: First mode shape and harmonic frequency

The next four mode shapes occurred at progressively higher natural frequencies. Again, this behavior was expected. The remaining mode shapes, along with the corresponding natural frequencies can be seen in Figure 5-2. While these mode shapes give a good indication of the behavior of the overall structure, the strictly two dimensional nature of the model raises some concerns, especially to the actual value of each of the natural frequencies. This 2D nature of the model also meant that any out of plane effects, such as the effects on displacement due to the orthotropic nature of the FR4

material, could not be considered in this analysis. Lastly, it is important to note the separation between the sensor and the package board in Figure 5-2 c. This occurred because the initial 2-D model allowed for separation to investigate any effects of not bonding the sensor to the package board with epoxy. Final packaging will of course, utilize an epoxy to securely fix the sensor in place.

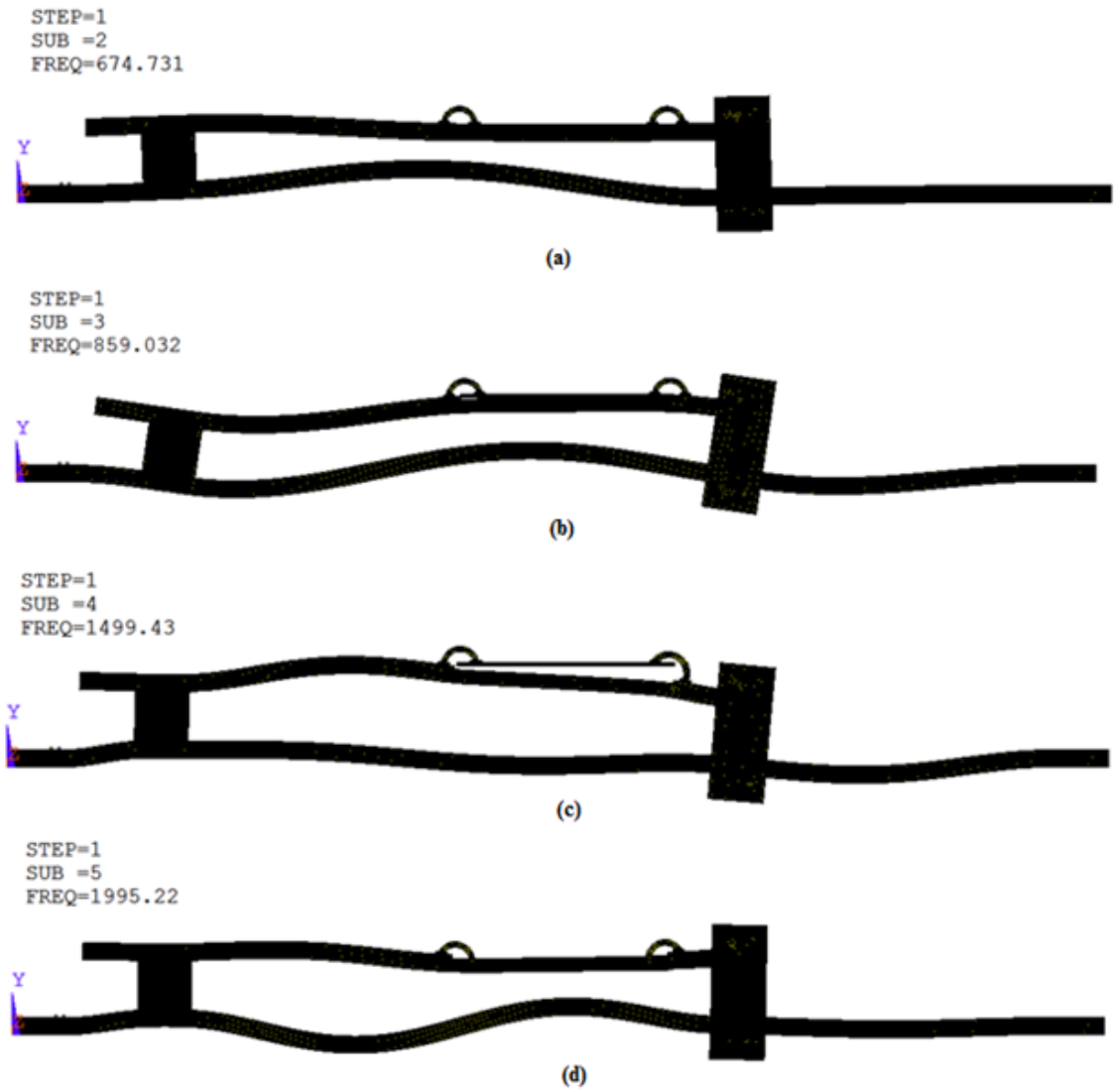

Figure 5-2: 2D modes 2 through 4 mode shapes

Three Dimensional Results

The three dimensional analysis yielded good results that showed nice modal shapes with deflection along all three axes. Again, the maximum deflection seems to center about the concentrated mass of the support bolt at the end of the package board. Another consistency with the 2D analysis is the steady increase in frequency of each mode shape. The first mode shape of the three dimensional result mimicked that of the two dimensional analysis closely and can be seen in Figure 5-3.

Figure 5-3: First mode shape of 3D model

The second mode shape of the 3D analysis differed from the 2D one. This mode shape shows a lateral vibration of the structure from left to right and is shown in Figure 5-4.

Figure 5-4: Second mode shape of 3D model

As expected, the last three mode shapes had very high natural frequencies and are shown in FIG. It is important to note that the displacements for all modal analyses are shown with a large scaling factor in order to help visualize the type of movement happening in each harmonic mode.

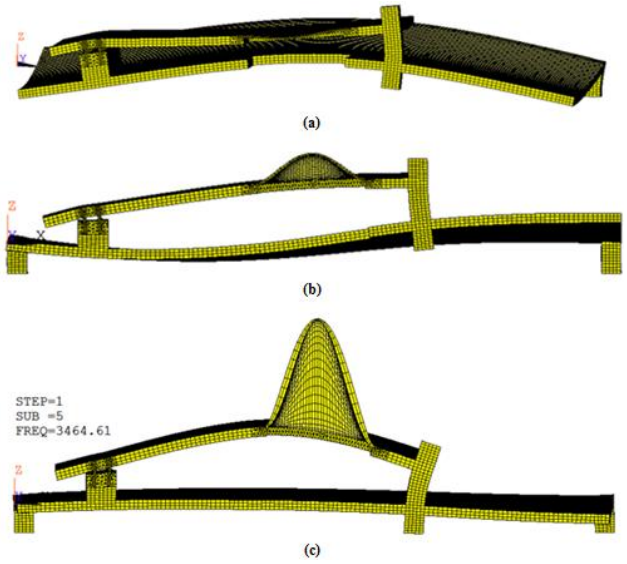

Figure 5-5: Modes 3-5 of the 3D model

There are a few notable differences between the 2D model and the 3D one. There of course is the obvious difference between 2d and 3D displacement as seen by the mode shapes of the two models. Another difference is how each model was constrained. As mentioned before, the 2D model had to be constrained at the interconnect pins, while the 3D model was fixed by the corner support bolts. The 3D nature of the second model also allowed for the inherent orthotropic nature of the FR4 material to have an effect. A non-uniform stiffness of the material would definitely affect displacement along the orthogonal exes. The natural frequencies of each mode for both 2D and 3D models are shown in Table 5-1 for easy comparison of the two models.

Table 5-1: 2D & 3D Natural Frequencies

Mode	2D f_n [Hz]	3D f_n [Hz]
1	229.96	709.08
2	674.73	1472.72
3	859.03	2107.94
4	1499.43	2953.91
5	1995.22	3464.61

The second analysis run on the 3D model was a harmonic loading test. As previously stated, this model was done to merely lay the groundwork for future vibrations study in order to adequately design for a given flight vehicle. In this case, the random vibrations loading for a sounding rocket was used as a guideline. It is important to note that the frequency range for loading, 0 to 60 Hz, is far lower than any of the modal frequencies of the structure.

Equivalent stress plots showed a fairly low stress values experienced over the entire structure aside from some very high values, most likely caused by sharp corner singularities in the structure. The stress plot for the entire structure, the radiation sensor, and the interconnect pins may be seen in Figure 5-6, Figure 5-7, and Figure 5-8 respectively.

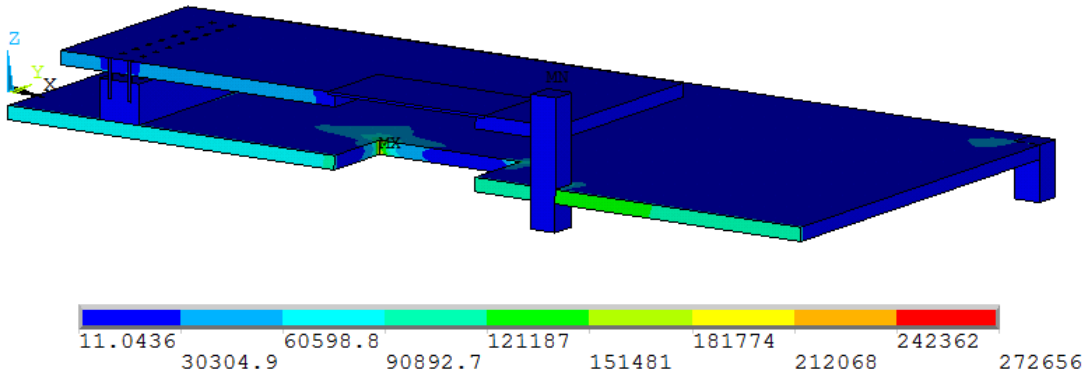

Figure 5-6: Equivalent stress plot for a 0.1g at 60 Hz loading

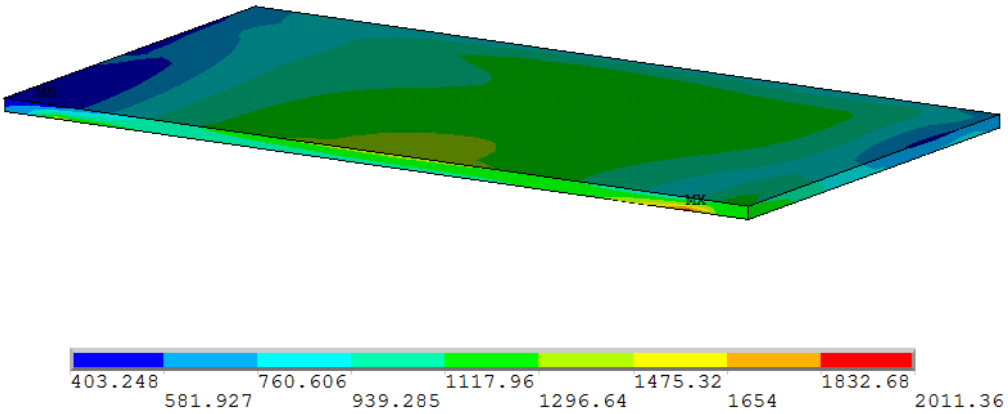

Figure 5-7: Radiation sensor equivalent stress

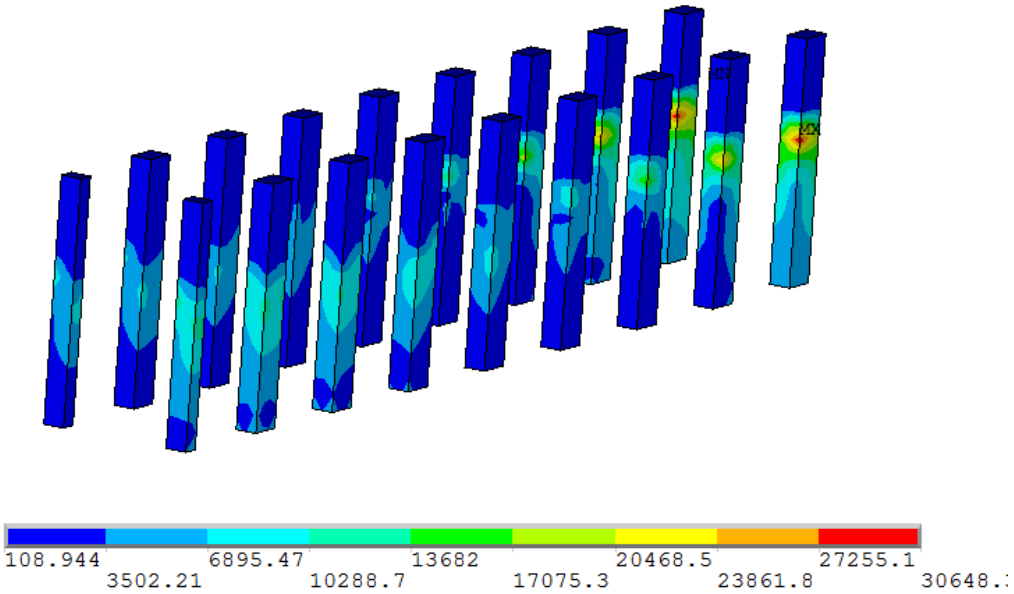

Figure 5-8: Interconnect pins equivalent stress

While most of the stress developed in the PCB structures remained below the yield stress of 55 ksi, there are regions of stress values much higher than that. Again, this is a result of the sharp corners in the geometry that create singularities and can be seen in Figure 5-9. The concentration of stress at sharp corners also occur in the interconnect pins as shown in Figure 5-8. The interconnect pins chosen for the structure were made of

phosphor bronze with a yield strength of over 65 ksi. Therefore the interconnect pins were in no danger of failing under the applied loading. Lastly, the sensor experienced a maximum stress of only 2000 psi. Again, this stress was far lower than the yield strength of the silicon sensor measured at 1000 ksi (Hsu, 2008).

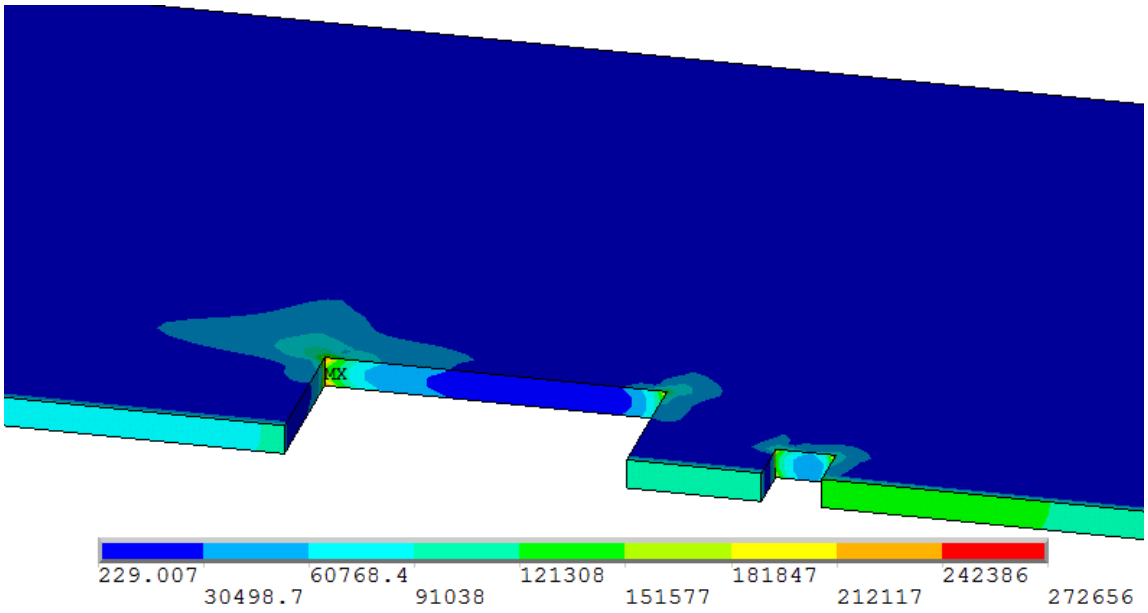

Figure 5-9: Stress concentrations at sharp corners

Balloon Test Sensor Results

The desired high altitude balloon test results consisted of a count of total radiation strikes with respect to altitude for the BOREALIS flights, and channel specific positional data for radiation strikes experienced during the HASP flight. The BOREALIS flight yielded good data showing an increase in detected radiation strikes with altitude. This behavior was expected due to the continuous decrease in atmosphere with altitude, and can be seen in Figure 5-10.

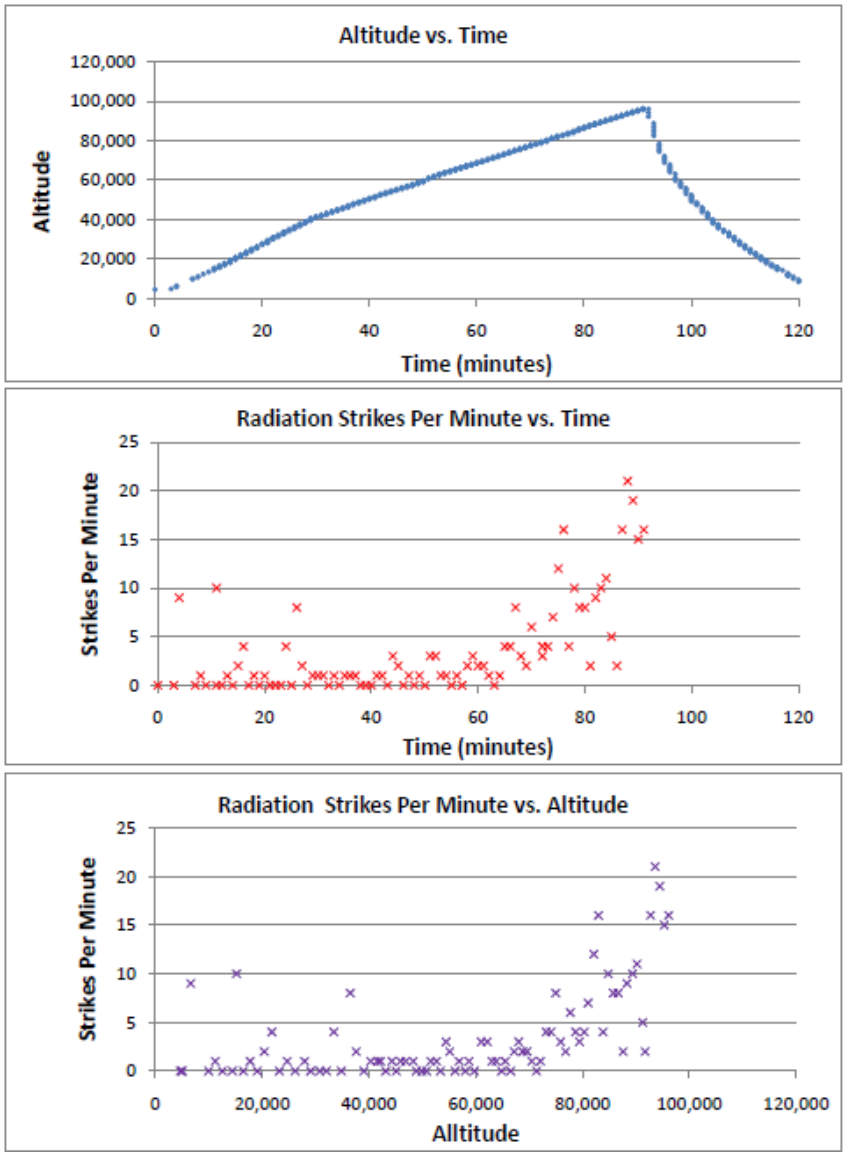

Figure 5-10: BOREALIS flight test sensor data

The BOREALIS data reflects that the total amount of radiation strikes, as well as their intensity increase with altitude in accordance with expected results. With less atmosphere at high altitudes, there are more radiation particles flying around. It makes intuitive sense that the more particles present, the more will strike the sensor and they will strike more often.

Unfortunately the HASP flight did not yield very good results. Something in the computer memory system failed and no radiation sensor data was stored. This meant that there was no way of telling how often or where radiation was striking the sensor. However, limited temperature data was recorded by the system validating some of the thermal models. This data is elaborated upon in the Maximum Altitude Results section.

Thermal Studies

Thermal Expansion Results

The thermal expansion study provided a good idea of where the most stress would be developed due to material expansion from thermal loading. As expected, the highest stress levels were at the interfaces between different materials. The maximum displacement due to thermal expansion occurred near the interconnect pins on the package board and was 0.018" as seen in Figure 5-11.

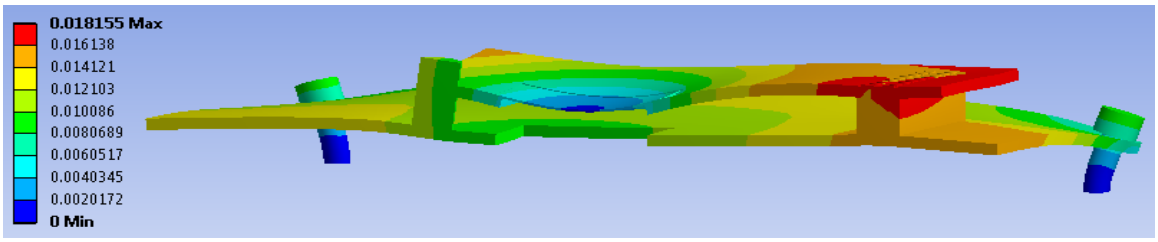

Figure 5-11: Thermal expansion displacement

While all stresses developed were below the yield strengths of each material, of particular interest was the stress developed in the connection pins in the vertical direction. If any connection pins were to fail, that could result in one of the sensor channels not being able to send a signal to the AMP board, and eventually the FPGA. This would

cause the system to never register any radiation strikes for that particular channel. Fortunately the stress developed in the pins was only 73 kPa, well below the yield stress of the phosphor bronze pins, as seen in Figure 5-12.

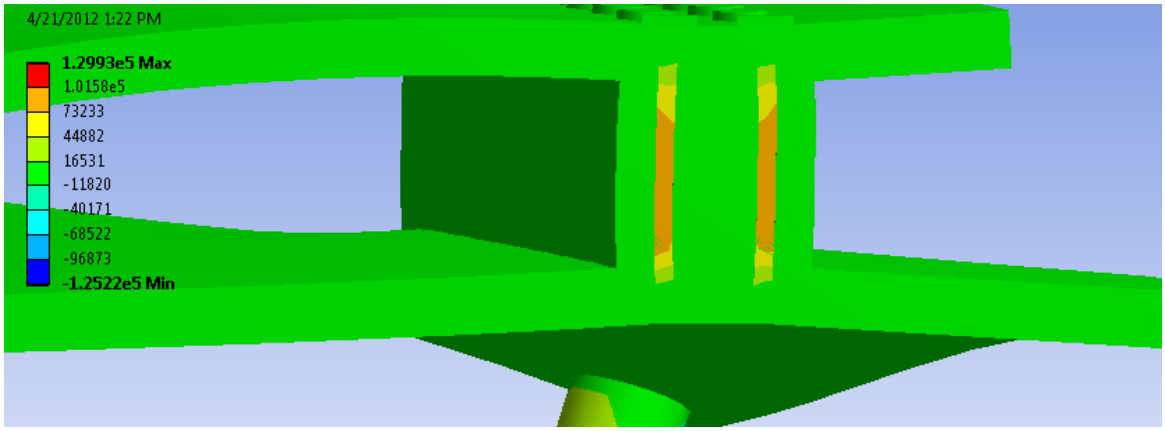

Figure 5-12: Connection pin stresses

HASP Integration Results

The integration model yielded temperature results that were a bit high. However, as the test included two heat generating FPGA boards instead of one, the design group was confident that the one board system would pass the integration requirements. The maximum temperature in Kelvin, experienced by the two FPGA boards can be seen in Figure 5-13. While the maximum temperature of 373.3 K, or 103 °C, was quite warm, it was still within the allowable operating temperature of the FPGA at 120 °C.

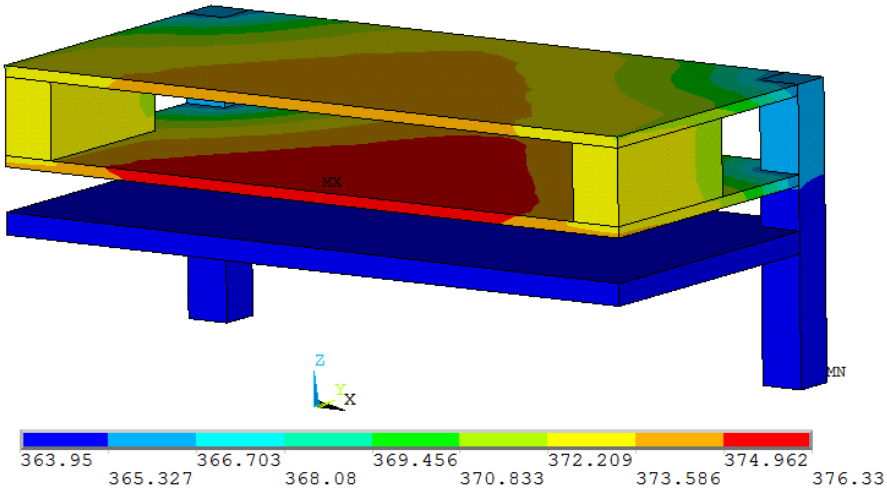

Figure 5-13: 50°C integration test results after 1 hour

As expected, the test payload had no trouble maintaining an acceptable temperature during the cold portion of the integration test. After one hour of being subjected to -60°C temperatures, a minimum temperature of 22°C, 295 K, was shown in the FPGA boards, as seen in Figure 5-14. This was well above the minimum operating temperature of -50°C for the FPGA.

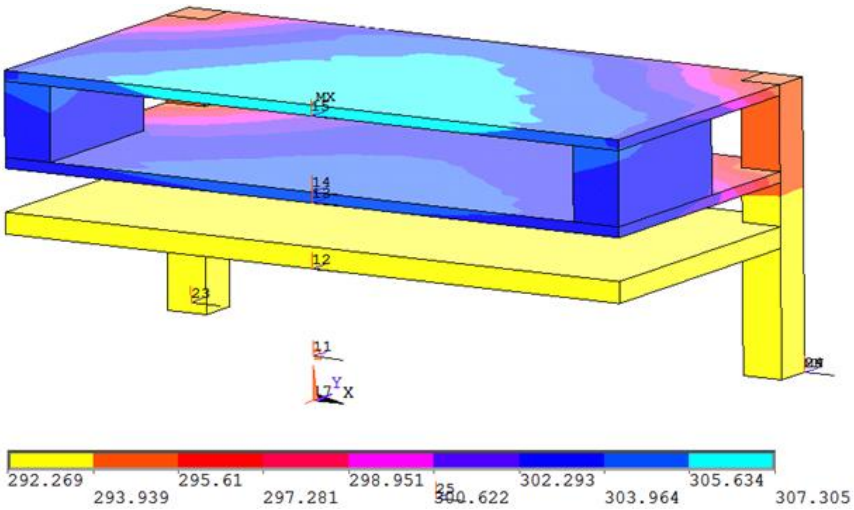

Figure 5-14: -60°C integration test temperature results after 1 hour

Maximum Altitude Results

The most critical results of the thermal analyses were from the maximum altitude tests. As previously mentioned, the maximum amount of solar energy would be hitting the payload for up to ten hours. Both a steady state and then a transient analysis were run with the same loading and meshing as described in the THERMAL ANALYSES chapter. The temperature results, in Kelvin, can be seen in Figure 5-15 for the entire structure, and Figure 5-16, for the FPGA board and aluminum support bushings.

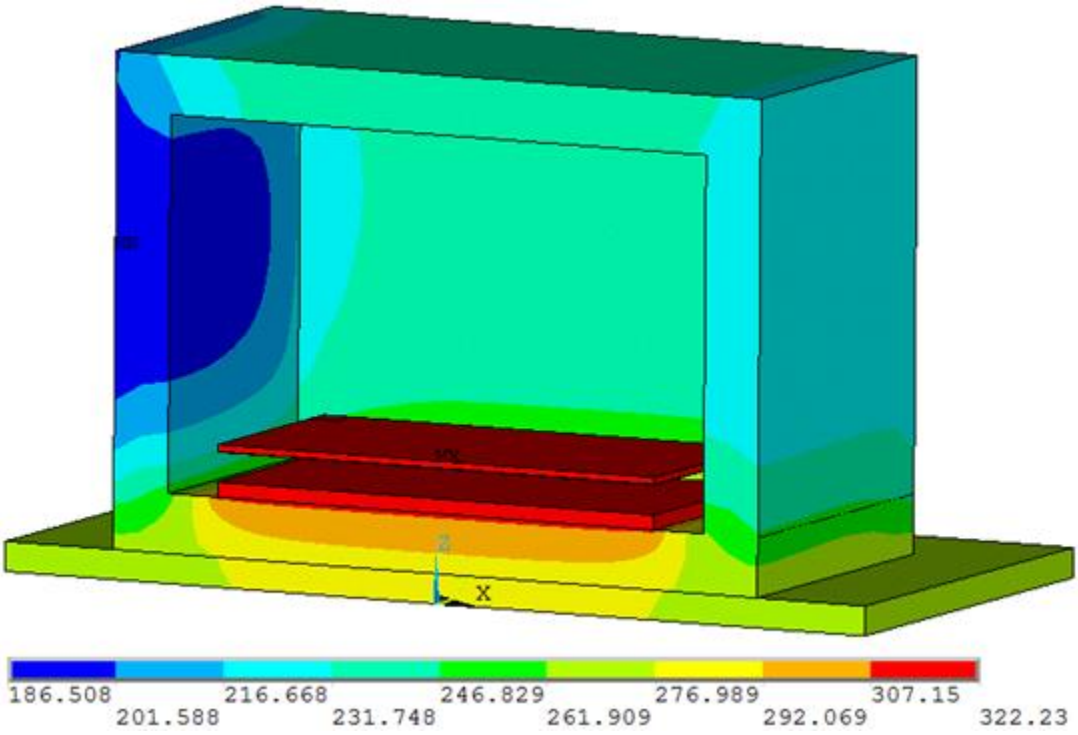

Figure 5-15: Max Altitude steady state temperature results in degrees Kelvin

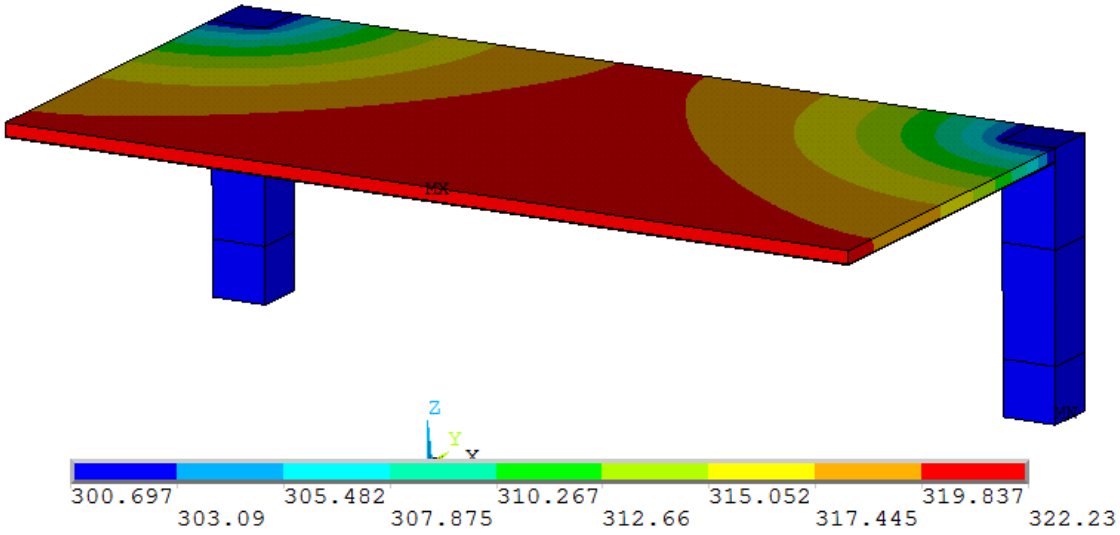

Figure 5-16: Max altitude steady state FPGA temperature distribution in degrees Kelvin

The maximum temperature result of 322.2 K, or 49°C, was very encouraging. As previously mentioned, initial temperature results were roughly twice as high without the use of the copper ground planes in the FPGA structure. The use of aluminum support bushings also helped with temperature management and the temperature distribution shows a thermal gradient that supports the theory. Notice the cooler temperature regions radiating outward from the support bushings in Figure 5-16. Further support of the aluminum bushings directing heat flow out the bottom of the structure can be seen by looking at the temperature distribution of the bottom of the structure in Figure 5-17. The effect of the copper heat sink can also be seen. The central region of the PVC mount plate is at a higher temperature than the outer edges due to the increased transfer of thermal energy from the heat sink.

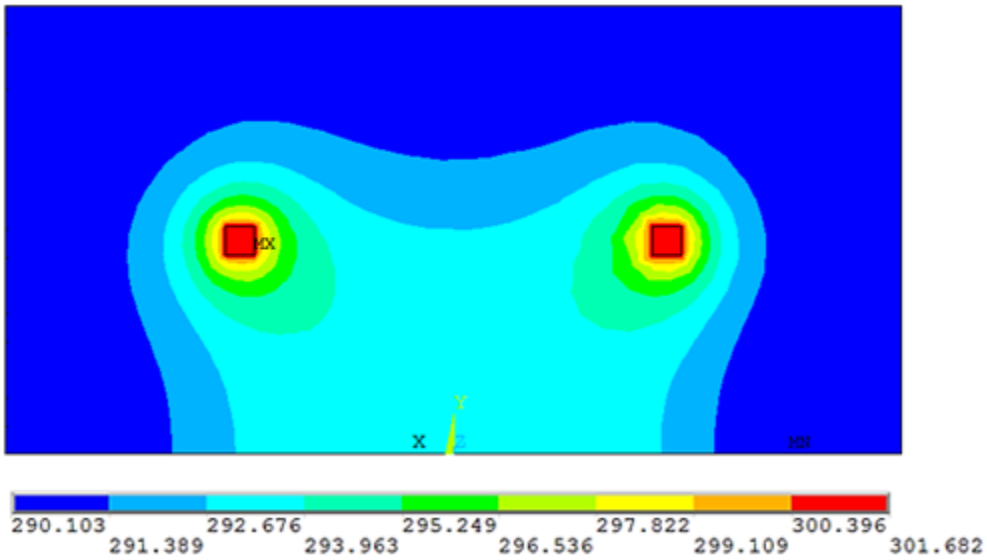

Figure 5-17: Max altitude steady state temperature distribution in degrees Kelvin, bottom view

The results of the maximum altitude FEA model were especially exciting as they were the only results that could be compared to actual temperature data. Before the HASP, flight, a single thermocouple was fixed to the FPGA processor in order to monitor and record the temperature. The results saved showed that the FPGA reached a maximum temperature of roughly 50°C, or 323 K. A rough plot of the recorded temperature data sent down from the HASP payload can be seen in Figure 5-18. The sharp spikes and discontinuities are a result of the signal being dropped during the download of information sets. The temperature profile shows a cooling as the structure passes through the cold layer of the atmosphere, recall Figure 2-8, and the subsequent heating as maximum altitude is reached.

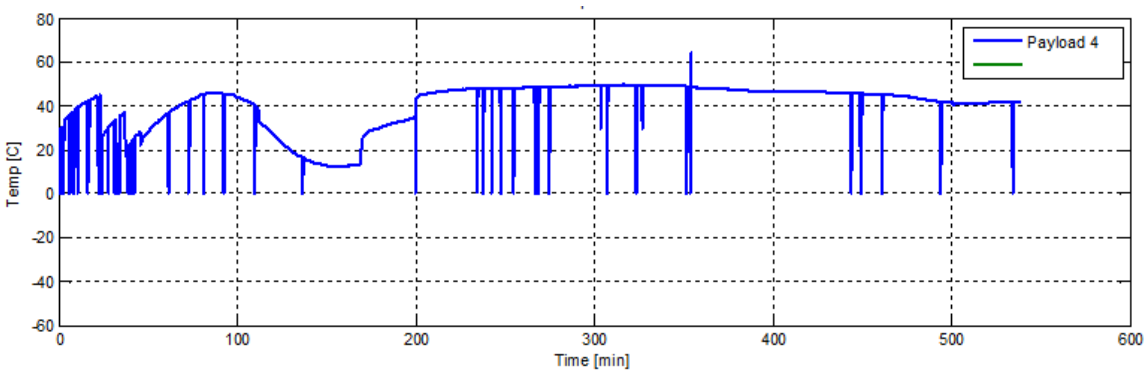

Figure 5-18: Temperature vs. time data from HASP flight

These results show that the maximum altitude thermal model was extremely accurate in predicting maximum temperatures reached in the FPGA structure with an error of less than one percent.

The transient analysis showed temperature results very similar to that of the steady state model. As expected, the maximum temperatures were a bit lower than those of the steady state analysis. The temperature distribution 10 hours into the transient analysis can be seen in Figure 5-19 and Figure 5-20.

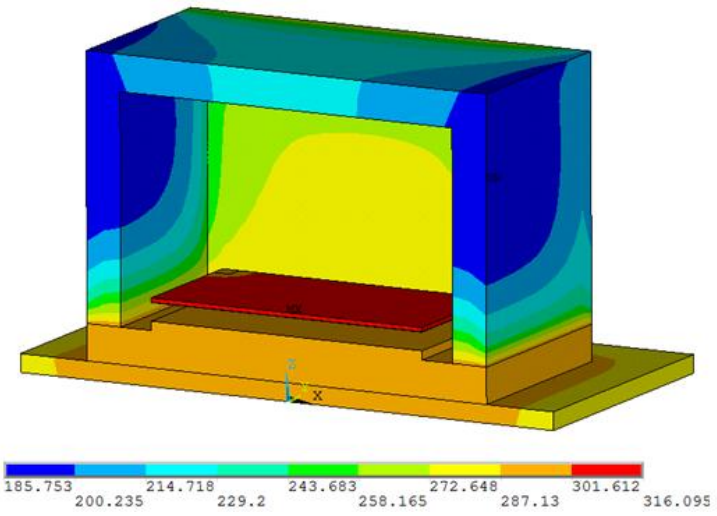

Figure 5-19: Max altitude 10 hour transient temperature results in degrees Kelvin

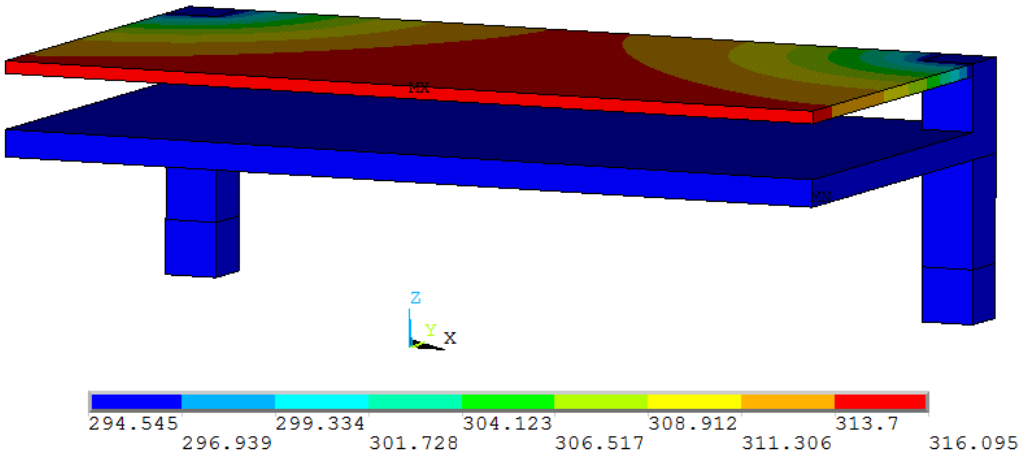

Figure 5-20: Max altitude 10 hour transient FPGA temperature distribution in degrees Kelvin

The transient analysis was very beneficial in that it ensured that the simulation modeled the maximum altitude portion of the actual HASP flight as closely as possible. The transient model also showed that the payload seemed to reach a thermal equilibrium fairly quickly. This can be seen in Figure 5-21 comparing the maximum temperature with time.

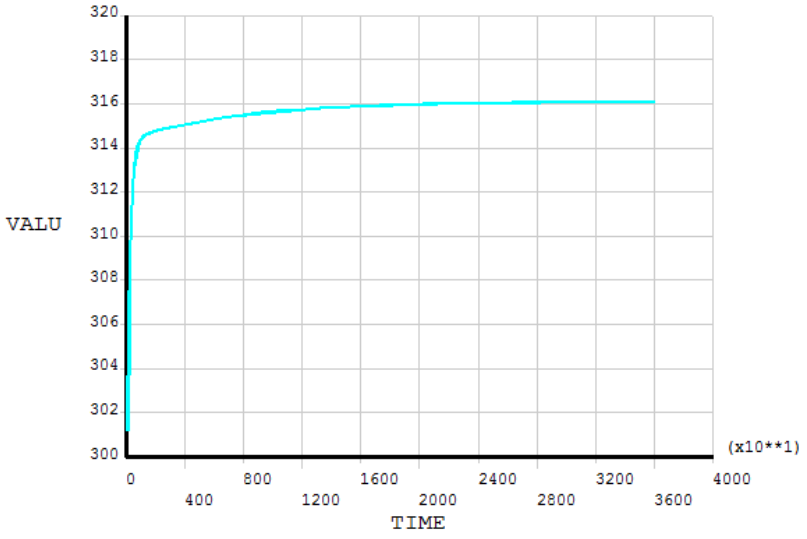

Figure 5-21: Max temperature [K] vs. time [s]

The maximum temperatures from the steady state and transient analyses are compared with the maximum temperature obtained from the thermocouple in Table 5-2.

Table 5-2: Maximum altitude model results comparison

Model	Max Temp [K]	Difference From Measured
Steady State	322.23	0.29%
10 Hour Transient	316.1	2.18%

Temperature Response to Varying Inputs: As previously described, the internal heat generation was varied for the maximum altitude payload analysis. By ranging the internal heat generation from the current value of 1.63W to a maximum of 6W, a trend was found between maximum FPGA temperature, and the heat generation rate. After running the simulation for each individual heat generation rate, the maximum temperature was plotted showing a linear response between heat input, and maximum temperature as seen in Figure 5-22.

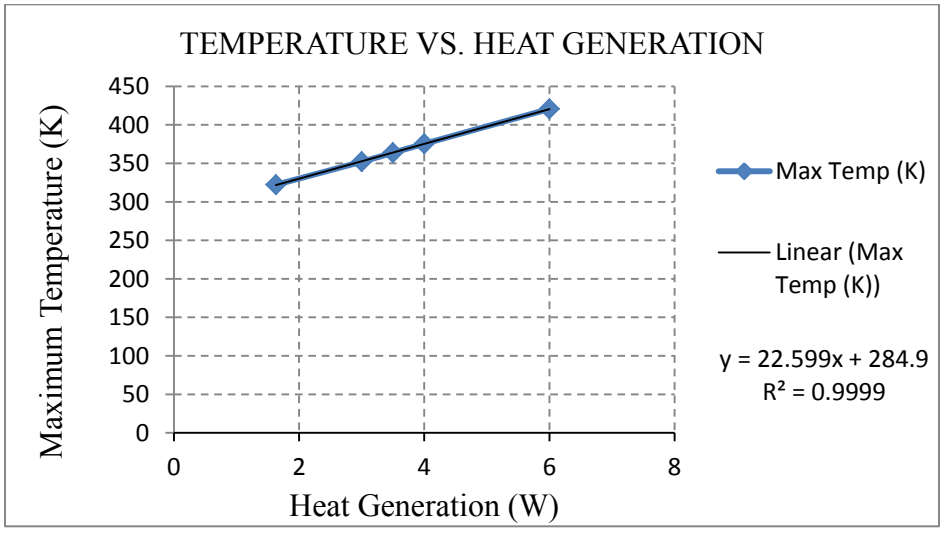

Figure 5-22: Maximum temperature vs. heat generation

By fitting a trend line to the data from Figure 5-22, it was shown that the maximum FPGA temperature went up 22.6 K for each additional watt of heat generation in the steady state, maximum altitude analysis.

As expected, the addition of a gap in the copper ground plane also resulted in an increase in maximum temperature of the FPGA board. This response was also linear showing a 7.1 K increase in maximum temperature for every 0.001 in (1 mil) increase of the ground plane gap. This data, along with the linear fit line can be seen in Figure 5-23.

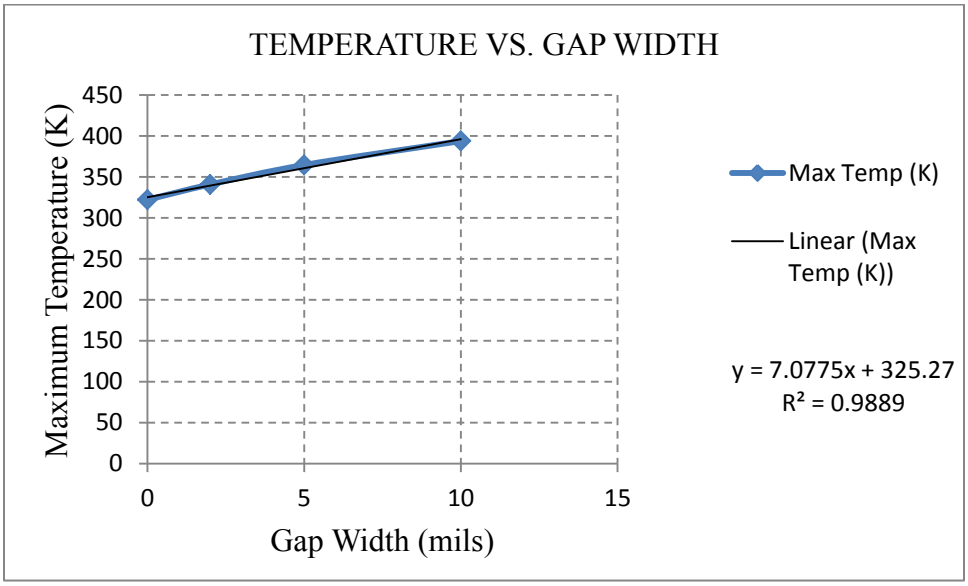

Figure 5-23: Max temperature vs. ground plane gap thickness

The temperature data from this ground plane gap study shows how the copper ground planes help direct heat out of the FPGA board. While increasing the gap does increase the maximum temperature, the total temperature increase is not as significantly affected by gap distance as it is by an increase in heat generation.

Future Work and Recommendations

While the BOREALIS flight and radiation testing at Texas A&M yielded good results for the radiation sensor itself, the HASP flight was not able to record radiation strikes. The most likely explanation for this problem is that the power board was overloaded with too much energy from radiation particles. This caused certain systems to fail during the operation. The power board has since been redesigned and has been lab tested to ensure that it will not fail even under unexpectedly high energy levels. Obviously future test flights are desired in order to see how the sensor performs at high altitude, inside a test payload.

While the vibration studies of this thesis were somewhat limited, they provide for direction in future support structure design. With the harmonic frequencies known, support structures can be tailored to avoid them when implemented in various rocket test platforms. The harmonic loading model will also provide a good starting point in order to apply various forces and frequencies to the RTC sub structure. Future work including more of the structure is possible but node count limitations within the ANSYS software will make additional geometry difficult to mesh. Perhaps shake table testing could also be performed in order to get good comparison data.

The thermal models for this project provided an adequate estimate of various temperature values for given test platforms. Further improvements could be made in order to better simulate the varying convective heat transfer through the atmosphere, but, as previously discussed, the current RTC configuration is in no danger of over cooling itself. However, if future test payloads significantly differ from the one used, new studies

will have to be performed. The current models will provide an excellent starting point for future analyses and provide excellent flexibility in making certain geometry and material property changes.

If the system heat generation is increased significantly, the maximum temperature in the FPGA board will soon exceed the allowable operating temperature. In order to counteract this effect, the rate in which heat is conducted away from the generation source will need to be increased. The rate of thermal conduction would be increased by the addition of copper ground planes to the structure, but the ground planes cannot interfere with the electronic systems functionality. A more effective solution would be to use heat pipes to direct heat away from the heat generation source to the exterior radiating surface of the payload. Careful analysis of the heat pipe would be necessary in order to ensure that enough heat was conducted to the payload exterior. A simple one dimensional conduction analysis could be performed for any necessary heat pipes to ensure adequate heat conduction. Incoming thermal energy from the heat generating device would be conducted through the length of the heat pipe, and then out the exterior. The rate at which thermal energy would leave the heat pipe would be dependent on the exterior surface it connects to and how quickly it could radiate heat out to its surroundings. The current maximum altitude FEA models provide a good simulation of how much thermal energy can be radiated back out to earth, or space depending on orientation and external temperatures.

REFERENCES CITED

ANSYS, Inc. (2011). ANSYS Help.

Benson, T. (2010, July 30). *Earth Atmosphere Model*. Retrieved 2012, from Nasa Glenn Research Center: http://www.grc.nasa.gov/WWW/k-12/airplane/atmosmet.html

Buerkle, T. M. (2012). *Ionizing Radiation Detector for Environmental Awareness in FPGA-Based Flight Computers.*

Hsu, T.-R. (2008). *MEMS and Microsystems.* Hoboken: John Wiley & Sons, Inc.

Hutton, D. V. (2004). *Fundamentals of Finite Element Analysis.* New York: McGraw-Hill Companies Inc.

Incropera, F. P., Dewitt, D. P., Bergman, T. L., & Lavine, A. S. (2007). *Introduction to Heat Transfer.* Hoboken: John Wiley & Sons, Inc.

LSU Department of Physics and Astronomy. (2012). *LSU Space Sciences Group*. Retrieved 2012, from High Altitude Student Platform: http://laspace.lsu.edu/hasp/

LSU Space Sciences Group. (2009, February 17). *HASP Student Payload Interface Manual.* Retrieved 2012, from HASP Technical Documentation: http://laspace.lsu.edu/hasp/documents/public/HASP_Interface_Manual_v21709.pdf

McQuiston, F. C., Parker, J. D., & Spitler, J. D. (2005). *Heating, Ventilating, and Air Conditioning.* Danvers: John Wiley & Sons, Inc.

Montana Space Grant Consortium. (2011). *BOREALIS Programs*. Retrieved from Montana Space Grant Consortium: http://spacegrant.montana.edu/BOREALIS.html

NASA Earth Obsevatory. (n.d.). *Solar Radiation and Climate Experiment*. Retrieved May 20, 2012, from NASA Earth Observatory: http://earthobservatory.nasa.gov/Features/SORCE/sorce.php

NASA Goddard Space Flight Center. (2005). General Environmental Verification Standard. *GSFC Technical Standards*, 2.4-20 - 2.4-21.

Texas A&M University. (2012). *Cyclotron Institute* . Retrieved 2012, from Cyclotron Institute Texas A&M University: http://cyclotron.tamu.edu/

APPENDICES

APPENDIX A

SOLAR INCIDENCE ANGLE CALCULATIONS

Solar Incidence:

Calculated for a Launch in Florida on September 10th

$d_n := 253$ Day of the year (Sept 10th in this case)

$\delta := 23.45\text{deg} \cdot \sin\left[360 \cdot \frac{(d_n + 284)}{365}\text{deg}\right]$ Solar declination angle $\delta = 4.216 \cdot \text{deg}$

$l := 34\text{deg}$ N Global Lattitude

$\text{long} := 104\text{deg}$ W Global Longitude

Time Adjustment for standard time zone vs. actual location:

LST = 9:30 AM - (LL-LS)*4min/deg + EOT

LL = location longitude = 34 deg
LS = standard longitude = 105 deg for mountain std time

$N := (d_n - 1) \cdot \left(\frac{360\text{deg}}{365}\right)$ +

$EOT := [229.2 \cdot (0.000075 + .001868 \cdot \cos(N) - .032077 \sin(N) - .014615 \cdot \cos(2 \cdot N) - .04089 \cdot \sin(2 \cdot N))] \cdot \text{min}$

$EOT = 2.777 \cdot \text{min}$

$LST := 9.5\text{hr} - (\text{long} - 105\text{deg}) \cdot 4\frac{\text{min}}{\text{deg}} + EOT$ Local standard time, adjusts for location in standard time zone

$h := 15\frac{\text{deg}}{\text{hr}} \cdot (LST - 12\text{hr})$

Solar time angle. Calculated as the difference between noon and the hour of the day in terms of a 360 deg rotation for a day. Before noon would be a negative angle and after noon would be a positive angle.
(i.e. the angle the earth has rotated at that time, minus 180deg) zero degrees corresponds with noon.

$h = -35.806 \cdot \text{deg}$

-35.806 deg corresponds to
9:30AM MST
when max altitude is reached

$\beta := \cos(l) \cdot \cos(h)\cos(\delta) + \sin(l) \cdot \sin(\delta)$ Solar altitude angle

$\beta = 40.774 \cdot \text{deg}$

$a := 0.2$ Absorptivity of exterior paint

$G := 1368\frac{W}{m^2}$ Incident solar energy at outer atmosphere

For ease of calculations, assume insulation faces are oriented along the cardinal directions. 1 face normal vector points due north, one points due east etc.

TOP FACE:

$\theta_t := \text{acos}(\sin(\beta))$

$\theta_t = 49.226 \cdot \text{deg}$ Solar incidence angle for top surface

$F_t := \cos(\theta_t) = 0.653$ Radiation Form Factor

$Q_t := F_t \cdot G$

$Q_t = 893.409 \cdot \frac{W}{m^2}$ **Incident Radiation on Top Face**

NORTH FACE:

$\psi_N := 0\text{deg}$ Surface facing direction measured clockwise from North.

$$\phi := \text{acos}\left(\frac{\sin(\delta)\cdot\cos(l) - \cos(\delta)\cdot\sin(l)\cdot\cos(h)}{\cos(\beta)}\right)$$

$\phi = 121.115 \cdot \text{deg}$ Solar azimuth angle clockwise from North (Does not depend on the face orientation, only the sun's orientation)

$\gamma_N := |\phi - \psi_N|$

$\gamma_N = 121.115 \cdot \text{deg}$ Surface solar azimuth angle. Angle between the solar azimuth and the surface facing direction.

$\theta_N := \text{acos}(\cos(\beta)\cdot\cos(\gamma_N))$

$\theta_N = 113.038 \cdot \text{deg}$ Solar incidence angle for NORTH surface

$F_N := \cos(\theta_N) = -0.391$ Radiation Form Factor, use value of 0 if negative

$Q_N := 0 \cdot F_N \cdot G$

$Q_N = 0 \cdot \frac{W}{m^2}$ **Incident Radiation on NORTH Face**

EAST FACE:

$\psi_E := 90deg$ Surface facing direction measured clockwise from North.

$\gamma_E := |\phi - \psi_E|$

$\gamma_E = 31.115 \cdot deg$ Surface solar azimuth angle. Angle between the solar azimuth and the surface facing direction.

$\theta_E := \text{acos}(\cos(\beta) \cdot \cos(\gamma_E))$

$\theta_E = 49.583 \cdot deg$ Solar incidence angle for EAST surface

$F_E := \cos(\theta_E) = 0.648$ Radiation Form Factor

$Q_E := F_E \cdot G$

$Q_E = 886.929 \cdot \frac{W}{m^2}$ **Incident Radiation on EAST Face**

SOUTH FACE:

$\psi_S := 180deg$ Surface facing direction measured clockwise from North.

$\gamma_S := |\phi - \psi_S|$

$\gamma_S = 58.885 \cdot deg$ Surface solar azimuth angle. Angle between the solar azimuth and the surface facing direction.

$\theta_S := \text{acos}(\cos(\beta) \cdot \cos(\gamma_S))$

$\theta_S = 66.962 \cdot deg$ Solar incidence angle for SOUTH surface

$F_S := \cos(\theta_S) = 0.391$ Radiation Form Factor

$Q_S := F_S \cdot G$

$Q_S = 535.353 \cdot \frac{W}{m^2}$ **Incident Radiation on SOUTH Face**

WEST FACE:

$\psi_W := 270deg$ Surface facing direction measured clockwise from North.

$\gamma_W := |\phi - \psi_W|$

$\gamma_W = 148.885 \cdot deg$ Surface solar azimuth angle. Angle between the solar azimuth and the surface facing direction.

$\theta_W := acos(cos(\beta) \cdot cos(\gamma_W))$

$\theta_W = 130.417 \cdot deg$ Solar incidence angle for WEST surface

$F_W := cos(\theta_W) = -0.648$ Radiation Form Factor, use value of 0 if negative

$Q_W := 0F_W \cdot G$

$Q_W = 0 \cdot \frac{W}{m^2}$ **Incident Radiation on WEST Face**

APPENDIX B

CONVECTION PROPERTY CALCULATIONS

Free Convection Film Coefficient Calculation

$\beta := .0031\,K^{-1}$ — Volumetric thermal expansion coefficient

$l := .11176\ m$ — Payload side wall length

$Pr := .703$ — Prandtl Number

$v := 17 \cdot 10^{-6}\ \frac{m^2}{s}$ — Kinematic Viscosity

$\alpha := 26 \cdot 10^{-6}\ \frac{m^2}{s}$ — Thermal Diffusivity

$k := 28 \cdot 10^{-3}\ \frac{W}{m \cdot K}$ — thermal conductivity

$Ra := \frac{9.8 \cdot \beta \cdot (323 - 288) \cdot l^3}{v \cdot \alpha} = 3.358 \times 10^6$ — Raleigh Number
Equation 9.25 Incropera

$Ra_c := 10^9$ — Critical value where flow transitions from laminar to turbulent. If Ra < Rac, the flow is laminar.

$$Nu := .68 + \frac{.670 \cdot Ra^{.25}}{\left[1 + \left(\frac{.492}{Pr}\right)^{\frac{9}{16}}\right]^{\frac{4}{9}}}$$

Nusselt Number
Equation 9.27 Incropera

$Nu = 22.669$

$h := \frac{k}{l} \cdot Nu$

$h = 5.679$ W/m^2*K

APPENDIX C

ANSYS INPUT CODES

2D Modal Analysis

```
!BOTTOM LINE KEYPTS (AMP BOARD)
/PREP7

K,1,0,0
K,2,.082,0
K,3,.098
K,4,.182
K,5,.198
K,6,.502
K,7,.518
K,8,.602
K,9,.618
K,10,2.5975
K,11,2.7225
K,12,3.802
K,13,3.818
K,14,3.902
K,15,3.918
K,16,4
K,69,    0.0425
K,70,    0.2375
K,71,    3.7625
K,72,    3.9575
K,73,    2.56
K,74,    2.76


!BOTTOM LINES (AMP BOARD)

L,1,69
L,69,2
L,2,3
L,3,4
L,4,5
L,5,70
L,70,6
L,6,7
L,7,8
L,8,9
L,9,73
L,73,10

L,11,74
L,74,71
L,71,12
L,12,13
L,13,14
L,14,15
L,15,72
L,72,16
```

```
!TOP KPTS (AMP BOARD)

K,      17,     0       ,0.062
K,      18,     0.0425  ,0.062
K,      19,     0.082   ,0.062
K,      20,     0.098   ,0.062
K,      21,     0.182   ,0.062
K,      22,     0.198   ,0.062
K,      23,     0.2375  ,0.062
K,      24,     0.4625  ,0.062
K,      25,     0.502   ,0.062
K,      26,     0.518   ,0.062
K,      27,     0.602   ,0.062
K,      28,     0.618   ,0.062
K,      29,     0.6575  ,0.062
K,      30,     2.56    ,0.062
K,      31,     2.5975  ,0.062
K,      32,     2.7225  ,0.062
K,      33,     2.76    ,0.062
K,      34,     3.7625  ,0.062
K,      35,     3.802   ,0.062
K,      36,     3.818   ,0.062
K,      37,     3.902   ,0.062
K,      38,     3.918   ,0.062
K,      39,     3.9575  ,0.062
K,      40,     4       ,0.062

!TOP LINES (AMP BOARD)

L,      17,     18
L,      18,     19
L,      19,     20
L,      20,     21
L,      21,     22
L,      22,     23
L,      23,     24
L,      24,     25
L,      26,     27
L,      28,     29
L,      29,     30
L,      30,     31
L,      32,     33
L,      33,     34
L,      34,     35
L,      35,     36
L,      36,     37
L,      37,     38
L,      38,     39
L,      39,     40

L,      1,      17
L,      16,     40
```

```
!BOTTOM KPTS (PKG BOARD)

K,      41,     0.26    ,0.242
K,      42,     0.4625  ,0.242
K,      43,     0.502   ,0.242
K,      44,     0.518   ,0.242
K,      45,     0.602   ,0.242
K,      46,     0.618   ,0.242
K,      47,     0.6575  ,0.242
K,      48,     2.56    ,0.242
K,      49,     2.5975  ,0.242
K,      50,     2.7225  ,0.242
K,      51,     2.76    ,0.242

!BOTTOM LINES (PKG BOARD)

L,      41,     42
L,      42,     43
L,      44,     45
L,      46,     47
L,      47,     48
L,      48,     49
L,      50,     51

!TOP KPTS (PKG BOARD)

K,      52,     0.26    ,0.304
K,      53,     0.502   ,0.304
K,      54,     0.518   ,0.304
K,      55,     0.602   ,0.304
K,      56,     0.618   ,0.304
K,      57,     1.61    ,0.304
K,      58,     1.61    ,0.292
K,      59,     2.4     ,0.292
K,      60,     2.4     ,0.304
K,      61,     2.56  ,0.304
K,      62,     2.5975  ,0.304
K,      63,     2.7225  ,0.304
K,      64,     2.76    ,0.304

!EPOXY PTS

K,      79,     1.59    ,0.304
K,      80,     1.55    ,0.304

K,      81,     1.55    ,0.313
K,      82,     1.59    ,0.313
K,      83,     1.561   ,0.313
K,      84,     1.579   ,0.313

K,      85,     2.42    ,0.304
K,      86,     2.46    ,0.304
K,      87,     2.42    ,0.313
```

```
K,      88,     2.431   ,0.313
K,      89,     2.449   ,0.313
K,      90,     2.46    ,0.313

!TOP LINES (PKG BOARD)

L,      52,     53
L,      53,     54
L,      54,     55
L,      55,     56
L,      56,     80
L,      80,     79
L,      79,     57
L,      57,     58
L,      58,     59
L,      59,     60

L,      60,     85
L,      85,     86
L,      86,     61
L,      61,     62
L,      63,     64

L,      41,     52
L,      51,     64

!EPOXY LINES
L,      80,81
L,81,83
L,83,84
L,84,82
L,82,79

L,85,87
L,87,88
L,88,89
L,89,90
L,90,86

!SENSOR KPTS & LINES

K,      65,     1.611,  0.292
K,      66,     1.611,  0.304
K,      67,     2.399,  0.304
K,      68,     2.399,  0.292

!EPOXY
K,      91,     1.66,   0.304
K,      92,     1.7,    0.304
K,      93,     1.66,   0.313
K,      94,     1.671,  0.313
K,      95,     1.689,  0.313
K,      96,     1.7,    0.313
```

```
K,      97,     2.35    ,0.304
K,      98,     2.31    ,0.304
K,      99,     2.31    ,0.313
K,      100,2.35,0.313
K,      101,2.321       ,0.313
K,      102,2.339       ,0.313

L,      65,     66
L,      66,     91
L,      91,     92
L,      92,     98
L,      98,     97
L,      97,     67
L,      67,     68
L,      68,     65

L,      91,     93
L,      93,94
L,      94,95
L,      95,96
L,      96,92

L,      98,99
L,      99,101
L,      101,102
L,      102,100
L,      100,97

!VERTICAL BOLT LINES

L,      2,      19
L,      3,      20
L,      4,      21
L,      5,      22
L,      6,      25
L,      7,      26
L,      8,      27
L,      9,      28
L,      24,     42
L,      25,     43
L,      26,     44
L,      27,     45
L,      28,     46
L,      29,     47
L,      30,     48
L,      31,     49
L,      32,     50
L,      33,     51
L,      10,     31
L,      11,     32
L,      12,     35
L,      13,     36
```

```
L,      14,     37
L,      15,     38
L,      43,     53
L,      44,     54
L,      45,     55
L,      46,     56
L,      49,     62
L,      50,     63

!NUT 3/32 IN TALL

K,75,   2.56,   -.09375
K,76,   2.76,   -.09375

L,73,75
L,75,76
L,76,74

!BOLT HEAD 3/32 IN TALL

K,77,   2.56,   .39775
K,78,   2.76,   .39775

L,61,77
L,77,78
L,78,64

!WIRES
K,      103,    1.625,  0.368
K,      104,    1.625,  0.35
K,      105,    2.385,  0.368
K,      106,    2.385,  0.35

LARC, 83, 95, 103
LARC, 84, 94, 104
LARC, 101, 89, 105
LARC, 102, 88, 106

!AMP BOARD AREAS
AL, 1, 2, 95, 22, 21, 41
AL, 4, 97, 24, 96
AL, 6, 7, 99, 28, 27, 26, 98
AL, 9, 101, 29, 100
AL, 102, 30, 31, 32, 113, 12, 11
AL, 114, 13, 14, 15, 115, 35, 34, 33
AL, 17, 117, 37, 116
AL, 118, 19, 20, 42, 40, 39

!PIN AREAS
AL, 95, 3, 96, 23
AL, 97, 5, 98, 25
AL, 8, 100, 105, 120, 51, 119, 104, 99
AL, 10, 102, 107, 122, 53, 121, 106, 101
```

```
AL, 16, 116, 36, 115
AL, 18, 118, 38, 117

!PLASTIC AREAS
AL, 103, 28, 104, 44
AL, 105, 29, 106, 45
AL, 107, 30, 108, 46
AL, 109, 32, 110, 48
AL, 111, 33, 112, 49

!PKG AREAS
AL, 65, 43, 44, 119, 50
AL, 120, 45, 121, 52
AL, 124, 49, 66, 64
A,46,47,48,49,62,61,86,85,60,59,58,57,79,80,56

!SENSOR AREA
AL, 77, 84, 83, 82,81, 80, 79, 78

!BOLT AREA
A,75,76,74,11,32,50,63,64,78,77,61,62,49,31,10,73

!EPOXY AREAS
AL, 67, 55, 71, 70, 69, 68
AL, 85, 79, 89, 88, 87, 86
AL, 90, 81, 94, 93, 92, 91
AL, 72, 61, 76, 75, 74, 73

!WIRE AREAS
AL, 74, 134, 92, 133
AL, 69, 132, 87, 131

!ELEMENT TYPES
ET,1,PLANE183,0,,2,,,0
ET,2,CONTA178,,,,,2

!MATERIAL PROPERTIES

!FR4 (orthotropic)
MP,EX, 1,       3.5E6
MP,EY,  1,      3.5E6
MP,EZ,  1,      3.0E6
MP,GXY, 1,      3.1E9
MP,DENS,1,      2.044E-3
MP,PRXY,1,      0.136
MP,PRXZ,1,      0.118
MP,PRYZ,1,      0.118
MP,ALPX,1,      14E-6
MP,ALPY,1,      13E-6
MP,ALPZ,1,      175E-6
MP,MU,1,        0.4

!CU WIRE
```

```
MP,EX, 2,       15.2E6
MP,DENS,2,      9.9E-3
MP,PRXY,2,      0.34
MP,ALPX,2,      10.8E-6

!PLASTIC SUPPORT (SLW BODY)
MP,EX, 3,       1.55E6
MP,DENS,3,      1.86E-3
MP,PRXY,3,      0.3
MP,ALPX,3,      1.386E-4

!CONNECTOR PINS
MP,EX, 4,       16E6
MP,DENS,4,      9.949E-3
MP,PRXY,4,      0.34
MP,ALPX,4,      9.89E-6

!SENSOR
MP,EX, 5,       16.3E6
MP,DENS,5,      2.58E-3
MP,PRXY,5,      0.28
MP,ALPX,5,      1.38E-6
MP,MU,5,        0.38

!Aluminum Bolt
MP,EX, 6,       10.6E6
MP,DENS,6,      3.12E-3
MP,PRXY,6,      0.33
MP,ALPX,6,      11.7E-6

!EPOXY
MP,EX, 7,       300E3
MP,DENS,7,      3.2E-3
MP,PRXY,7,      0.33
MP,ALPX,7,      27.2E-6

!PLASTIC BUSHING (MOLDED POLYAMIDE)
MP,EX, 8,       980E3
MP,DENS,8,      1.63E-3
MP,PRXY,8,      0.42
MP,ALPX,8,      12E-6

!REAL CONSTANTS FOR CONTA178
R,1,-3.25E6,0,,,,
RMORE,1,-0
R,2,-16.3E6,0,,,,
RMORE,2,-0

!LINE SIZING
!PIN ENDS
        LSEL,S,LINE,,3
        LSEL,A,LINE,,5
        LSEL,A,LINE,,23
```

```
        LSEL,A,LINE,,25
        LSEL,A,LINE,,8
        LSEL,A,LINE,,10
        LSEL,A,LINE,,51
        LSEL,A,LINE,,53
        LSEL,A,LINE,,36
        LSEL,A,LINE,,16
        LSEL,A,LINE,,38
        LSEL,A,LINE,,18
!SENSOR EDGES
        LSEL,A,LINE,,77
        LSEL,A,LINE,,83
!EPOXY
        LSEL,A,LINE,,67,76
        LSEL,A,LINE,,85,94

LESIZE,ALL,0.0005

!PIN EDGES
        LSEL,S,LINE,,95,102
        LSEL,A,LINE,,104,107
        LSEL,A,LINE,,115,122
        LESIZE,ALL,0.002

!REST
        LSEL,ALL
        LESIZE,ALL,0.004

!MESHING

!CONTACT ELEMENTS
        !PKG SHELF
                MAT,1
                REAL,1
                TYPE,2
                LMESH,58
        !SENSOR BOTTOM
                MAT,5
                REAL,2
                TYPE,2
                LMESH,84

        !PKG BOTTOM
                !MAT,1
                !REAL,1
                !TYPE,2
                !LMESH,47
        !AMP TOP
                !MAT,1
                !REAL,1
                !TYPE,2
                !LMESH,31
```

```
!PLANE ELEMENTS
        !FR4 BOARDS
                MAT,1
                REAL,1
                TYPE,1
                AMESH,1,8
                AMESH,20,23
        !CU WIRE
                MAT,2
                TYPE,1
                AMESH,30,31
        !PLASTIC SUPPORT
                MAT,3
                AMESH,15,17
        !PINS
                MAT,4
                AMESH,9,14
        !SENSOR
                MAT,5
                AMESH,24
        !AL BOLT
                MAT,6
                AMESH,25
        !EPOXY
                MAT,7
                AMESH,26,29
        !PLASTIC BUSHING
                MAT,8
                AMESH,18,19

!DOF CONSTRAINTS
DL,2,,UY,0
DL,3,,ALL,0
DL,5,,ALL,0
DL,6,,UY,0
DL,15,,UY,0
DL,16,,ALL,0
DL,18,,ALL,0
DL,19,,UY,0

FINISH

/SOLU
ANTYPE,MODAL
MODOPT,LANB,5


MXPAND,5
SOLVE
FINISH
```

3D Modal Analysis

```
/FILENAM,Half_Modal_3,1
/CWD,'D:\Temp\AL_ANSYS'

/PREP7
/pnum,volu,1

!!!!!!!!!! PARAMETERS !!!!!!!!!!!!

t1 = 0.062                          ! FR4 thickness
t2 = 0.012                          ! Sensor thickness
senlen = 0.79                       ! sensor length
senw = 0.395                        ! sensor half width
h1 = 0.18                           ! SLW connector height
slw_w = .195                        ! SLW WIDTH
slw_l = .85                         ! SLW half length
lp = 2.5                            ! PKG length
wp = 1.0                            ! PKG half width
la = 4                              ! AMP length
wa = 2                              ! AMP half width
gap = 0.03125                       ! gap between PKG and SLW
htot = 2*t1+h1+gap                  ! distance between bottom of AMP and top of PKG
cblength = 0.25                     ! corner bolt length
tpinlength = 0.177                  ! top pin length
boltdia = 0.125                     ! bolt radius

!!!! Coord Systems !!!!!

clocal,11,CART, 0,0,t1              !! origin on top of AMP board
clocal,12,CART, 0,0,h1              !! origin on top of SLW connector
clocal,13,CART, 0,0,gap             !! origin on bottom of PKG board
clocal,14,CART, 0,0,t1              !! origin on top of PKG board


!!!!!!!!!!!!!!!!!!!!!!!!!!!!!!!!
!!!!!!!!! GEOMETRY !!!!!!!!!!!!
!!!!!!!!!!!!!!!!!!!!!!!!!!!!!!!!

csys,0
blc4,0,0,la,wa,t1                  ! AMP board
cm,AMP,volu                         ! creates AMP component
vsel,none                           ! deselects all volumes

csys,11
wpcsys
blc4,0.4625,0,0.195,0.85,h1         ! SLW connector body
cm,SLW,volu                         ! creates SLW component
vsel,none                           ! deselects all volumes

csys,13
wpcsys
```

```
blc4,0.26,0,lp,wp,t1                    ! PKG board
cm,PKG,volu                             ! creates PKG component
vsel,none                               ! deselects all volumes


!!!!!!!!! CREATE THRU HOLE !!!!!!!!!!!!!!
csys,0
wpcsys
blc4,1.645,0,0.71,0.355,htot            ! Thru hole volume thru AMP & PKG
cm,thru_hole,volu                       ! creates thru_hole component
vsel,s,volu, ,PKG
vsel,a,volu, ,AMP
cm,FR4,volu                             ! Groups FR4 volumes into a component (this gets deleted
after vsbv command)

allsel,all
vsbv,FR4,thru_hole,,delete,delete    ! subtracts thru hole volume from amp & pkg, deletes vol#4  (THIS
DELETES ALL COMPONENTS)
vsel,s,loc,z,0,t1,1,1                   ! select AMP
cm,AMP,volu                             ! recreates AMP component

csys,13
vsel,s,loc,z,0,t1,1,1                   ! select PKG
cm,PKG,volu                             ! recreates PKG component


!!!!!!!!! CREATE SENSOR AND ITS SHELF IN PKG !!!!!!!!!

vsel,none                               ! deselects all volumes
csys,14
wpcsys
blc4,1.61,0,0.79,0.395,-0.012           ! sensor volume
cm,SENSOR,volu                          ! creates SENSOR component
allsel,all
vsbv,PKG,SENSOR,,delete,keep            ! creates shelf for sensor

csys,13
vsel,s,loc,z,0,t1,1,1                   ! select PKG & SENSOR
vsel,u,volu, ,SENSOR                    ! unselects SENSOR
cm,PKG,volu                             ! recreates PKG component
allsel,all


!!!!!!!! CREATE TOP PINS AND HOLES !!!!!!!!!!

csys,14
wpcsys
vsel,none                                   ! deselects all volumes
blc4,0.502,0.092,0.016,0.025,-tpinlength    ! genereates 1st whole pin in PKG
vgen,8,all, , ,0,0.1,0,0,1,0                ! generates the 1st row of whole pins in PKG
blc4,0.502,0,0.016,0.0125,-tpinlength       ! creates 1st half pin in PKG
vgen,2,all, , ,0.1,0,0,0,1,0                ! generates the 2nd row of pins in PKG
cm,TPINS,volu                               ! creates top pins (TPINS) component
```

```
allsel,all
vsbv,PKG,TPINS, ,delete,keep                    ! subtracts top pin volumes from PKG
vsbv,SLW,TPINS, ,delete,keep                    ! subtracts top pin volumes from SLW

csys,13
vsel,s,loc,z,0,t1,1,1                           ! select PKG
vsel,u,volu, ,SENSOR
cm,PKG,volu                                     ! recreates PKG component
csys,11
vsel,s,loc,z,0,h1,1,1                           ! selects SLW and top pins
cm,SLW,volu                                     ! recreates SLW component

!!!!!!! CREATE END SUPPORT BOLT !!!!!!!!!!

csys,0
clocal,60,0,0,0,-.125
wpcsys
vsel,none

blc4,.26+lp,0,-boltdia,boltdia,htot+.25

cm,BOLT,volu                                    ! creates bolt component
clocal,61,0, .26+lp-boltdia,0,0, 0,0,90

allsel,all
vsbv,PKG,BOLT, ,delete,keep                     ! subtracts BOLT volumes from PKG
allsel,all
csys,13
vsel,s,loc,z,0,t1,1,1                           ! select PKG
vsel,u,volu, ,SENSOR                            ! unselects SENSOR
cm,PKG,volu                                     ! recreates PKG component

allsel,all
vsbv,AMP,BOLT, ,delete,keep                     ! subtracts BOLT volumes from AMP
csys,0
vsel,s,loc,z,0,t1,1,1                           ! selects AMP and pins
cm,AMP,volu                                     ! recreates AMP component

!!!!!!! CREATE CORNER BOLTS !!!!!!!!!!!!!!!!!!!!!!!!!!

csys,11
wpcsys
vsel,none
blc4,0,wa-.125,.125,.125,-cblength          ! creates corner bolt
vgen,2,all, , ,4-.125,0,0,0,1,0                 ! creates 2nd corner bolt
cm,CBOLTS,volu                                          ! creates bolts component (CBOLTS)

allsel,all
vsbv,AMP,CBOLTS, ,delete,keep                   ! subtracts CBOLTS volumes from AMP
csys,0
vsel,s,loc,z,0,t1,1,1                           ! selects AMP and pins
cm,AMP,volu                                     ! recreates AMP component
```

```
allsel,all
vglue,all

!! RECREATE COMPONENETS !!
csys,14
clocal,15,CART,1.61,0,0, 0,0,90          ! creates coord. plane on left edge of sensor
clocal,16,CART,0,0,0.035, 0,0,0          ! creates coord. plane on left edge of sensor hole
csys,15
clocal,17,CART,0,0,senlen, 0,0,0         ! creates coord. plane on right edge of sensor
csys,14
clocal,18,CART,2.355,0,0, 0,0,90         ! creates coord. plane on left edge of sensor hole
csys,0
clocal,19,cart,0,0.355,0, 0,90,0         ! creates plane @ inside edge of sensor hole
clocal,20,cart,0,0,-0.04, 0,0,0          ! creates plane @ inside edge of sensor
csys,0
clocal,21,CART,0.502,0,0, 0,0,90         ! creates coord. plane on left outer face of TPINS (positive z to
the right)
clocal,22,CART,0,0,0.016, 0,0,0          ! creates coord. plane on left inner face of TPINS
clocal,23,CART,0,0,0.084, 0,0,0          ! creates coord. plane on right inner face of TPINS
clocal,24,CART,0,0,0.016, 0,0,0          ! creates coord. plane on right outer face of TPINS

seltol,1e-8

csys,12
vsel,s,loc,z,0,gap
cm,TPINS,volu                            ! top pins
csys,0
vsel,s,loc,z,0,t1
csys,21
vsel,u,loc,z,0,.016
csys,23
vsel,u,loc,z,0,.016
cm,AMP,volu                              ! amp

csys,11
vsel,s,loc,z,0,h1
vsel,r,loc,y,0,slw_l
csys,16
vsel,u,loc,z,0,10
cm,SLW,volu                              ! SLW
csys,0
vsel,s,loc,y,1.5,2
cm,CBOLTS,volu                                   ! corner bolts
csys,15
vsel,s,loc,z,0,senlen
vsel,u,volu,,amp
cm,SENSOR,volu

csys,0
clocal,25,0, .125,1.875,0, 0,0,90
csys,0
clocal,26,0, 3.875,1.875,0, 0,0,90
```

```
csys,11
clocal,27,0, .4625,0,0, 0,0,90
clocal,28,0, 0,0,slw_w

csys,13
vsel,s,loc,z,0,t1
vsel,u,volu,,sensor
cm,pkg,volu                                    ! package board

csys,61
vsel,s,loc,z,0,boltdia
cm,BOLT,volu                                   ! support bolt

allsel,all
save,presplit,model

finish
/prep7

!! SPLIT UP AMP !!
vsel,s,volu,,amp
!csys,25
!wpcsys
!vsbw,amp, ,delete
csys,28
clocal,30,0, 0,0,t1
csys,61
clocal,31,0, 0,0,boltdia
csys,25
clocal,32,0, 0,0,-.5, 0,90,0
csys,0
clocal,33,0, -.5,slw_l,0, 0,90,0
csys,27
clocal,50,0, 0,0,-t1
csys,0
clocal,40,0, -.5,boltdia,0, 90,,90


csys,28
wpcsys
vsbw,all, ,delete
csys,16
wpcsys
vsbw,all, ,delete
csys,18
wpcsys
vsbw,all, ,delete
csys,31
wpcsys
vsbw,all,,delete
csys,61
wpcsys
vsbw,all,,delete
```

```
csys,26
wpcsys
vsbw,all,,delete
csys,27
wpcsys
vsbw,all,,delete

csys,33
wpcsys
vsbw,all,,delete
csys,32
wpcsys
vsbw,all,,delete

csys,19
wpcsys
vsbw,all,,delete

csys,25
wpcsys
vsbw,all,,delete

csys,18
vsel,r,loc,z,0,2
csys,19
vsel,r,loc,z,0,1
csys,31
clocal,38,0, 0,boltdia,0, 0,90,0
wpcsys
vsbw,all,,delete

csys,0
vsel,s,loc,z,0,t1

cm,AMP,volu

!! SPLIT TPINS !!!!!!!!!!!!!!!
vsel,s,volu,,tpins
csys,12
wpcsys
vsbw,all,,delete
csys,13
wpcsys
vsbw,all,,delete

cm,TPINS,volu

!! SPLIT PKG !!!!!!!!!!!!!!! free mesh all of it !!
vsel,s,volu,,pkg

csys,15
clocal,40,0, 0,0,-t1
csys,17
```

```
clocal,41,0, 0,0,t1
csys,16
clocal,34,0, 0,senlen/2,0, 0,90,0
csys,34
clocal,35,0, 0,0,-t1

csys,41
wpcsys
vsbw,all,,delete
csys,40
wpcsys
vsbw,all,,delete
csys,35
wpcsys
vsbw,all,,delete

csys,27
wpcsys
vsbw,all,,delete
csys,28
wpcsys
vsbw,all,,delete

csys,41
vsel,r,loc,z,0,1
csys,38
wpcsys
vsbw,all,,delete
csys,61
wpcsys
vsbw,all,,delete

csys,13
vsel,s,loc,z,0,t1
vsel,u,volu,,tpins
vsel,u,volu,,sensor

cm,PKG,volu

allsel,all

!! SPLIT SENSOR !!!!!!!!!!!!!!!!!!!
vsel,s,volu,,sensor
csys,16
wpcsys
vsbw,all,,delete

csys,18
wpcsys
vsbw,all,,delete

csys,19
wpcsys
```

```
vsbw,all,,delete

cm,SENSOR,volu

!! SPLIT BOLTS !!!!!!!!!!!!!!!!!!!!!!
vsel,s,volu,,cbolts
csys,0
wpcsys
vsbw,all,,delete
cm,cbolts,volu

vsel,s,volu,,bolt
csys,0
wpcsys
vsbw,all,,delete
csys,11
wpcsys
vsbw,all,,delete
csys,13
wpcsys
vsbw,all,,delete
csys,14
wpcsys
vsbw,all,,delete
cm,bolt,volu

allsel,all
save,geo1,model

!!!!!!!!!!!! MATERIAL PROPERTIES !!!!!!!!!!!!!!!!

!!! add Tref to mps for thermal calcs!!!!!!!!!!!!

finish

/prep7
!FR4 (orthotropic)
MP,EX, 1,       3.5E6
MP,EY,  1,      3.5E6
MP,EZ,  1,      3.0E6
MP,GXY, 1,      3.1E9
MP,GYZ, 1,      3E9
MP,GXZ, 1,      3E9
MP,DENS,1,      2.044E-3
MP,PRXY,1,      0.136
MP,PRXZ,1,      0.118
MP,PRYZ,1,      0.118
MP,ALPX,1,      14E-6
MP,ALPY,1,      13E-6
MP,ALPZ,1,      175E-6
MP,MU,1,        0.4

!PLASTIC SUPPORT (SLW BODY)
```

```
MP,EX, 2,         1.55E6
MP,DENS,2,        1.86E-3
MP,PRXY,2,        0.3
MP,ALPX,2,        1.386E-4

!CONNECTOR PINS
MP,EX, 3,         16E6
MP,DENS,3,        9.949E-3
MP,PRXY,3,        0.34
MP,ALPX,3,        9.89E-6

!SENSOR
MP,EX, 4,         16.3E6
MP,DENS,4,        2.58E-3
MP,PRXY,4,        0.28
MP,ALPX,4,        1.38E-6
MP,MU,4,          0.38

!Aluminum Bolt
MP,EX, 5,         10.6E6
MP,DENS,5,        3.12E-3
MP,PRXY,5,        0.33
MP,ALPX,5,        11.7E-6


!!!!!!!!!!!!!!!!!!!!!! ELEMENT TYPES !!!!!!!!!!!!!!!!!!!!!!!!!!!!!!!

et,1,solid186                   ! 20  node solid structural element. 3 disp DOF
et,2,conta173
et,3,targe170
real,1
et,4,solid185                   ! 8  node solid structural element. 3 disp DOF

!!!!!!!!!!!!!!!!!!!!!! MESHING !!!!!!!!!!!!!!!!!!!!!!!!!!!!!!!!!!!!!

!! DIVIDE SLW !!!!!!!!!
vsel,s,volu,,slw
csys,14
clocal,51,0, 0,0,-tpinlength-.01
wpcsys
vsbw,all,,delete
cm,slw,volu
csys,51
vsel,r,loc,z,-1,0
csys,19
wpcsys
vsbw,all,,delete
cm,MAP_SLW,volu

csys,11
vsel,s,loc,z,0,h1
vsel,u,volu,,tpins
csys,33
```

```
vsel,r,loc,z,0,1
csys,0
vsel,r,loc,x,0,2
cm,slw,volu

!!!!!!!!! ASSIGN MATERIALS, REAL CONST, ELEM SYS !!!!!!!!!!!

vsel,s,volu,,PKG
vsel,a,volu,,AMP
vatt,1,-1,-1,0                          ! sets mat'l. props and element type for FR4 matls (1)

vsel,s,volu,,SLW
vatt,2,-1,-1,0                          ! sets mat'l. props and element type for SLW (2)

vsel,s,volu,,TPINS
vatt,3,-1,-1,0                          ! sets mat'l. props and element type for PINS (3)

vsel,s,volu,,SENSOR
vatt,4,-1,-1,0                          ! sets mat'l. props and element type for SENSOR

vsel,s,volu,,BOLT
vsel,a,volu,,CBOLTS
vatt,5,-1,-1,0                          ! sets mat'l. props and element type for BOLT & NUT

allsel,all
save,premesh,all

!!! MESHING !!!!!!!!!!!

finish
/prep7

!!!!!!!! MAPPED MESH !!!!!!!!!!!
csys,0
vsel,s,volu,,amp                    ! mapped amp volumes
vsel,a,volu,,map_slw
vsel,a,volu,,bolt
vsel,a,volu,,cbolts
aslv,r
lsla,r
lsel,u,tan1,z,1,1
lsel,u,tan2,z,1,1
lesize,all,t1/2

        type,4
        mshkey,1
        mshape,0,3d
        esize,t1/3
        vmesh,all

allsel,all
vsel,s,volu,,sensor
aslv,r
```

```
lsla,r
lsel,u,tan1,z,1,1
lsel,u,tan2,z,1,1
lesize,all,t1/3

        type,4
        mshkey,1
        mshkey,1
        mshape,0,3d
        esize,t2/2
        vmesh,all

allsel,all
vsel,s,volu,,tpins

        type,4
        mshkey,1
        mshkey,1
        mshape,0,3d
        esize,t2
        vmesh,all


allsel,all
vsel,s,volu,,pkg
csys,27
vsel,r,loc,z,-1,0
aslv,r
lsla,r
lsel,u,tan1,z,1,1
lsel,u,tan2,z,1,1
lesize,all,t1/2

        type,4
        mshkey,1
        mshkey,1
        mshape,0,3d
        esize,t1/3
        vmesh,all

allsel,all
vsel,s,volu,,pkg
csys,28
vsel,r,loc,z,0,3
csys,40
vsel,u,loc,z,0,2
aslv,r
lsla,r
lsel,u,tan1,z,1,1
lsel,u,tan2,z,1,1
lesize,all,t1/2
        type,4
        mshkey,1
```

```
            mshkey,1
            mshape,0,3d
            esize,t1/3
            vmesh,all

allsel,all
vsel,s,volu,,pkg
csys,40
vsel,r,loc,z,0,2
csys,35
vsel,r,loc,z,-1,0
aslv,r
lsla,r
lsel,u,tan1,z,1,1
lsel,u,tan2,z,1,1
lesize,all,t1/2,,,,0
            type,4
            mshkey,1
            mshkey,1
            mshape,0,3d
            esize,t1/3
            vmesh,all

allsel,all
vsel,s,volu,,pkg
csys,41
vsel,r,loc,z,0,1
csys,35
vsel,u,loc,z,-1,0
aslv,r
lsla,r
lsel,u,tan1,z,1,1
lsel,u,tan2,z,1,1
lesize,all,t1/2,,,,0
            type,4
            mshkey,1
            mshkey,1
            mshape,0,3d
            esize,t1/3
            vmesh,all

allsel,all
save,prefree,all

!!!!! FREE MESH !!!!!!!!!!!!!!!!!
finish

/prep7

vsel,s,volu,,pkg
csys,27
vsel,r,loc,z,0,slw_w
```

```
        type,1
        mshkey,0
        mshape,1,3d
        !mopt,tetexpnd,2
        smrtsize,6
        vmesh,all

allsel,all
vsel,s,volu,,pkg
csys,40
vsel,r,loc,z,0,1
csys,35
vsel,r,loc,z,0,1
        type,1
        mshkey,0
        mshape,1,3d
        !mopt,tetexpnd,2
        smrtsize,6
        vmesh,all
allsel,all
vsel,s,volu,,slw
vsel,u,volu,,map_slw
        type,1
        mshkey,0
        mshape,1,3d
        !mopt,tetexpnd,2
        smrtsize,6
        vmesh,all

allsel,all


!!!!!!!!!! CONTACT !!!!!!!!


allsel,all
save,meshed,all


!!! DOF CONSTRAINTS !!!!

csys,11
nsel,s,loc,z,-cblength          ! selects nodes on bottom face of corner bolts
d,all,all,0                     ! fixes all DOF's of all the bottom nodes

!csys,0                         ! amp edges fixed option
!nsel,s,loc,z,0,t1
!nsel,r,loc,x,0
!d,all,all,0

!csys,0
!nsel,s,loc,z,0,t1
!nsel,r,loc,x,4
```

```
!d,all,all,0

csys,0
nsel,s,loc,y,0
d,all,uy,0                    ! fixes all uy for all the symmetry plane nodes
allsel,all

/SOLU
ANTYPE,MODAL
MODOPT,LANB,5
MXPAND,5

allsel,all
SOLVE
FINISH
```

Maximum Altitude Steady State

```
/FILENAM,HASP_ground_rad_plates,1
/CWD,'D:\Temp\AL_ANSYS'

/prep7
/pnum,volu,1

!!!!!!!!! PARAMETERS !!!!!!!!!

        !!!!! MOUNT PLATE !!!!!!!!!
                w_mplate = 0.200025                     ! mount plate width
                t_mplate = 0.00635                      ! mount plate thickness from HASP

        !!!!! BOTTOM INSULATION !!!!!!!!
                b_ins_th = 0.0127                       ! insulation thickness
                b_ins_w = 0.15                          ! bottom insulation width (square)
                ! width is the same as bottom insulation width

        !!!!! SIDE INSULATION !!!!!
                s_ins_th = 0.0127                       ! side insulation thickness
                s_ins_h = 0.08001                       ! side insulation height

        !!!!! TOP INSULATION !!!!!!
                t_ins_th = 0.0127                       ! top insulation thickness
                ! width is the same as bottom insulation width

        !!!!! PAYLOAD CAVITY CUTOUT !!!!
                cutwidth = b_ins_w - 2*s_ins_th

        !!!!! POWER BOARD !!!!!!!!!!!!
                wpboard = 0.1016                        ! board widths.
                bspace    = 0.011049                    ! space between power and FPGA boards
                pheight = 0.009525                      ! bottom of power board from bottom
insulation
                FR4thick = 0.001575                     ! FR4 thickness in meters

        !!!!! CONNECTOR DIMS !!!!!!!!
                congap = 0.001079                       ! dist. b/w edge of board and connector
                conwidth = 0.007493                     ! connector width
                conlen = 0.051308                       ! connector length
                conspc = 0.091948                       ! space b/w connectors

        !!!!! MESHING PARAMETERS !!!!!!
                tranlen = fr4thick

        !!!!! CONVECTION LOAD PARAMS !!!!
                h = 24.445                      !W/m^2*K
                Tamb = 275.21    !K

        !!!!! COPPER RAD. PLATE PARAMS !!!!!
```

```
wplate = wpboard                        ! square width of Cu plate. (same area as
PCB's)
sink_th = 3.175e-3                      ! thickness (1/8th inch)

!!!!! BUSHINGS !!!!!!!!!
bushwidth = 0.00635
bushheight = t_mplate + b_ins_th + pheight + FR4thick !+ sink_th

!!!!! COPPER GROUND PLANE PARAMS !!!!
plane_th = 3.429E-5                     ! single ground plane thickness
wplane = wpboard                        ! width of plane

!!!!! RADIATION LOAD PARAMS !!!!!
a = .25                                 ! outer coating absorptivity
Tsun = 5000        !K                   ! temp of sun
Tearth = 288                            ! temp of earth
Tspace = 4                              ! temp of space
G = 1358                                ! solar flux at top of atmosphere (W/m^2)
Atop = b_ins_w*b_ins_w/2                ! top area being irradiated
Lside = s_ins_h + b_ins_th + t_ins_th   ! height of payload (discounting mount
plate)
Aside = Lside*b_ins_w/2                 ! side area being irradiated
Aback = Lside*b_ins_w                   ! back area

Ft = 0.653                              ! Top Face Radiation Form Factor
Fn = 0.0                                ! North Face Radiation Form Factor
Fe = 0.648                              ! East Face Radiation Form Factor
Fs = 0.391                              ! South Face Radiation Form Factor
Fw = 0.0                                ! West Face Radiation Form Factor
flux = a*G                              ! Absorbed solar flux value (W/m^2)


!!!!!!!!!!!!!!!!!!!!!!!!!!!!!!!!!!!!
!!!!!!!! GEOMETRY !!!!!!!!!!
!!!!!!!!!!!!!!!!!!!!!!!!!!!!!!!!!!!!

boptn,keep,no

!! MOUNTPLATE

blc4,-w_mplate/2, -w_mplate/2, w_mplate, w_mplate, t_mplate          !mountplate
cm,mountplate,volu

!! BOTTOM INSULATION

vsel,none
clocal,11,cart, 0,0,t_mplate
wpcsys
blc4, -b_ins_w/2, -b_ins_w/2, b_ins_w, b_ins_w, b_ins_th

cm,B_INS,volu                                                !! bottom insulation
```

```
!! SIDE INSULATION

        clocal,12,cart, 0,0,b_ins_th                    !! top of bottom insulation
        wpcsys
        vsel,none
        blc4, -b_ins_w/2, -b_ins_w/2, b_ins_w, b_ins_w, s_ins_h

        cm,S_INS,volu                                   !!! side insulation

!! CUTOUT
        vsel,none
        blc4, -cutwidth/2, -cutwidth/2, cutwidth, cutwidth, s_ins_h
        cm,cutout,volu

        allsel,all
        vsbv,s_ins,cutout,,delete,delete                !! Subtract cutout from side ins. block

        vsel,s,loc,z,0,s_ins_h
        cm,S_INS,volu                                   !! recreates side insulation

!! COPPER RAD PLATE (HEAT SINK)

        csys,12
        wpcsys
        vsel,none
        blc4,-wplate/2,-wplate/2,wplate,wplate,sink_th  ! rad plate
        cm,radplate,volu

        !vsbv,b_ins,radplate,,delete,keep
        !vsel,u,volu,,radplate
        !vsel,u,volu,,mountplate
        !cm,b_ins,volu

!! POWER BOARD
        csys,12
        clocal,13,cart, 0,0,pheight                     !! bottom of powerboard
        wpcsys
        vsel,none
        blc4, -wpboard/2, -wpboard/2, wpboard,wpboard,FR4thick
        cm,PBOARD,volu

!! FPGA board

        clocal,14,cart,0,0,FR4thick                     !! coord sys on top of pboard
        clocal,15,cart,0,0,bspace                       !! bottom of FPGA
        !wpcsys
        !vsel,none
        !blc4, -wpboard/2, -wpboard/2, wpboard,wpboard,FR4thick
        !cm,FPGA,volu                                   !! creates FPGA component

!! CONNECTORS

        !csys,14
```

```
        !wpcsys
        !vsel,none
        !blc4, -wpboard/2+congap,-conlen/2,conwidth,conlen,bspace
        !vgen,2,all,,,conspc,0,0,0,1,0                  !! creates second connector
        !cm,ESQ,volu                                    !! creates ESQ connectors component

!! GROUND PLANES

        !csys,15
        !wpcsys
        !vsel,none
        !blc4, -wpboard/2, -wpboard/2, wpboard,wpboard,4*plane_th

        !cm,FPGA_GRND,volu                              !! creates fpga ground plane

        csys,13
        wpcsys
        vsel,none
        blc4, -wpboard/2, -wpboard/2, wpboard,wpboard,3*plane_th
        cm,POWER_GRND,volu                              !! creates power board ground
plane

        allsel,all
        vsbv,pboard,power_grnd,,delete,keep
        csys,14
        vsel,s,loc,z,-fr4thick+3*plane_th,0
        cm,pboard,volu

!! SUPPORT BUSHINGS

        csys,0
        !clocal,40,0, 0,0,-sink_th
        wpcsys
        vsel,none
        blc4, -wpboard/2, -wpboard/2, bushwidth, bushwidth, bushheight
        vgen,2,all,,,wpboard-bushwidth,0,0,0,1,0
        vgen,2,all,,,0,wpboard-bushwidth,0,0,1,0
        cm,BUSHINGS,volu                                !! creates bushings comp.

        vsel,a,volu,,mountplate
        vsel,a,volu,,b_ins
        vsel,a,volu,,pboard
        vsel,a,volu,,power_grnd
        vsel,a,volu,,radplate

        vovlap,all

        csys,0
        clocal,23,0, -wpboard/2,wpboard/2,0
        clocal,24,0, wpboard,0,0
        clocal,25,0, 0,-wpboard,0
        clocal,26,0, -wpboard,0,0
```

```
vsel,s,loc,z,0,t_mplate
vsel,u,loc,y,0,bushwidth
csys,23
vsel,u,loc,y,-bushwidth,0

cm,mountplate,volu

csys,23
vsel,s,loc,y,-bushwidth,0
csys,26
vsel,a,loc,y,0,bushwidth
cm,BUSHINGS, volu

csys,12
vsel,s,loc,z,0,sink_th
vsel,u,volu,,bushings
cm,radplate,volu

csys,11
vsel,s,loc,z,0,b_ins_th
vsel,u,volu,,bushings
vsel,u,volu,,radplate
cm,B_INS,volu

csys,13
vsel,s,loc,z,0,3*plane_th
vsel,u,volu,,bushings
cm,power_grnd,volu

vsel,s,loc,z,3*plane_th,fr4thick
vsel,u,volu,,bushings
cm,pboard,volu


!! TOP INSULATION

csys,12
clocal,16,cart,0,0,s_ins_h                    !! top of side insulation
wpcsys
vsel,none
blc4, -b_ins_w/2, -b_ins_w/2, b_ins_w, b_ins_w, t_ins_th

cm,TOP_INS,volu                               !! creates top insulation component

!! SYMMETRY SPLIT

allsel,all
csys,0
clocal,17,cart,0,0,0,0,90,0
wpcsys
vsbw,all,sepo,delete
csys,0
vsel,s,loc,y,0,-1
```

```
        vdele,all,,,1

!! GLUE VOLUMES TO SHARE COINCIDENT AREAS !!
        allsel,all
        vglue,all

!! RECREATE DELETED COMPONENTS !!!!!!

        csys,0
        vsel,s,loc,z,0,t_mplate
        csys,23
        vsel,u,loc,x,0,bushwidth
        csys,24
        vsel,u,loc,x,-bushwidth,0
        cm,MOUNTPLATE,volu

        !csys,23
        !vsel,s,loc,y,-bushwidth,0
        !vsel,u,volu,,mountplate
        !cm,BUSHINGS, volu

        csys,12
        vsel,s,loc,z,0,sink_th
        vsel,u,volu,,bushings
        cm,radplate,volu

        csys,11
        vsel,s,loc,z,0,b_ins_th
        vsel,u,volu,,bushings
        vsel,u,volu,,radplate
        cm,B_INS,volu                       !! bottom insulation comp

        csys,13
        vsel,s,loc,z,0,3*plane_th
        vsel,u,volu,,bushings
        cm,power_grnd,volu

        vsel,s,loc,z,3*plane_th,fr4thick
        vsel,u,volu,,bushings
        cm,pboard,volu

        !csys,14
        !vsel,s,loc,z,0,bspace
        !vsel,u,volu,,bushings
        !cm,ESQ,volu                        !! ESQ connectors component

        vsel,s,volu,,bushings
        vsel,a,volu,,pboard
        vsel,a,volu,,power_grnd
        vsel,a,volu,,radplate
        cm,SYSTEM,volu                      !! creates internal systems component

        csys,12
```

```
        vsel,s,loc,z,0,s_ins_h
        vsel,u,volu,,system
        vsel,u,volu,,radplate
        cm,S_INS,volu                                   !! side insulation component

        csys,16
        vsel,s,loc,z,0,t_ins_th
        cm,TOP_INS,volu                                 !! top insulation component

!! SPLIT SIDE AND TOP INSULATION FOR MAPPED MESH !!!
        csys,12
        clocal,27,0, cutwidth/2,0,0, 90,90,0
        clocal,28,0, 0,0,-cutwidth
        csys,12
        clocal,29,0, 0,cutwidth/2,0,0,90,0

        vsel,s,volu,,s_ins
        vsel,a,volu,,top_ins
        csys,28
        wpcsys
        vsbw,all,,delete
        csys,27
        wpcsys
        vsbw,all,,delete
        csys,29
        wpcsys
        vsbw,all,,delete

        !! Recreate components
                csys,12
                vsel,s,loc,z,0,s_ins_h
                vsel,u,volu,,system
                cm,s_ins,volu                           !! side insulation
                csys,16
                vsel,s,loc,z,0,t_ins_th
                cm,top_ins,volu                         !! top insulation

!!!!!!!!!!!!!!!!!!!!!!!!!!!!!!!!!!!!!!!!!!!!!!!!!!!!!!
!!!!!!!!!!!! THERMAL PROPERTIES !!
!!!!!!!!!!!!!!!!!!!!!!!!!!!!!!!!!!!!!!!!!!!!!!!!!!!!!!
! FR4
        mp,kxx,1,0.27
        mp,c,1,915                      ! J/kg*K
        mp,dens,1,1.82E3                ! kg/m^3

! Polystyrene Insulation     ! values from isolparma extruded polystyrene boards
                                ! (http://www.isolparma.it/ING/pdf/XPS.pdf)
        mp,kxx,2,0.036
        mp,dens,2,30                    ! kg/m^3
        mp,c,2,1200                     ! J/kg*K

! Aluminum bushings (assumed 2024 T6) (values from Incropera)
        mp,kxx,3,177                    ! W/m*K
```

```
        mp,dens,3,2790                  ! kg/m^3
        mp,c,3,875                      ! J/kg*K
        mp,emis,3,0.1                   ! emisivity =.1

! Outer layer (White Paint)
        mp,emis,4,0.95                                  !! Krylon Flat White #1502
        mp,kxx,4,0.000017               ! W/m*K         !! Incropera
        mp,dens,4,801                   ! kg/m^3        !! Sherwin Williams Spec Sheet
! ESQ connectors
        mp,kxx,5,3.976                  ! W/m*K
        mp,c,5,1500                     ! J/kg*K
        mp,dens,5,1610                  ! kg/m^3

! Copper
        mp,dens,6,8933                  ! kg/m^3
        mp,kxx,6,401                    ! W/m*K
        mp,c,6,385                              ! J/kg*K
        mp,emis,6,.05                   ! http://www.thermoworks.com/emissivity_table.html

! Air Inside Payload
        mp,dens,7,1.009                 ! kg/m^3
        mp,kxx,7,0.0243                 ! W/m*K
        mp,c,7,1006.5                   ! J/kg*K

! PVC base plate
        mp,dens,8,527
        mp,kxx,8,0.19                   !http://www.engineeringtoolbox.com/thermal-conductivity-
d_429.html
        mp,c,8,900
        mp,emis,8,.85                   !http://www.thermoworks.com/emissivity_table.html

!!!!!!!!!!!!!!!!!!!!!!!!!!!!!!!!!!!!!!!!!!!!!!!!!!!!!!!!!!!!
!!!!!!!!!!!!!!!! ELEMENTS & MESHING !!!!
!!!!!!!!!!!!!!!!!!!!!!!!!!!!!!!!!!!!!!!!!!!!!!!!!!!!!!!!!!!!


csys,0

et,1,solid70                            ! 8 node, 3D thermal elem. 1 DOF (temp)
et,2,surf152                            ! radiation surface element
real,2
keyopt,2,4,1
keyopt,2,5,1
keyopt,2,8,1
keyopt,2,9,1
keyopt,2,11,0

r,2,1,5.6704E-8                         ! form factor=1, Stefan Boltzmann constant (kg/s^3*K^4)

et,3,solid87
et,4,solid90

!!!!!!!!!!!!!!!!!!!!!! MESHING !!!!!!!!!!!!!!!!!!!!!!!!!!!!!!!!!!!!
```

```
!!!!!!!!! ASSIGN MATERIALS, REAL CONST, ELEM. TYPE, ELEM SYS !!!!!!!!!!!

        !! SET MOUNT PLATE
        vsel,s,volu,,mountplate
        vatt,8,-1,-1

        !! SET INSULATION PROPS
        vsel,s,volu,,s_ins
        vsel,a,volu,,top_ins
        vsel,a,volu,,b_ins
        vatt,2,-1,-1

        !! FR4
        vsel,s,volu,,pboard
        vatt,1,-1,-1

        !! ESQ
        !vsel,s,volu,,esq
        !vatt,5,-1,-1

        !! BUSHINGS
        vsel,s,volu,,bushings
        vatt,3,-1,-1

        !! GROUND PLANES
        vsel,a,volu,,power_grnd
        vatt,6,-1,-1

        !! HEAT SINK RAD PLATE
        vsel,s,volu,,radplate
        vatt,6,-1,-1

!! GROUND PLANES

        !csys,0
        !seltol,1e-8
        !vsel,s,volu,,power_grnd
        !vsel,a,volu,,fpga_grnd
        !aslv,s
        !lsla,s
        !lsel,u,tan1,x,1,1
        !lsel,u,tan2,x,1,1
        !lsel,u,tan1,y,1,1
        !lsel,u,tan2,y,1,1
        !lesize,all,,,-1,,1

allsel,all
save,presplit,all

!! SPLIT PCB BOARDS, GRND PLANES, & RAD PLATE FOR MAPPED MESHING !!!!!!
finish
/prep7
```

```
allsel,all
vsel,s,volu,,power_grnd
vsel,a,volu,,pboard
vsel,a,volu,,radplate
csys,23
clocal,30,0, bushwidth,0,0, 0,0,90
clocal,36,0, 0,-bushwidth,0, 0,90,0
csys,24
clocal,31,0, -bushwidth,0,0, 0,0,90
clocal,37,0, 0,-bushwidth,0, 0,90,0

csys,30
wpcsys
vsbw,all,,delete
csys,31
wpcsys
vsbw,all,,delete
csys,36
wpcsys
vsbw,all,,delete

csys,13
vsel,s,loc,z,0,3*plane_th
vsel,u,volu,,bushings
cm,power_grnd,volu
vsel,s,loc,z,3*plane_th,fr4thick
vsel,u,volu,,bushings
cm,pboard,volu

vsel,s,volu,,power_grnd
cm,CU_PLANES,volu                    !! creates copper planes component

!csys,30
!vsel,u,loc,z,-1,0
!csys,31
!vsel,u,loc,z,0,1
!cm,MAPPED_CU,volu

csys,12
vsel,s,loc,z,0,sink_th
vsel,u,volu,,bushings
!csys,30
!clocal,41,0, 0,-congap-conwidth-tranlen,0, 0,90,0
!wpcsys
!vsbw,all,,delete
cm,radplate,volu

!! Split b_ins for mapped mesh

vsel,s,volu,,b_ins
vsel,a,volu,,bushings
csys,12
```

```
clocal,50,0, 0,0,-bushwidth/2
wpcsys
vsbw,all,,delete

csys,23
vsel,s,loc,y,-bushwidth,0
csys,26
vsel,a,loc,y,0,bushwidth
vsel,u,volu,,mountplate
vsel,u,volu,,radplate
vsel,u,volu,,pboard
vsel,u,volu,,power_grnd
cm,BUSHINGS, volu

csys,12
vsel,s,loc,z,-b_ins_th,0
vsel,u,volu,,bushings
cm,b_ins,volu

csys,50
vsel,u,loc,z,0,1
cm,b_ins_coarse,volu
vsel,s,volu,,b_ins
vsel,u,volu,,b_ins_coarse
cm,b_ins_fine,volu

allsel,all
save,premesh,all

!!!!!!! MAPPED MESH !!!!!!!!!!!
finish
/prep7

vsel,s,volu,,power_grnd
mat,6
type,1
mshkey,1
mshape,0,3d
esize,bushwidth/4
vmesh,all

allsel,all
vsel,s,volu,,pboard
mat,1
type,1
mshkey,1
mshape,0,3d
esize,bushwidth/4
vmesh,all

!! Mapped mesh bushings
vsel,s,volu,,bushings
mat,3
```

```
        type,1
        mshkey,1
        mshape,0,3d
        esize,bushwidth/4
        vmesh,all

!! Mapped side and top insulation
        vsel,s,volu,,s_ins
        vsel,a,volu,,top_ins
        mat,2
        type,1
        mshkey,1
        mshape,0,3d
        esize,t_ins_th/2
        vmesh,all

!! Mapped mesh Rad Plate
        vsel,s, volu,,radplate
        mat,6
        type,1
        mshkey,1
        mshape,0,3d
        esize,sink_th/2
        vmesh,all

allsel,all
save,prefree,all

!! Free mesh remaining
        vsel,s,volu,,mountplate
        aslv,s
        lsla,s
        lsel,u,line,,105,108
        lsel,u,line,,153,168
        lsel,u,line,,117,120
        lesize,all,t_mplate,,,,0

        mshkey,0
        mshape,1,3d
        mopt,expnd,2
        mopt,trans,3
        smrtsize,9
        vmesh,all

        allsel,all
        vsel,s,volu,,b_ins_coarse
        mshkey,0
        mshape,1,3d
        mopt,expnd,2
        mopt,trans,3
        smrtsize,9
        vmesh,all
```

```
allsel,all
vsel,s,volu,,b_ins_fine
mshkey,0
mshape,1,3d
mopt,expnd,2
mopt,trans,3
smrtsize,9
vmesh,all

allsel,all
save,prerad3,all

finish
/prep7

!! APPLY SURFACE ELEMENTS !!!!!!!!!!!!!!

!coord systems to find faces.
csys,16
clocal,32,0, 0,0,t_ins_th          ! top face, center of area
clocal,33,0, b_ins_w/2,0,0         ! right face, top left corner
clocal,34,0, -b_ins_w,0,0          ! left face, top right corner
csys,32
clocal,35,0, 0,b_ins_w/2,0         ! back face, top center

csys,32
n,100000,0,b_ins_w/4, .5           ! top space temp node

csys,32
asel,s,loc,z,-1e-8,1e-8            !! TOP FACE
nsla,s,1
esln,s,0
type,2
mat,4
real,2
esurf,100000                       !! puts surface elems on top surf.
!Solflux_top = G*a*Atop            !! solar flux on top of payload
!sf,all,hflux,flux                 !! applies flux on nodes
esel,r,type,,2                     !! select surface elements
sfe,all,1,hflux,1,Ft*flux          !! applies flux on element faces.

csys,34
n,100001,-.5,b_ins_w/4,-Lside/2    !! space node for left face
vsel,s,volu,,s_ins
vsel,a,volu,,top_ins
aslv,s
asel,r,loc,x,-1e-8,1e-8            !! LEFT FACE
nsla,s,1
esln,s,0
csys,12
esel,u,cent,z,-1,0

type,2
```

```
mat,4
esurf,100001
!Solflux_left = G*e*Aside                !! solar flux on left of payload
!sf,all,hflux,flux                       !! applies flux
esel,r,type,,2
sfe,all,1,hflux,1,Fn*flux

csys,35
n,100002,0,.5,-Lside/2                   !! space node for back face
vsel,s,volu,,s_ins
vsel,a,volu,,top_ins
aslv,s
asel,r,loc,y,-1e-8,1e-8                  !! BACK FACE
nsla,s,1
esln,s,0
csys,12
esel,u,cent,z,-1,0
type,2
mat,4
esurf,100002
!Solflux_back = G*e*Aback                !! solar flux on back of payload
!sf,all,hflux,flux                       !! applies flux
esel,r,type,,2
esel,u,cent,Y,-1,0
sfe,all,1,hflux,1,Fe*flux

csys,33
n,100003,.5, b_ins_w/4,-Lside/2          ! space temp node for right face

vsel,s,volu,,s_ins
vsel,a,volu,,top_ins
aslv,s
asel,r,loc,x,-1e-8,1e-8                  !! RIGHT FACE
nsla,s,1
esln,s,0
csys,12
esel,u,cent,z,-1,0
type,2
mat,4
esurf,100003
esel,r,type,,2
esel,u,cent,Y,-1,0
sfe,all,1,hflux,1,Fs*flux

csys,0
n,100004,0, 0, -.5                       ! earth temp extra node

allsel,all
vsel,s,volu,,mountplate
vsel,a,volu,,bushings
aslv,s
asel,r,loc,z,-1e-8,1e-8                  !! bottom face
nsla,s,1
```

```
        esln,s,0
        type,2
        mat,4
        esurf,100004

allsel,all
TUNIF,293

allsel,all
save,meshed3,all

        vsel,s,volu,,power_grnd
        vsum,default
        *get,P_volume,volu,power_grnd,volu

!!!!!!!!!!!!! APPLY LOADS IN SOLUTION PROCESSOR !!!!!!!!!!!

finish

/solu
antype,0
outres,all,all
nsubst,1
kbc,0

!! POWER BOARD HEAT GEN !!  !actually the gen value of fpga which is what actual temp was
measured on

        GEN1 = 1.631                                    ! 1.631W genned throughout board
        vsel,s,volu,,power_grnd
        eslv,s
        bfe,all,hgen,1,GEN1/P_volume

        !/pbf,hgen,,1                                   !! shows heat gen

!! RADIATION !!
        d,100000,temp,Tspace
        d,100001,temp,Tspace
        d,100002,temp,Tspace
        d,100003,temp,Tspace
        d,100004,temp,Tearth

allsel,all
save,loaded3,all

!!! SOLUTION !!!!!

finish
/solu
allsel,all
solve
save
finish
```

```
/post1
/DSCALE,ALL,1.0
/EFACET,1
PLNSOL, TEMP,, 0

vsel,s,volu,,pboard
vsel,a,volu,,bushings
vsel,a,volu,,power_grnd
eslv
nslv
/DSCALE,ALL,1.0
/EFACET,1
PLNSOL, TEMP,, 0
```